REPUBLIC OF TÜRKİYE
ADANA ALPARSLAN TÜRKEŞ SCIENCE AND TECHNOLOGY UNIVERSITY

GRADUATE SCHOOL

DEPARTMENT OF BIOENGINEERING

FABRICATION OF MOLECULARLY IMPRINTED NANOPARTICLE BASED QUARTZ CRYSTAL MICROBALANCE (QCM) SENSORS FOR ANGIOTENSIN-II DETECTION FROM HUMAN SERUM

OKAN ZENGER

Ph.D.

ADANA 2025

REPUBLIC OF TÜRKİYE
ADANA ALPARSLAN TÜRKEŞ SCIENCE AND TECHNOLOGY UNIVERSITY

GRADUATE SCHOOL

DEPARTMENT OF BIOENGINEERING

FABRICATION OF MOLECULARLY IMPRINTED NANOPARTICLE BASED QUARTZ CRYSTAL MICROBALANCE (QCM) SENSORS FOR ANGIOTENSIN-II DETECTION FROM HUMAN SERUM

OKAN ZENGER

Ph.D.

THESIS ADVISOR

PROF. GÖZDE BAYDEMİR PEŞİNT

ADANA, 2025

DECLARATION OF CONFORMITY

I hereby declare that all the information presented in this thesis has been obtained and documented in accordance with academic rules and scientific ethical standards. All visual and written materials, as well as the results, have been appropriately referenced and presented in line with the principles of academic integrity. The data have not been altered or distorted in any manner, and the results completely represent the research findings. None of the content of this thesis has been submitted as part of another thesis or academic research.

09/07/2025

[Signature]

Okan ZENGER

ÖZET

İNSAN SERUMUNDAN ANJİYOTENSİN-II TESPİTİ İÇİN MOLEKÜLER BASKILANMIŞ NANOPARTİKÜL TABANLI KUVARS KRİSTAL MİKROTERAZİ (QCM) SENSÖRLERİNİN ÜRETİMİ

Okan ZENGER
Doktora, Biyomühendislik Anabilim Dalı
Danışman: Prof. Dr. Gözde BAYDEMİR PEŞİNT
Temmuz 2025, 100 sayfa

Anjiyotensin II (AngII), renin-anjiyotensin sisteminin önemli bir efektör peptididir ve hücresel büyüme, fibrozis ve apoptoz süreçlerinin düzenlenmesinde büyüme faktörü olarak görev yapar. AngII, hipertansiyon, kardiyovasküler hastalıklar ve influenza ile SARS-CoV-2 gibi enfeksiyonlar da dahil olmak üzere birçok hastalığın ve bozukluğun patofizyolojisinde kritik bir rol oynamaktadır. Ayrıca tümör gelişimindeki potansiyel rolü açısından da araştırılmaktadır. Ancak, AngII'nin biyolojik sıvılardaki konsantrasyonunun çok düşük olması, kararsız yapısı ve biyolojik sıvıların karmaşık doğası, bu molekülün anlık ve hassas tespitini oldukça güç hale getirmektedir. Moleküler baskılama, hedef molekülün doğal tanıma bölgelerini taklit eden, yüksek seçiciliğe sahip sentetik reseptörlerin hazırlanmasına olanak tanıyan bir tekniktir. Bu çalışmada, AngII'nin seçici tespiti için ~50 nm boyutunda nanoparçacık formunda sentezlenen moleküler baskılanmış polimerler (MIP'ler), tanıma elemanı olarak kuvars kristal mikroterazi (QCM) sensör çiplerine entegre edilmiştir. AngII baskılanmış (AngII-MIP) ve baskılanmamış (NIP) nanoparçacıkların sentezi ve karakterizasyonunun ardından, QCM tabanlı sensörler (AngII-MICqcm ve NICqcm) üretilmiş ve kinetik bağlanma analizlerinde kullanılmıştır. AngII-MICqcm sensörü, 0.25 pg/mL gibi son derece düşük konsantrasyonlardaki AngII'yi tespit edebilme yeteneğiyle yüksek bir duyarlılık göstermiştir. Seçicilik çalışmaları kapsamında, Anjiyotensin I (AngI) ve vazopressin (Vasp) molekülleriyle gerçekleştirilen yarışmalı analizlerde, sırasıyla AngII lehine 6.09 ve 7.44'lük seçicilik oranları elde edilmiştir. Hesaplanan baskılama faktörü (IF) değerleri, AngII için 5.58, AngI için 3.67 ve Vasp için 4.50 olarak bulunmuş ve MIP tabanlı sensörün üstün seçiciliğini doğrulamıştır. Yeniden kullanılabilirlik testleri sonucunda, 10. döngü sonrasında QCM çipinin AngII adsorpsiyon kapasitesinin

yaklaşık %96'sını koruduğu belirlenmiştir. Ayrıca, AngII-MICqcm çipi kullanılarak insan serum örneklerinde gerçekleştirilen analizlerde, bu karmaşık biyolojik ortamda dahi 1 pg/mL düzeyindeki son derece düşük miktarlarda AngII başarıyla tespit edilmiştir.

Anahtar Kelimeler: Anjiyotensin II, moleküler baskılanmış nanoparçacıklar, kuvars kristal mikroterazi (QCM), gerçek zamanlı analiz, etiketsiz tespit

ABSTRACT

FABRICATION OF MOLECULARLY IMPRINTED NANOPARTICLE BASED QUARTZ CRYSTAL MICROBALANCE (QCM) SENSORS FOR ANGIOTENSİN-II DETECTION FROM HUMAN SERUM

Okan ZENGER
Ph.D., Department of Bioengineering
Supervisor: Prof. Gözde BAYDEMİR PEŞİNT
July 2025, 100 pages

Angiotensin II (AngII) is a significant effector peptide of the renin-angiotensin system (RAAS) that serves as a growth factor, regulating cellular growth, fibrosis, and apoptosis. AngII plays a critical role in the pathophysiology of several diseases and disorders, including hypertension, cardiovascular diseases, and infections such as influenza and SARS-CoV-2. It is also being explored for its potential role in tumor progression. However, the spontaneous detection of AngII remains challenging due to its low physiological concentration, instability, and the complex nature of biological fluids. Molecular imprinting is a technique that enables the preparation of highly selective synthetic receptors that mimics the natural recognition sites for the molecule of interest. In this study, molecularly imprinted polymers (MIPs) were synthesized in nanoparticle form (~50 nm) and employed as recognition elements in quartz crystal microbalance (QCM) sensor chips for the selective detection of AngII. Following the synthesis and characterization of AngII-imprinted (AngII-MIP) and non-imprinted (NIP) nanoparticles, QCM-based sensors (AngII-MICqcm and NICqcm) were fabricated and used in kinetic binding studies. The AngII-MICqcm sensor demonstrated high sensitivity, with the ability to detect AngII at concentrations as low as 0.25 pg/mL. Selectivity tests using Angiotensin I (AngI) and vasopressin (Vasp) as competing molecules revealed selectivity ratios of 6.09 and 7.44 in favor of AngII, respectively. The calculated imprinting factor (IF) values were 5.58 for AngII, 3.67 for AngI, and 4.50 for Vasp, confirming the superior selectivity of the MIP-based sensor. Upon reusability test, it was found that after the 10th cycle, the QCM chip retained about 96% of its AngII adsorption capacity. Human serum samples were used in studies to detect AngII using

the AngII-MICqcm chip. Even in this complex environment, the instrument was able to detect incredibly minute amounts of AngII (1 pg/mL).

Keywords: Angiotensin II, molecularly imprinted nanoparticles, quartz crystal microbalance (QCM), real-time analysis, label-free detection

Dedication

To Prof. Gözde Baydemir Peşint,
whose constant support and belief in me have shaped both my academic journey and personal growth. Her ability to see potential when I was unsure of myself has been a lasting source of inspiration.

And to my mom, Zühal Ketre Zenger,
for always being there for me, not only celebrating my successes with pride but also supporting me with love and patience through my early mistakes.

ACKNOWLEDGEMENTS

First, I would like to thank my dear supervisor, Prof. Gözde Baydemir Peşint, for her valuable guidance, professional advice, constructive criticism and suggestions during my research, as well as her sincere interest and efforts to be always there for me in need, like a family.

I am deeply grateful to my thesis jury members, Assoc. Prof. Hatice İmge Oktay Başeğmez, Prof. Dilek Göktürk, Prof. Dilek Alagöz, and Prof. Deniz Yıldırım, for their warm attitude, insightful suggestions, and supportive presence throughout the evaluation of my work.

My heartfelt thanks go to my teammates, Burcu Eren Yüngeviş, Kardelen Cemek Şahin, and Pırıl Arısoy, for their support and friendship. With the right people by your side, even the impossible becomes not only possible, but also much easier.

There are no words strong enough to convey my gratitude to my beloved family, whose endless support, belief in me, and unconditional love have been my greatest source of strength. They have stood beside me in every success and helped me recover from every mistake. I owe everything to them.

I would also like to extend a special thanks to my dear nephew Emir Utku, whose unexpected wisdom beyond his years, his companionship, and even our funny little fights during games have been an irreplaceable source of joy and relief throughout the most stressful times.

This thesis study was supported by TÜBİTAK under the project number 220Z052. I would like to express my sincere gratitude to TÜBİTAK for not only providing financial support, but also for encouraging young researchers like me to pursue scientific curiosity and innovation.

This thesis was conducted at the Nanotechnology Research Laboratory of Adana Adana Alparslan Türkeş Science and Technology University, established with support from the Çukurova Development Agency (Project No: TR62/18ÜRET/0032), whose contribution was key to the success of this and many other studies.

TABLE OF CONTENTS

LIST OF FIGURES

LIST OF TABLES

LIST OF ABBREVIATIONS

AngII	: Angiotensin II
AngI	: Angiotensin I
Vasp	: Vasopressin
RAAS	: Renin-Angiotensin-Aldosterone System
ACE	: Angiotensin Converting Enzyme
AT1R	: Angiotensin Type 1 Receptor
AT2R	: Angiotensin Type 2 Receptor
MIP	: Molecularly Imprinted Polymer
NIP	: Non Imprinted Polymer
LOQ	: Limit of Quantification
LOD	: Limit of Detection
PVA	: Poly (Vinyl Alcohol)
SDS	: Sodium Dodecyl Sulfate
VIM	: 1-Vinylimidazole
EGDMA	: Ethylene Glycol Dimethacrylate
HEMA	: 2-Hydroxyethyl Methacrylate
APS	: Ammonium Persulfate
PBS	: Phosphate Buffered Saline
TEM	: Transmission Electron Microscope
SEM	: Scanning Electron Microscope
FTIR	: Fourier Transform Infrared Spectroscopy
AFM	: Atomic Force Microscope
AngII-MIP	: AngII-Imprinted Polymer
AngII-MICqcm	: QCM chip coated with AngII-MIP nanoparticles
NICqcm	: QCM chip coated with NIP nanoparticles
Cqcm	: Non-coated QCM chip
UV	: Ultraviolet
EDTA	: Ethylenediaminetetraacetic Acid

LIST OF SYMBOLS

L	: Liter
mL	: Milliliter
µL	: Microliter
mg	: Milligram
ng	: Nanogram
pg	: Picogram
nm	: Nanometer
T	: Temperature
°C	: Celsius degree
min	: Minute
h	: Hour
mM	: Millimolar
ΔF	: Change in Frequency
Δm	: Change in Mass
Ka	: Binding constant
Kd	: Dissociation constant
C	: Analyte concentration
1/n	: Freundlich surface heterogeneity index
k	: Selectivity coefficient
k’	: Relative selectivity coefficient

1. INTRODUCTION

Cardiovascular diseases (CVDs) represent the most common cause of mortality worldwide. Every single year, over 20 million people lose their lives to CVDs, accounting for approximately one-third of all global deaths (WHO, 2021; Henein et al., 2022; Gaidai et al., 2023). A key player in this global burden is high blood pressure, or hypertension. It silently raises the risk of heart attacks, strokes, and kidney failure and promotes atherosclerosis. Approximately 50% of hypertensive individuals are unaware of their condition. This makes early detection and better screening not just important but urgent (Mensah et al., 2023). Even though cardiovascular diseases are highly prevalent, early detection is still challenging. One reason is that blood pressure readings alone may not reflect real pathophysiology, especially in asymptomatic individuals. In many cases, these diseases are silent; they can slowly get worse without any clear warning signs. The result is that numerous individuals get diagnosed later than necessary, when irreversible damage has occurred (Gaidai et al., 2023; WHO, 2023; Chong et al., 2024). At this point, biomarkers, which are measurable indicators that help detect diseases even before symptoms appear, become really important.

The renin-angiotensin-aldosterone system (RAAS) constitutes a sophisticated endocrine cascade essential for long-term regulation of arterial pressure and extracellular volume (Perazella & Setaro, 2003). Its activation is initiated by the hepatic release of angiotensinogen, typically in response to reductions in perfusion pressure, lowered distal tubular sodium concentration, or sympathetic stimuli, which is cleaved by renin enzyme secreted from the kidneys to generate the inactive decapeptide angiotensin I (Ang I). Ang I is subsequently converted into the potent vasoconstrictor angiotensin II (Ang II) through the action of angiotensin-converting enzyme (ACE), which is abundantly present on vascular endothelium, especially within the pulmonary circulation (Figure 1.1) (Burnier and Brunner, 2000; Suzuki et al., 2003; Sparks et al., 2014; Crowley & Coffman, 2014).

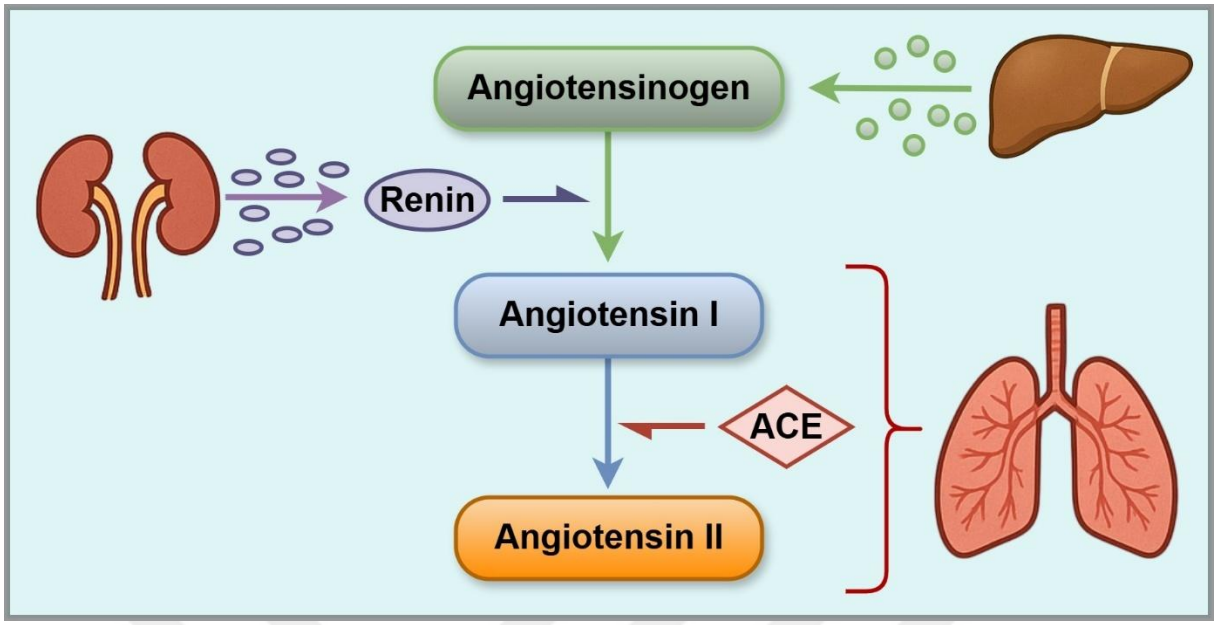

Figure 1.1. Schematic representation of the biosynthesis of AngII. Angiotensinogen, produced primarily in the liver, is cleaved into AngI by renin enzyme released from the kidneys. AngI is then converted into the active vasoconstrictor peptide AngII by ACE, mainly in the lungs.

Ang II, the principal effector peptide of the RAAS, performs multiple functions, i.e., inducing arteriolar vasoconstriction, stimulating aldosterone synthesis from the adrenal cortex, promoting renal sodium retention and potassium excretion, and enhancing thirst and vasopressin (Vasp) release, thus increasing blood pressure and preserving extracellular fluid volume. Recent reviews emphasize RAAS's broader physiological impact, including its role in tissue remodeling, inflammation, and metabolic regulation, as well as emerging interest in local RAAS pathways across various organs (Şerbetçi and Boğa, 2022). AngII demonstrates its physiological effects primarily by binding to two distinct G protein-coupled receptor subtypes: angiotensin type 1 (AT1R) and type 2 (AT2R) receptors. The majority of AngII's well-characterized actions, such as vasoconstriction, aldosterone secretion, sodium retention, and sympathetic activation, are mediated via AT1R receptors. These receptors are widely expressed across various tissues, including the kidneys, myocardium, vascular smooth muscle, central nervous system, adrenal cortex, platelets, adipose tissue, and the placenta (Sparks et al., 2014; Crowley & Coffman, 2014). In contrast, AT2R receptors are less abundantly expressed in adult tissues but are believed to modulate physiological responses by antagonizing or counterbalancing AT1R-mediated effects, contributing to vasodilation, anti-inflammatory

signaling, and tissue repair processes. For example, binding of AngII molecule to AT1R causes vasoconstriction, whereas AT2R stimulation will result in vasodilation (Figure 1.2) (Ardaillou, 1998; Crowley & Coffman, 2014; Busse et al., 2017).

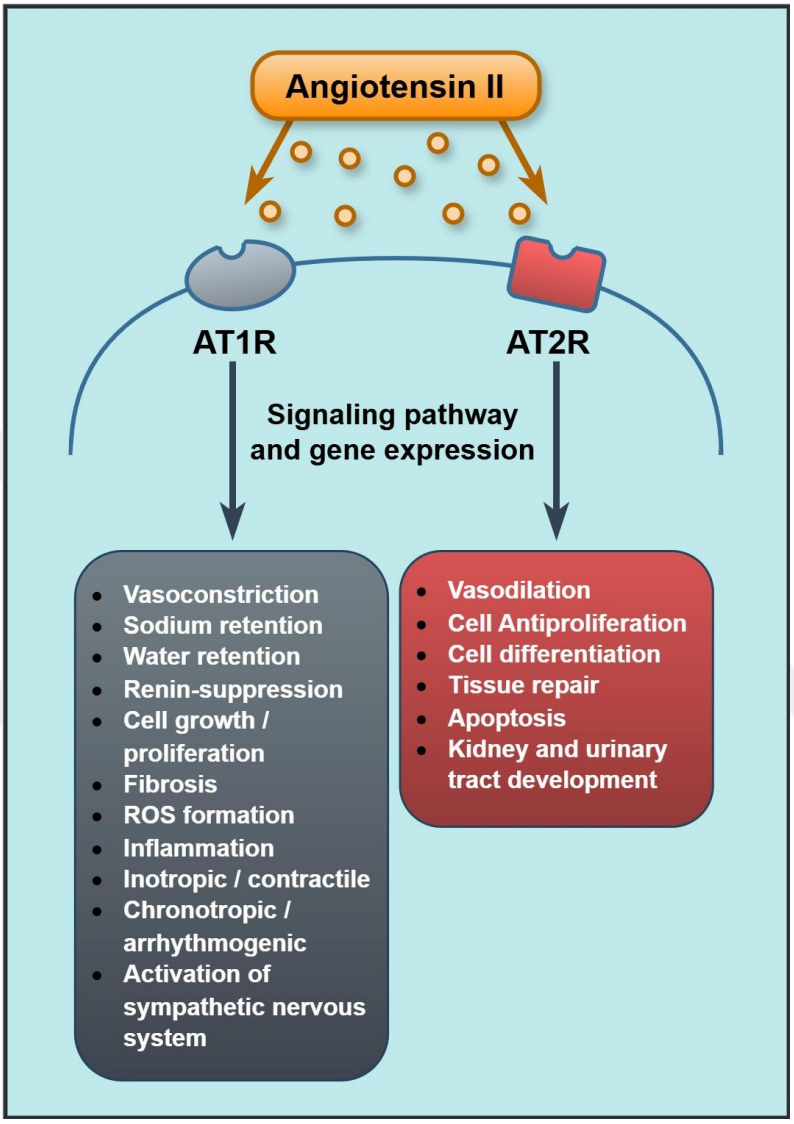

Figure 1.2. Biological effects of AngII upon binding to AT1R and AT2R receptors. These receptors exert counter-regulatory functions, playing opposing roles in vascular homeostasis and disease progression.

AngII molecule consists of 8 amino acids (Figure 1.3). It serves as a critical biomarker in the diagnosis and monitoring of various pathological conditions, including infectious diseases, neoplasms, and, most notably, cardiovascular disorders (Yıldırım and Baydemir Peşint, 2021).

Despite its clinical relevance, the quantification of AngII in blood samples remains a technically demanding and cost-intensive process. Although routine analytical methods are available in clinical laboratories, unstable nature of the peptide, its very low physiological concentration, and the complex matrix of biological fluids pose significant challenges to accurate and efficient detection (Cheng et al., 2005; Sriramula et al., 2008; Yıldırım and Baydemir Peşint, 2021).

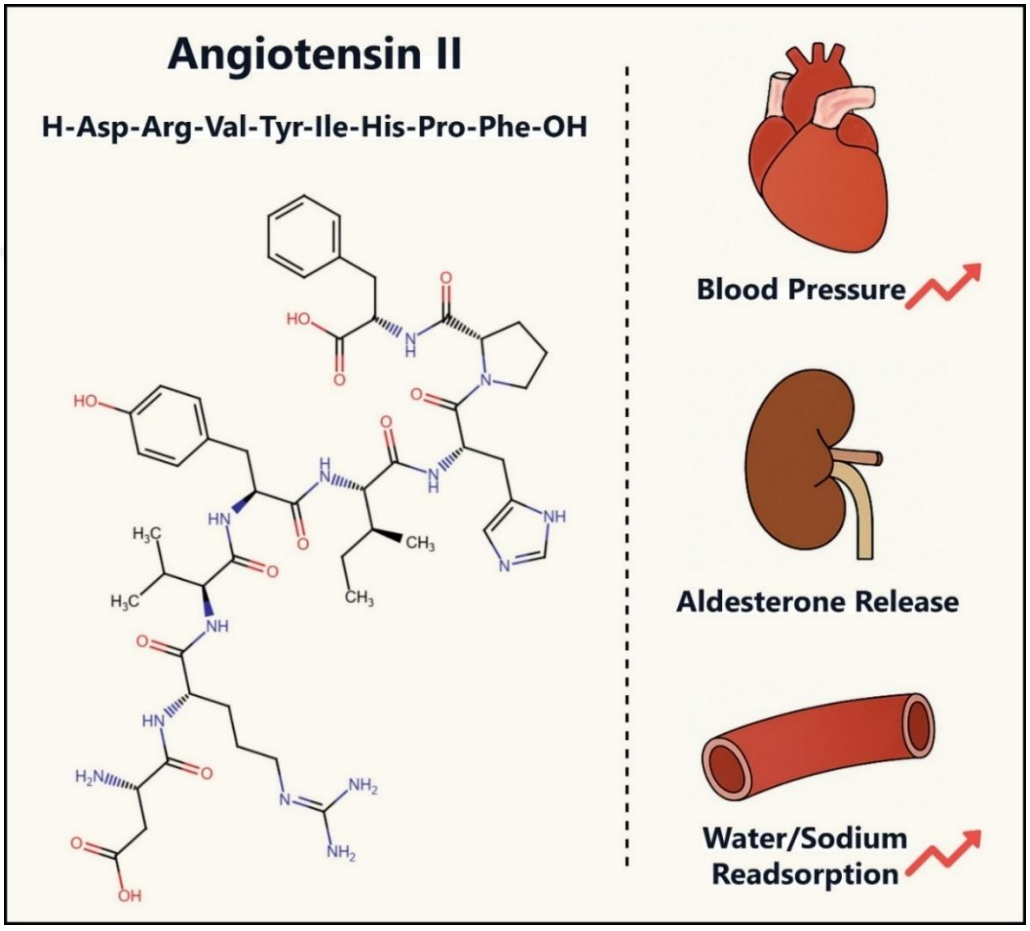

Figure 1.3. Molecular structure and physiological effects of AngII. The left panel illustrates the primary amino acid sequence (H-Asp-Arg-Val-Tyr-Ile-His-Pro-Phe-OH) and chemical structure of AngII. The right panel highlights its major physiological actions: increasing blood pressure via vasoconstriction, stimulating aldosterone release from the adrenal cortex, and enhancing sodium and water reabsorption. Molecular formula: $C_{50}H_{71}N_{13}O_{12}$; Molecular weight: 1,046.2 g/mol (National Center for Biotechnology Information, 2022).

AngII has central effects in vasoconstriction, aldosterone release, antidiuretic hormone synthesis, and salt reabsorption from kidney tubules, and all these effects lead to the development of hypertension. The most important effect in hypertension is the direct contraction effect of AngII on arterial smooth muscles (Forrester et al., 2018; Wu & McGoogan, 2020; Yıldırım and Baydemir Peşint, 2021; Deng et al., 2024). AngII is present in blood at very low levels (reference range: 5-40 pg/mL in serum) and is unstable because of its reactivity, which makes its detection particularly challenging. High-performance liquid chromatography-radioimmunoassay (HPLC-RIA) is the most commonly used method for the detection and determination of AngII biological fluids (Brosnihan & Chappell, 2017; Deng et al., 2024). To analyze AngII using HPLC-RIA, a notable amount of time and effort is required. Therefore, alternative methods are being explored for the detection of AngII in human serum (Cheng et al., 2005; Sriramula et al., 2008; Yıldırım and Baydemir Peşint, 2021).

Molecular imprinting, a rapidly advancing technology, holds great promise (BelBruno, 2018). It involves creating synthetic structures that mimic natural molecular recognition processes for example, binding of an enzyme to a substrate, entry of a virus into the cell through a receptor, recognition of antigen/antibody in the immune system, a drug to a biological target, formation of messenger RNA from DNA template molecules, binding of odor molecules to olfactory receptors found in nasal cavity, etc. (Vasapollo et al., 2011; BelBruno, 2018; Nergiz et al., 2024).

The fundamental characteristics that molecularly imprinted polymers (MIPs) are expected to possess are given below:

1) They should be stable enough to create a permanent memory specific to the template molecule.

2) They are important to have a porous structure so that the target molecule can be easily removed from the imprinted regions (template removal), and then adsorption can be carried out in the same way.

There are some basic components required for the MIP synthesis procedure. These are the target molecule (template), monomer(s), crosslinker, initiator, and solvent. After polymerization, the

template molecule is removed from the polymer to form cavities that will take the three-dimensional structure of the target molecule in the MIP structure so that the cavities can recognize the template molecule in terms of size, structure, and chemical characteristics and allow the target molecule to bind under optimum conditions (Figure 1.4) (Li et al., 2019; Yıldırım and Baydemir Peşint, 2021). MIPs have come into prominence in a wide variety of applications, including the food industry, environmental monitoring, drug delivery systems, forensic sciences, medical sciences, etc., due to their ease of preparation, exceptional stability and reusability under harsh physical and chemical conditions, and excellent recognition properties for the template molecule (Schirhagl, 2014; Saylan et al., 2017; Ding et al., 2020; Yıldırım and Baydemir Peşint, 2021).

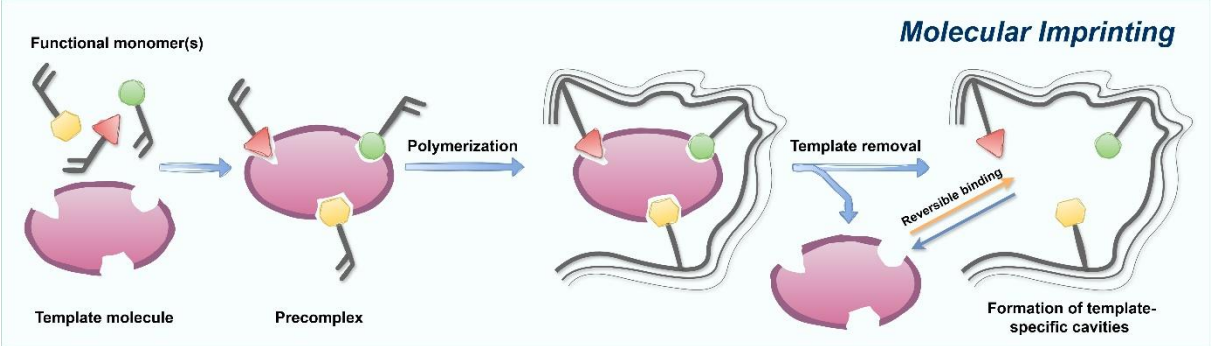

Figure 1.4. Representative illustration of molecular imprinting technique: precomplexation, polymerization around precomplex, removal of the template molecule and formation of template-specific cavities.

MIPs can be synthesized in various forms such as cryogels, hydrogels, monoliths, microbeads, nanofibers, nanoparticles, smart polymers, and many more (Kartal & Denizli, 2014; Wackerlig & Lieberzeit, 2015; Morsi et al., 2023). As seen in Figure 1.5, each type has different structural and chemical properties and comes with different advantages based on their type (Nergiz et al., 2024). Cryogels have macroporous structure which enables ease of mass transfer, they are perfect for separation and purification. Hydrogels exhibit high biocompatibility and they are widely used in medical applications, especially in areas such as wound dressing materials and controlled drug release, due to their excellent biocompatibility. Since monoliths offer mechanical and chemical stability, they perfectly fit in flow-through systems. Microbeads are versatile materials that can be utilized in batch processes due to their readily dispersion. Smart

polymers exhibit stimuli-responsive behavior, enabling controlled release of molecules under stimulations such as temperature, pH, ionic strength, etc. Nanomaterials, on the other hand, are promising materials with elevated surface-to-volume ratios and quantum effects, and their adjustable surface properties enable unique optical, magnetic, mechanical, and catalytic behaviors. Nanomaterials, in general, offers fast binding kinetics, high sensitivity, high binding capacity, adaptability to sensor applications due to their small size (Webster et al., 2005). Among them, nanoparticles have large surface area-to-volume ratios and high binding kinetics. They are particularly advantageous for applications requiring high sensitivity (Xu et al., 2021; Nergiz et al., 2024).

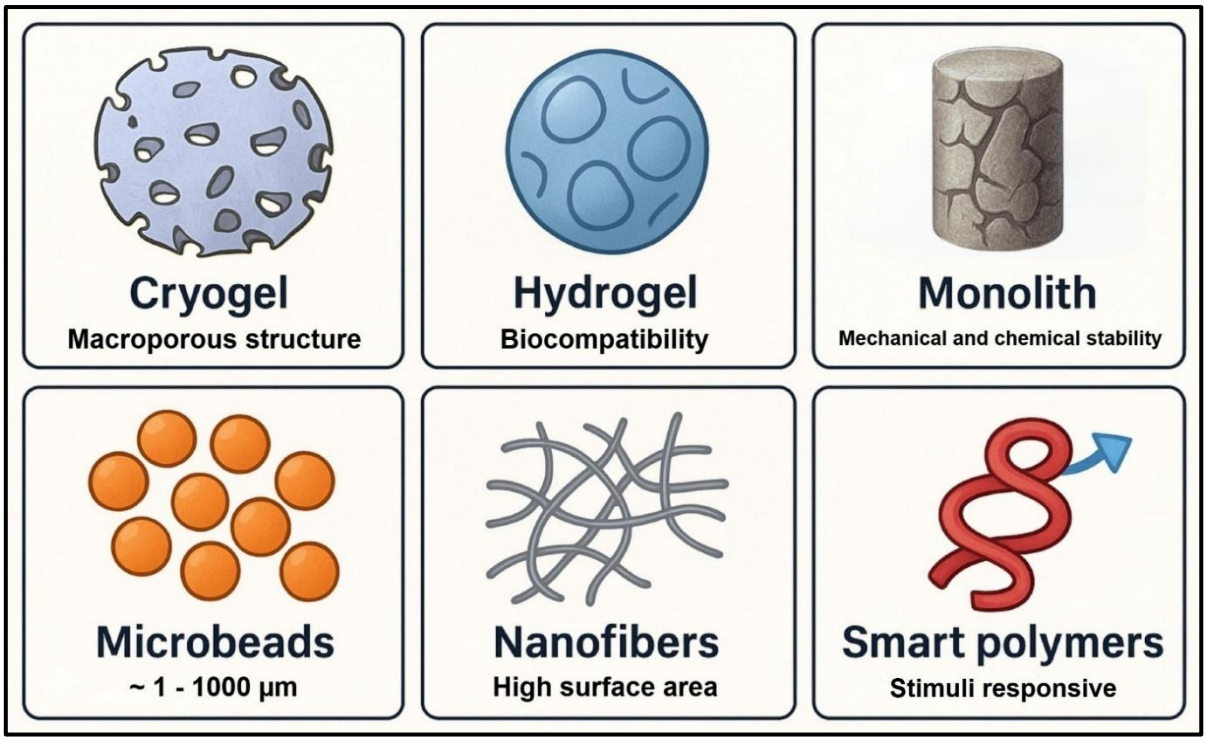

Figure 1.5. Various formats of MIPs and their key advantages: cryogels (interconnected macroporous structure, ease of diffusion), hydrogels (biocompatibility, potential for wound-dressing materials), monoliths (stability under chemically and mechanically harsh conditions), microbeads (~1-1000 µm, ease of dispersion), nanofibers (high surface area, adaptability to sensor applications), and smart polymers (stimuli-responsiveness).

Molecularly imprinted nanoparticles (nanoMIPs) combine the advantages of nanoparticles and MIPs, making them ideal for biorecognition applications (Canfarotta et al., 2016; Qiao et al., 2022; Nergiz et al., 2024).

In analytical science, a common approach is to maximize efficiency and impact by combining various substances, materials, methods, and devices that are distinguished by their unique properties and advantages, provided they do not negatively affect one another. Nanoparticles, for example, integrate seamlessly into biosensor architectures; their sub-100 nm dimensions maximize surface area and accelerate mass transport, thereby boosting signal intensity and response kinetics (Bajaj et al., 2023). Quartz crystal microbalance (QCM) transducers add a complementary capability: a thin quartz wafer, sandwiched between two electrodes, oscillates at its resonant frequency under an alternating voltage. Any adsorbed mass decreases the oscillation, producing a proportional frequency shift that can be quantified with sub-nanogram precision (Liu et al., 2021; Aylaz & Andaç, 2022; Karabulut et al., 2022). Because the measurement is label-free, continuous, and operable in both gas and liquid phases, QCM has become a workhorse for biochemical interaction studies (Diltemiz et al., 2017). When the sensor surface is functionalised with highly selective recognition elements such as nano-MIPs, the platform can monitor binding events in real time while discriminating against non-target species (Lin et al., 2004; Reimhult et al., 2008; Yang & Zhang, 2009; Diltemiz et al., 2017). Thus, the nanoparticle-based QCM represents a synergistic convergence of nanoscale recognition and picogram-mass sensing, well suited for demanding bioanalytical tasks.

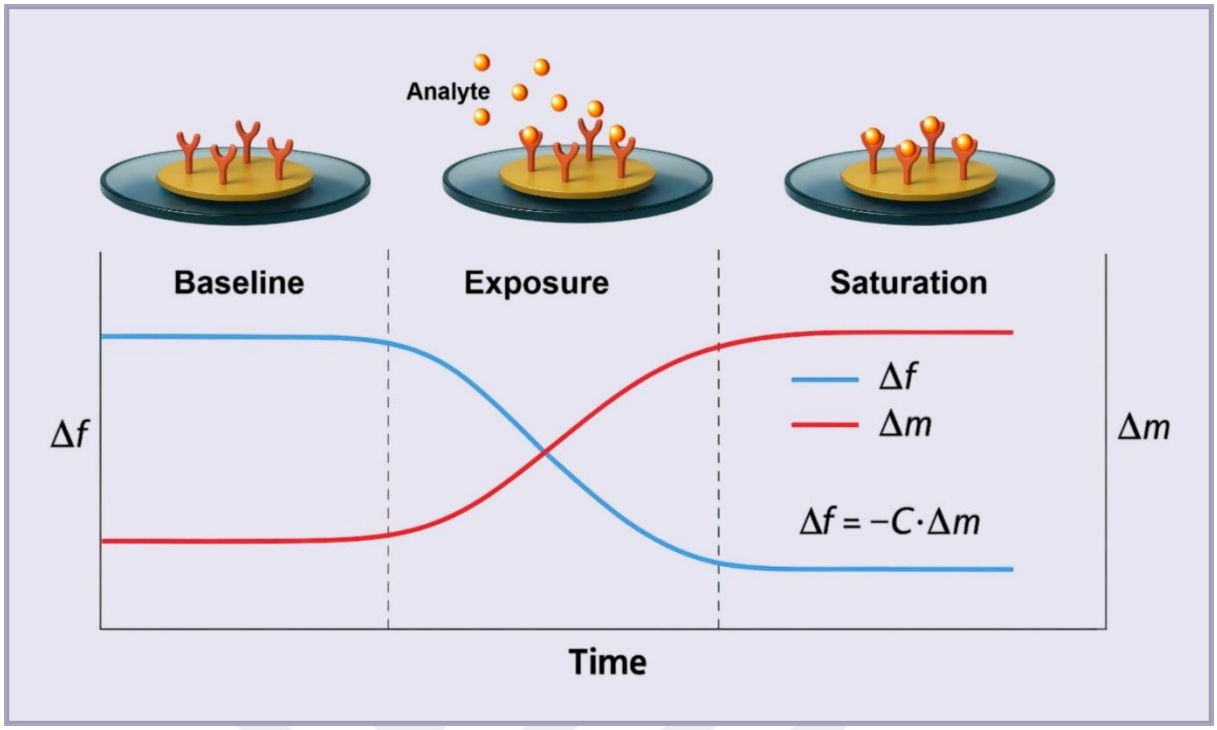

Figure 1.6. Working principle of a QCM sensor showing the inverse correlation of frequency shift (Δf) and mass change (Δm) during the binding process.

Integrating nano-MIPs into high-sensitivity transducers combines three complementary assets: template-driven selectivity, nanoscale surface engineering, and picogram-level mass sensing. The resulting hybrid architecture provides an exceptional surface-area-to-volume ratio that accelerates mass transfer, exposes a larger fraction of recognition sites, and shortens equilibration times. Such kinetic and thermodynamic gains are critical when quantifying angiotensin II, whose serum concentration rarely exceeds the low-picomolar range. In practice, nano-MIP–functionalised sensors have demonstrated rapid, selective capture in complex matrices without extensive pre-treatment, underscoring their utility for precise bioanalysis in clinical fluids. In this study, nanoMIPs were synthesized with the size below 50 nm and well-characterized, and employed as recognition elements in QCM sensor chips for the selective, ultra-sensitive, real-time and label-free detection of AngII in human serum.

2. THEORETICAL FOUNDATIONS AND LITERATURE REVIEW

2.1. Background and Motivation

2.1.1. Global Burden of Hypertension and Cardiovascular Diseases

Cardiovascular diseases (CVDs) still are the prominent cause of mortality worldwide. They constitute around 17.9 million deaths yearly, an estimated 32% across all global deaths, according to the World Health Organization (WHO, 2023). Among these items, hypertension constitutes the most popular risk determinant impacting beyond 1.28 billion adults aged 30-79 globally since the majority are from low- and middle-income nations. Unfortunately, nearly half of adults exhibit hypertension yet remain ignorant of their condition, highlighting an important deficiency in screening alongside management (WHO, 2021; Mensah et al., 2023; Chong et al., 2024).

Hypertension increases the hazard of heart attack, stroke, as well as kidney failure. It additionally impairs the vascular endothelium long-term and promotes atherosclerosis's progression, along with alternative degenerative diseases (Mills et al., 2020). Maturing demographics, poor eating habits, lack of physical activity, and escalating levels of diabetes and obesity are anticipated to further increase CVDs' burden (Roth et al., 2020; Mills et al., 2020; Henein et al., 2022; Gaidai et al., 2023).

2.1.2. Challenges in Early Diagnosis and Monitoring

Early detection and diagnosis is still the main issue in CVDs, even though its high prevalence (Yıldırım and Baydemir Peşint, 2021). Diagnosis of hypertension, i.e., hight blood pressure, conventionally depends on routine blood pressure measurements. However, blood pressure screening alone does not always reflect the full picture, especially in asymptomatic people. In many cases, these diseases are silent; they can slowly get worse without any clear warning signs (Braunwald, 2008; Kario, 2018). Current approaches for the diagnosis of CVDs, such as imaging techniques (e.g., angiography, echocardiography, etc.) and biochemical analysis (e.g., troponin levels, lipid profiles, etc.), are often lack of cost-effectiveness or inadequate for real-

time and routine application in healthcare (Yıldırım and Baydemir Peşint, 2021). These limitations result in delays in diagnosis and treatment, decreasing the possibility of an effective therapeutic intervention (Yıldırım and Baydemir Peşint, 2021). This is where biomarkers become crucial.

2.1.3. Role of Biomarkers in Improving Diagnostics

Biomarkers are measurable indicators that help detect diseases, even when there are no symptoms yet. They have emerged as vital tools in health for early detection and monitoring of disease, and follow-up of treatment, as well as the risk assessment long before any clear sign of the disease (Yıldırım and Baydemir Peşint, 2021; Nergiz et al., 2024). Troponins, B-type natriuretic peptide (BNP), C-reactive protein (CRP), and AngII are remarkable biomarkers in definition of CVD mechanisms, as well as diagnosis, prognosis and further follow-up of CVDs (Miura et al., 2011; Maisel et al., 2019; Mueller et al., 2019).

AngII, a key effector hormone in RAAS, is significantly involved in the regulation of blood pressure, fluid balance, and vascular remodeling. Any increase in AngII levels can be related with heart failure, hypertension, myocardial infarctions, and chronic renal illness (Pagliaro & Penna, 2005; Chappell, 2012; Oparil & Schmieder, 2015). Therefore, detecting and quantifying AngII levels in biological fluids can offer valuable information for early diagnosis and monitoring of CVDs. However, due to its short half-life and extremely low concentration in human serum (in the picomolar range), accurate and real-time detection of AngII remains technically challenging using conventional methods like ELISA or LC-MS/MS (Nguyen Dinh Cat & Touyz, 2011). Emerging biosensor technologies, particularly those integrating MIPs with platforms like QCM, hold the potential to overcome these challenges by enabling selective, sensitive, and label-free detection of target biomarkers such as AngII in real time and complex biological matrices (Karabulut et al., 2022; Tang et al., 2024).

2.2. Importance of Angiotensin II

2.2.1. Physiological Function of AngII in RAAS

The classical RAAS cascade begins with the hepatic release of angiotensinogen, which is then cleaved by renin, an enzyme secreted by the juxtaglomerular cells of the kidneys, into AngI.

AngI is subsequently converted into AngII by ACE, primarily in the lungs (Karnik et al., 2015; Yıldırım and Baydemir Peşint, 2021).

AngII is the principal effector molecule of RAAS and performs its biological effects predominantly through binding to two G-protein coupled receptors: AT1R and Angiotensin AT2R (Laghlam et al., 2021; Leal et al., 2022). Most physiological and pathological effects of AngII, including vasoconstriction, aldosterone release, and sympathetic activation, are mediated via AT1R, while AT2R is thought to mediate vasodilatory, anti-inflammatory, and antiproliferative effects (Benigni et al., 2010; Shanks & Ramchandra, 2021).

2.2.2. Blood Pressure Regulation, Vasoconstriction, and Electrolyte Balance

AngII is a robust vasoconstrictor which operates on vascular smooth muscle cells to raise systemic vascular resistance and, as a result, arterial blood pressure. AngII works on AT1R to make the adrenal cortex release aldosterone (Rossi et al., 2021; Verma et al., 2021; Swiderski et al., 2023). This helps the distal nephron keep sodium and get rid of potassium. This retention of sodium causes blood volume to rise, which raises blood pressure even more (Carey et al., 2018). In addition to direct vasoconstriction and aldosterone synthesis, AngII also enhances sympathetic nervous system activity and promotes the secretion of antidiuretic hormone (vasopressin), which increases water reabsorption from the kidneys (Shanks & Ramchandra, 2021; Maranduca et al., 2023). These mechanisms work together to keep the body's circulation stable during stress or fluid loss (Crowley & Coffman, 2012).

2.2.3. Clinical Relevance of AngII in Hypertension, Hypotension, Heart Failure, and Kidney Disease

Dysregulation of AngII production or receptor function has been associated with the pathogenesis of various cardiovascular and renal disorders (Yıldırım and Baydemir Peşint, 2021). Chronic overactivity of the RAAS, especially increased AngII levels or AT1R signaling, is closely linked to the emergence and progression of hypertension (Rossi et al., 2021; Verma et al., 2021; Swiderski et al., 2023). AngII contributes to vascular remodeling, inflammation, endothelial dysfunction, and heightened arterial stiffness, all indicative of hypertensive illness (Li et al., 2016; Yıldırım and Baydemir Peşint, 2021).

In heart failure, AngII worsens myocardial hypertrophy and fibrosis, diminishes cardiac output, and deteriorates prognosis. Similarly, in chronic kidney disease, sustained AngII activation intensifies glomerular hypertension, proteinuria, and tubular-interstitial fibrosis (Mogensen et al., 2000; Shanks & Ramchandra, 2021; Maranduca et al., 2023). Moreover, clinical trials demonstrate that RAAS inhibition using ACE inhibitors or AT1R blockers enhances survival and decelerates disease development in individuals with heart failure, diabetic nephropathy, and post-myocardial infarction (Yusuf et al., 2000; Brenner et al., 2001). Significantly, AngII is associated with hypotension under certain clinical conditions. In cases of septic shock or remarkable vasodilatory conditions, exogenous AngII treatment has been utilized to restore vascular tone and blood pressure (Khanna et al., 2017; Shanks & Ramchandra, 2021).

2.2.4. Diagnostic Significance of Detecting AngII Levels

Although AngII plays a pivotal role in various disease mechanisms, its regular clinical measurement is constrained by its low concentrations in human serum (picomolar range), fast degradation due to its reactivity and low stability, and the technical difficulties involved in its quantification (Cheng et al., 2005; Sriramula et al., 2008; Yıldırım and Baydemir Peşint, 2021). Standard methods like radioimmunoassay (RIA) and liquid chromatography-mass spectrometry (LC-MS/MS) are very specific, but they are time-consuming and laborious, and most of the time require sample processing (Basu et al., 2021; Yıldırım and Baydemir Peşint, 2021).

Is there a faster route from sample to decision? Emerging evidence points to biosensor architectures as the answer (Brosnihan & Chappell, 2017; Deng et al., 2024). A genuinely ultra-sensitive, selective and real-time Ang II sensor could flag incipient disease and let clinicians fine-tune renin–angiotensin therapy from one outpatient visit to the next (Emdin et al., 2015). In pilot trials in our laboratory, a nanoparticle-imprinted QCM chip generated a stable signal within five minutes of serum application—no solid-phase extraction, no cryogenic shipping. By migrating the assay to the bedside (or even the home), such point-of-care formats promise individualized therapy and agile monitoring of patient status (Saylan et al., 2019; Haupt et al., 2020; Akgönüllü et al., 2023).

2.3. Detection of Angiotensin-II from Human Serum

2.3.1. Complex Nature of Biological Matrices

Biological fluids such as human serum, plasma, saliva, urine, cerebrospinal fluid, and tears are complex matrices composed of a broad spectrum of biomolecules, including proteins, peptides, lipids, electrolytes, hormones, metabolites, and exogenous substances (Figure 2.1) (Cavalier et al., 2012; Spagnolie, 2015; Plebani, 2016). These fluids reflect both the physiological and pathological states of the organism, making them valuable sources for biomarker discovery and diagnostic applications. However, their biochemical complexity presents significant analytical challenges.

Blood, composed of blood cells and plasma, circulates throughout the body. It is a vital biological fluid that carries substances such as oxygen and glucose to cells as part of the circulatory system. Over half of blood is plasma, a liquid containing ~90% water. Serum, unlike plasma, lacks clotting agents like fibrinogen and is mainly used for blood typing and diagnostic testing (Luque-Garcia et al., 2006), while plasma is often used in blood-clotting disorders (Bowen et al., 2014; see Figure 2.1). In serum, highly abundant proteins like albumin and immunoglobulins can mask low-abundance molecules such as angiotensin II (AngII), leading to lower signal during detection (Geyer et al., 2017). It requires sample preparation process including pre-treatment, enrichment, or fractionation steps to enhance its analytical sensitivity (Pisitkun et al., 2006).

Routine biomarker studies must choose between serum and plasma as analytical matrices. In this work, serum was preferred because plasma relies on anticoagulants—EDTA, citrate, or heparin—that chelate Zn^{2+} and Ca^{2+}, weakening divalent-ion bridges crucial for surface-based assays. In preliminary experiments, EDTA-treated plasma lowered the quartz-crystal microbalance (QCM) signal for Ang II by approximately 12 % (Bowen et al., 2014). Serum, obtained after coagulation, is free of such additives and therefore introduces minimal ionic interference. The clotting cascade simultaneously consumes thrombin, plasmin and related proteases, which slows peptide degradation and prolongs the analytical stability of labile targets (Böttger et al., 2017). Consistent with these observations, Luque-García et al. (2006) reported that peptide fingerprints remain temporally more stable in serum than in plasma. Consequently,

serum constitutes a more predictable matrix for quantifying low-abundance, instability-prone molecules such as Ang II.

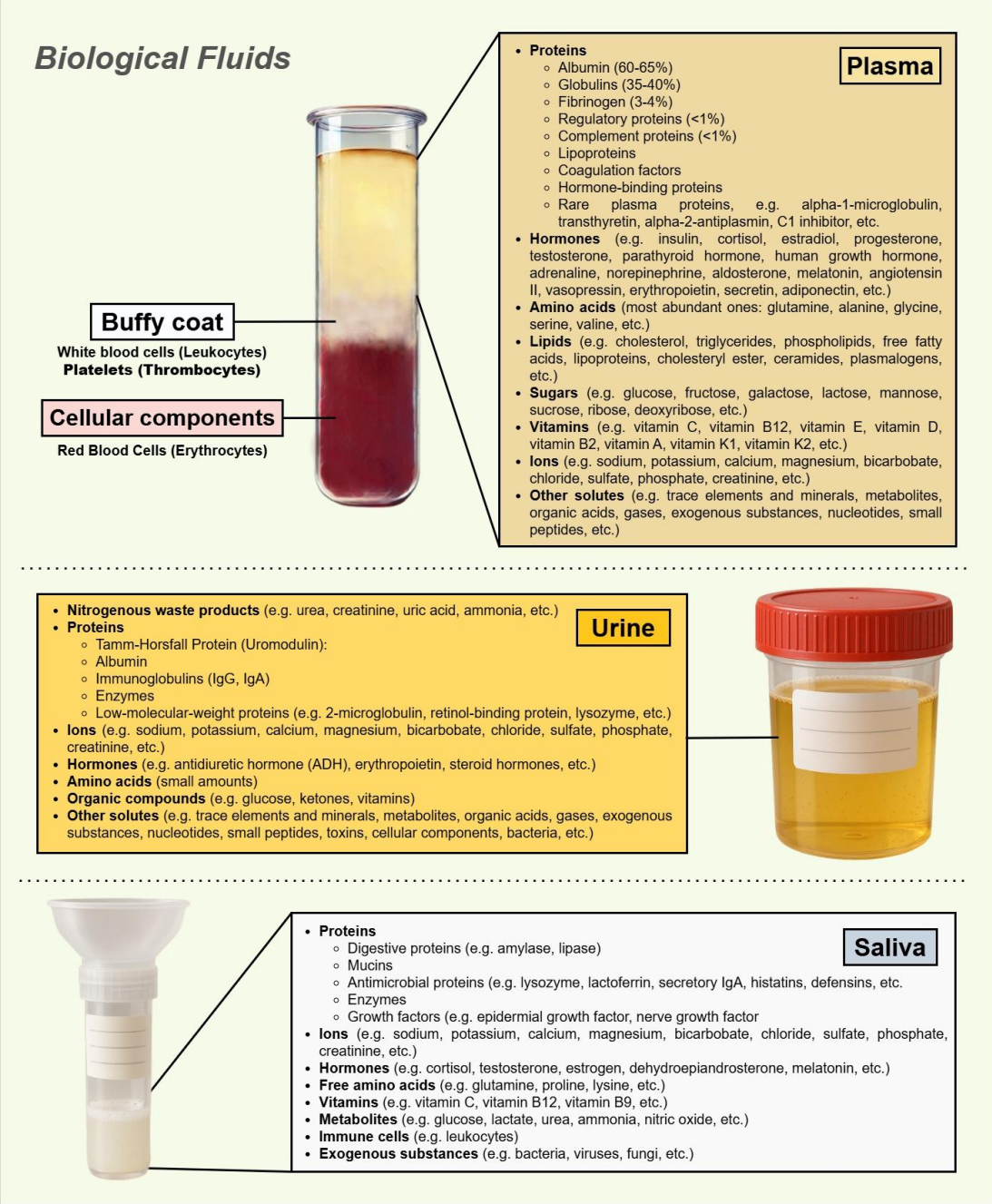

Figure 2.1. Overview of the molecular composition of plasma, urine, and saliva, illustrating the biochemical complexity of these biological fluids and their relevance for biomarker discovery and diagnostics.

2.3.2. Challenges: Low Abundance, Interference, and Stability

Ang II circulates at the edge of instrumental noise—typically 5–40 pg/mL—so analytical platforms must operate in the low-picomolar regime to capture physiologically relevant fluctuations. Conventional immuno-assays such as RIA or ELISA can reach this region only after multi-step enrichment or signal amplification, which adds time and dilution risk (Basu et al., 2021). Beyond scarcity, the serum matrix itself challenges specificity: abundant albumin, electrolytes, and near-isobaric peptides (e.g., vasopressin, angiotensin I) compete for binding sites and can suppress or distort the analytical read-out (Liu et al., 2019). A further complication is biochemical fragility—Ang II undergoes rapid proteolysis by dipeptidyl- and amino-peptidases, with half-lives measured in minutes (Ferrario & Varagic, 2010). In our pre-study stability check, >40 % of the native peptide was lost within 30 min at 25 °C when protease inhibitors were omitted.

Direct, purification-free measurement of Ang II in serum would therefore accelerate decision-making in both routine clinics and high-acuity settings (Catt et al., 1967; Kappelgaard et al., 1976). Eliminating solid-phase extraction cuts sample handling time and reduces the probability of analyte loss—an especially important consideration for short-lived peptides. Real-time tracking of Ang II could, for example, map the immediate biochemical response to antihypertensive therapy or warn of catecholamine surges during septic shock (Crapnell et al., 2020; Choi et al., 2021; Nazir & Iqbal, 2023).

A viable technical route combines MIPs with piezoelectric transducers such as quartz-crystal microbalance (QCM) chips. Tailored imprinting chemistry generates cavities complementary in size, shape and electrostatics to Ang II, thus suppressing cross-reactivity even in the presence of vasopressin. QCM, in turn, converts picogram-scale mass uptake into a frequency shift that can be monitored in seconds and without fluorescent or enzymatic labels. In our laboratory prototype, a nano-MIP layer (thickness ≈ 75 nm) deposited on a 10 MHz quartz wafer delivered a limit of detection of 0.7 pg/mL in undiluted serum while maintaining signal stability for at least 20 measurement cycles. Properly optimised, such MIP/QCM hybrids can bypass extensive preprocessing, furnishing rapid, sensitive and selective Ang II quantification in complex biological matrices.

2.4. Molecularly Imprinted Polymers (MIPs)

Molecular imprinting traces its conceptual roots to the pioneering adsorption studies of Polyakov in the early 1930s, although the lock-and-key analogy with antibody–antigen recognition was articulated much later (Sajini & Mathew, 2021). In essence, functional monomers assemble around a template molecule through covalent or non-covalent interactions; subsequent polymerization with an appropriate cross-linker "freezes" this arrangement. Once the template is extracted, the resulting material—called a MIP—retains three-dimensional cavities that are complementary to the target in size, shape and distribution of chemical functionalities (Chen et al., 2016; Saylan et al., 2019). These tailor-made binding pockets confer a level of molecular selectivity that rivals many biological receptors.

Because the imprinting step is embedded within a robust polymer matrix, MIPs withstand extremes of pH, temperature and organic solvent content that would rapidly inactivate proteins or antibodies. This resilience, coupled with low production cost, explains their growing use in biosensing, controlled drug release, preparative chromatography and even scaffold design for tissue engineering (Li et al., 2016; Algieri et al., 2014; Motamedi et al., 2022).

2.4.1. Definition and Mechanism

From a mechanistic viewpoint, a MIP is a synthetic polymer network endowed with template-shaped recognition sites. During polymerization, functional monomers orient themselves around the template, while cross-linkers establish a rigid three-dimensional framework. Removal of the template—by solvent extraction, Soxhlet elution or enzymatic cleavage—creates vacant sites that exhibit high affinity and specificity for the original molecule (Wulff, 1995; Haupt & Mosbach, 2000). In practical terms, the fidelity of these binding sites depends on: the strength and directionality of pre-polymerization interactions, the cross-link density that dictates cavity rigidity, and the porogenic environment, which governs accessibility of analyte molecules. Fine-tuning these parameters allows researchers to engineer MIPs capable of discriminating between molecules that differ by a single functional group—an ability central to ultra-selective biosensing applications such as the Ang II assay developed in the present study.

MIPs are synthesized via three basic steps:

1. Preparation of pre-complex which consists of the target molecule (template) and a convenient functional monomer;
2. Polymerization of crosslinkers and main monomers around the pre-complex;
3. Removal of template molecule from the polymeric system to generate specific adsorption cavities complementary to the template molecule in size, shape and placement of functional groups (Akgönüllü et al., 2023).

The mechanism of molecular imprinting typically involves non-covalent, covalent, or semi-covalent interactions between the template and monomers:

- Non-covalent imprinting relies on hydrogen bonds, ionic interactions, and van der Waals forces formed between the template and monomer in a pre-polymerization complex. It is the most commonly utilized approach due to its simplicity and versatility (Haupt & Mosbach, 2000; Sellergren, 2001).
- Covalent imprinting involves forming covalent bonds between the template and functional monomer before polymerization. These bonds are later broken to remove the template (Wulff, 1995, Hansen, 2007). Covalent bonds provide homogenous binding sites but limit template selection and slow binding/dissociation, hindering equilibrium. While this approach allows for more homogeneous binding sites, it is limited by fewer applicable monomers and more challenging template removal (Andersson et al., 1995).
- Semi-covalent imprinting combines covalent interactions during synthesis and non-covalent recognition during rebinding.

2.4.2. Polymerization Methods Used in the Synthesis of MIPs

The polymerization strategy selected for a MIP exerts a decisive influence on particle morphology, binding-site accessibility, and ultimately on the analytical utility of the material. Over the past three decades, several routes have been refined to balance ease of synthesis with performance. The most frequently exploited approaches are bulk, suspension, precipitation, emulsion and surface-imprinting protocols; each carries a characteristic mix of benefits and trade-offs.

2.4.2.1. Bulk polymerization

Bulk polymerization remains the workhorse technique owing to its minimal equipment requirements. Functional monomers, cross-linker and template are dissolved in a porogenic solvent; an initiator then triggers network formation, yielding a monolithic plug (Balke & Hamielec, 1973; Demir et al., 2007). After curing, the monolith is crushed and sieved to obtain particles in the 25- to 100-μm range. Although straightforward, the post-grinding step introduces two persistent drawbacks: (i) irregular particle geometry, and (ii) heterogeneous distribution of binding sites—factors that can erode both kinetics and capacity in chromatographic applications (Nikolaidis et al., 2011).

2.4.2.2. Suspension polymerization

In suspension polymerization the pre-polymer mixture is dispersed as micrometre-scale droplets within an immiscible continuous phase—typically water stabilised by a surfactant. Polymerization proceeds inside each droplet, producing nearly spherical beads with narrow size distribution (Chaudhary & Sharma, 2019). The resulting geometric uniformity suits high-performance liquid chromatography (HPLC) packings and batch adsorption studies. Reported limitations include lower overall yield and partial leaching of the template into the aqueous medium, which can reduce imprinting efficiency (Brooks, 2010; Chaudhary & Sharma, 2019).

2.4.2.3. Precipitation polymerization

Precipitation polymerization operates in a large excess of porogen. As chains grow, they reach a critical length at which solubility is lost, and the nuclei precipitate, continuing to polymerise as discrete spheres (Zhang et al., 2022). Because particles form in situ, no grinding is required; diameters often fall below 5 μm with relatively tight dispersity. These features make the method attractive for solid-phase extraction cartridges and sensor coatings where rapid mass transfer is essential (Li et al., 2013; Zhang et al., 2022).

2.4.2.4. Emulsion polymerization

Emulsion polymerization is carried out in a system containing water, monomers, initiators, and surfactants (Thickett and Gilbert, 2007; Arısoy and Baydemir Peşint, 2025). The

polymerization takes place in micelles formed by the surfactant, resulting in nanoparticles (Figure 2.2). This technique is beneficial for the preparation of MIPs with high surface areas and small particle sizes, ideal for certain sensor or catalysis applications (Thickett and Gilbert, 2007; Lovell and Schork, 2020).

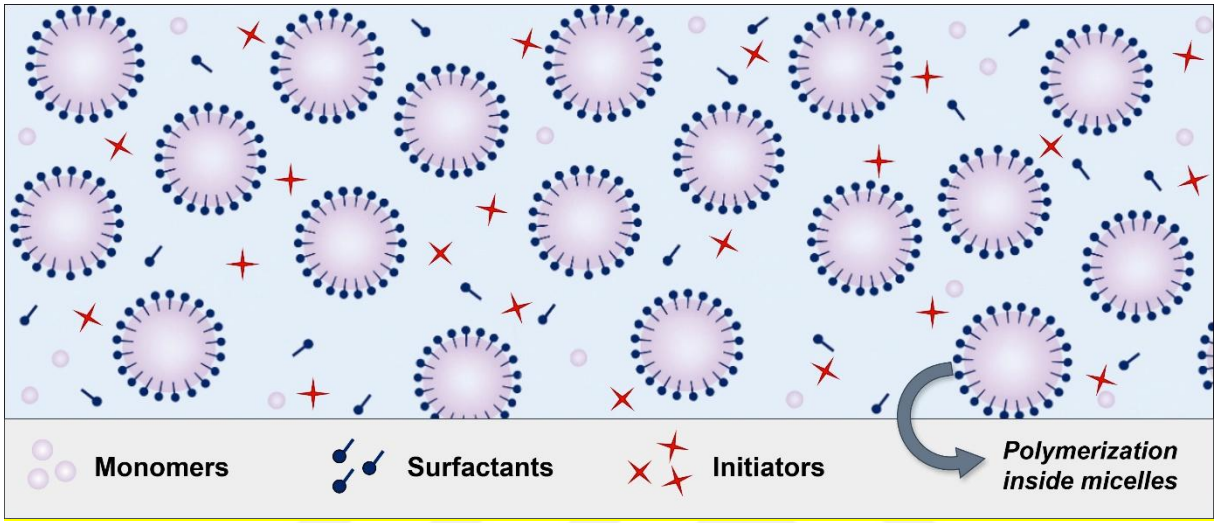

Figure 2.2. Schematic representation of miniemulsion polymerization.

2.4.3. Molecular imprinting types

Beyond the chemical processes used to form MIPs, the manner in which the template is introduced and the recognition sites are created—referred to as imprinting techniques—also plays a key role in determining the performance of the final material. Several imprinting strategies have been developed to address challenges related to template removal, site accessibility, and the imprinting of large or complex molecules. Major imprinting techniques include: conventional imprinting, surface imprinting, epitope imprinting, stimuli-responsive imprinting, dummy template imprinting, ion imprinting, multi-template imprinting, multi-functional monomer imprinting, solid-phase imprinting, and hierarchical imprinting (Table 2.1).

Table 2.1. Imprinting strategies used in MIP fabrication, highlighting each method's operational principle and advantage.

Strategy	Operational Principle	Typical Advantage	Reference
Conventional imprinting	Template is homogeneously dispersed throughout the bulk polymer.	Simple set-up; widely used benchmark.	Zenger & Baydemir Peşint, 2022
Stimuli-responsive imprinting	Binding affinity shifts under an external trigger (pH, temperature, light, magnetic field).	On-demand capture or release; smart drug carriers.	Puoci et al., 2008
Dummy-template imprinting	Safe structural analogue replaces a toxic/unstable/expensive target during polymerization.	Removes hazardous analytes from the workflow; lowers cost.	Abdella & Ulber, 2025; Bedair et al., 2025
Ion imprinting	Target metal ions coordinate with monomers; removal leaves ion-sized chelation sites.	Trace-metal selectivity for environmental/food analytics.	Rao et al., 2006
Multi-template imprinting	Two or more templates introduced simultaneously.	Multiplex recognition—useful in environmental monitoring.	Murdaya et al., 2022; Wang et al., 2023
Multi-functional-monomer imprinting	Complementary monomers mimic heterogeneous binding domains.	Higher affinity via synergistic interactions.	Niu et al., 2024
Surface imprinting	Recognition sites generated only at, or very near, the particle surface (silica, magnetic cores, polymer beads).	Faster mass transfer and easier template removal—crucial for large biomolecules.	Ding & Heiden, 2014; Dong et al., 2021
Epitope imprinting	A stable peptide fragment (epitope) of a large biomolecule serves as template.	High precision for proteins without handling the full macromolecule.	Dietl et al., 2021; Khumsap et al., 2021
Solid-phase (immobilized) imprinting	Template covalently attached to a solid support; polymer grows around it and is eluted as nanoMIPs.	Near-perfect site fidelity, rapid template removal.	Canfarotta et al., 2016; Kalecki et al., 2020
Hierarchical imprinting	Mixed-scale templates/porogens create tiered pore networks (macro↔nano).	Enhanced mass transfer; multi-tiered binding sites.	Titirici & Sellergren, 2004

Both the polymerization method and the imprinting approach must be carefully chosen and optimized to create MIPs with desired properties for specific applications.

2.4.4. Key Reagents for MIP Synthesis

The synthesis of MIPs requires a set of key components, each with a specific role (Yıldırım and Baydemir Peşint, 2021). The selection of convenient ingredients is one of the most crucial steps in the molecular imprinting process. The template molecule (or target/analyte), functional monomers, crosslinkers, initiators and solvent (porogen) are required for the preparation of MIPs, and the amount of each determines the structure of the polymer, such as pore size, stability, mechanical strength, etc. (Wullf, 1995). The template molecule serves as the model around which the polymer forms specific binding sites. Functional monomers are selected based on their ability to form reversible interactions (secondary interactions such as hydrogen bonds, ionic interactions, and hydrophobic forces) with the template molecule (Nergiz et al., 2024), while crosslinkers provide structural stability to fix these sites in place. A solvent is used as the interaction medium to dissolve all these components and to create a interconnected porous network in the polymer. Initiators, on the other hand, trigger the polymerization reaction through heat, UV light, or chemical reactions (Saylan et al., 2019; Akgönüllü et al., 2023). These components work together to create a polymer capable of selectively recognizing the original target after template removal (Zenger and Baydemir Peşint, 2022). Each reagent is discussed in detail below.

2.4.4.1. Template

The template molecule is critical to the molecular imprinting process because it determines the chemical and spatial arrangement of functional monomers during the synthesis of the pre-polymerization complex (Zenger and Baydemir Peşint, 2022). For optimal performance, template molecules should be chemically and thermally stable under polymerization conditions, highly soluble in the chosen porogenic solvent, and readily available at a reasonable cost, especially when large-scale synthesis is considered (Chen et al., 2011; Okay and Lozinsky, 2014). While molecular imprinting has been successfully applied to a broad spectrum of targets, from small drug-like compounds to complex biomacromolecules, not all analytes are equally suitable. Small, rigid molecules are often favored due to their well-defined structures, which facilitate the formation of precise and reproducible binding sites within the polymer matrix

(Nergiz et al., 2024). Larger templates, including peptides (e.g. AngII), proteins, and whole cells, can also be employed (Figure 2.3), yet they introduce several technical limitations (Dainiak et al., 2007; Okay and Lozinsky, 2014; Baydemir and Denizli, 2015; Ertürk and Mattiasson, 2017). These macromolecules often exhibit conformational flexibility and structural heterogeneity, which can hinder the generation of high-fidelity binding cavities. Moreover, steric hindrance and limited diffusion into the polymer network may compromise template removal and rebinding efficiency. Therefore, the reaction conditions must be modified according to the nature of the template (Okay and Lozinsky, 2014; Baydemir and Denizli, 2015).

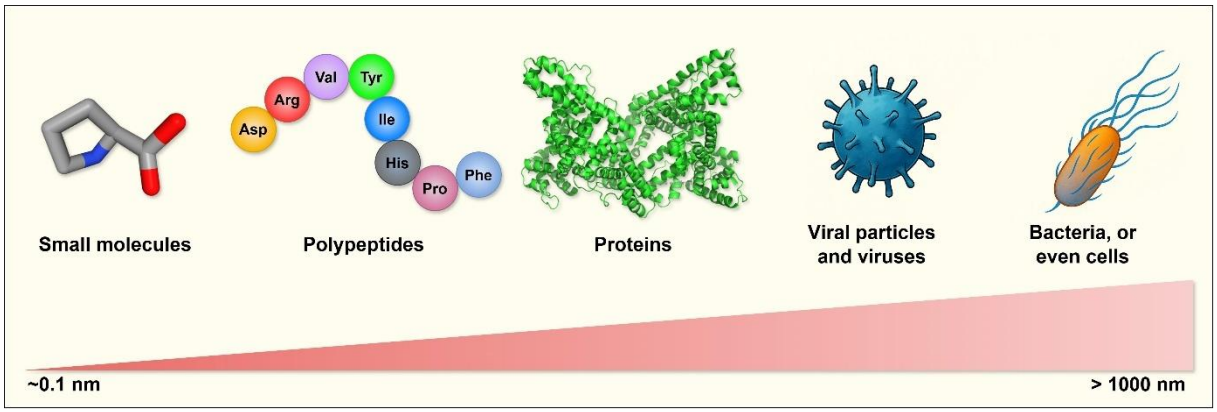

Figure 2.3. Representative illustration for the size range of template molecules used in molecular imprinting technology.

2.4.4.2. Functional Monomers

The role of the functional monomer is to provide functional groups to form a prepolymerization complex with the target molecule (template). It is important to choose a suitable functional monomer that can form specific donor-receptor or antibody-antigen complexes before the functional monomer polymerization and interact strongly with the template molecule (Yıldırım and Baydemir Peşint, 2021). Basically, functional monomers interact with the functional groups of the target molecule, creating a pre-complex structure. Commonly used functional monomers are acrylic acid, methacrylic acid, 2-vinylpyridine, 4-vinylpyridine, 1-vinylimidazole, and acrylamide, etc. (Figure 2.4) (Yan & Row, 2006; Golker et al., 2013). When forming the precomplex structure, it is important to carefully determine the ratio of template and functional monomer(s). If the amount of functional monomer is lower than required, the maximum

adsorption capacity may not be achieved because a sufficient number of specific recognition sites cannot be formed in the polymer. On the other hand, an excess amount of monomer may cause an increase in non-specific binding, which may negatively affect the accuracy of the data obtained and cause the results to not reflect the truth (Yan & Row, 2006; Golker et al., 2013; Niu et al., 2024).

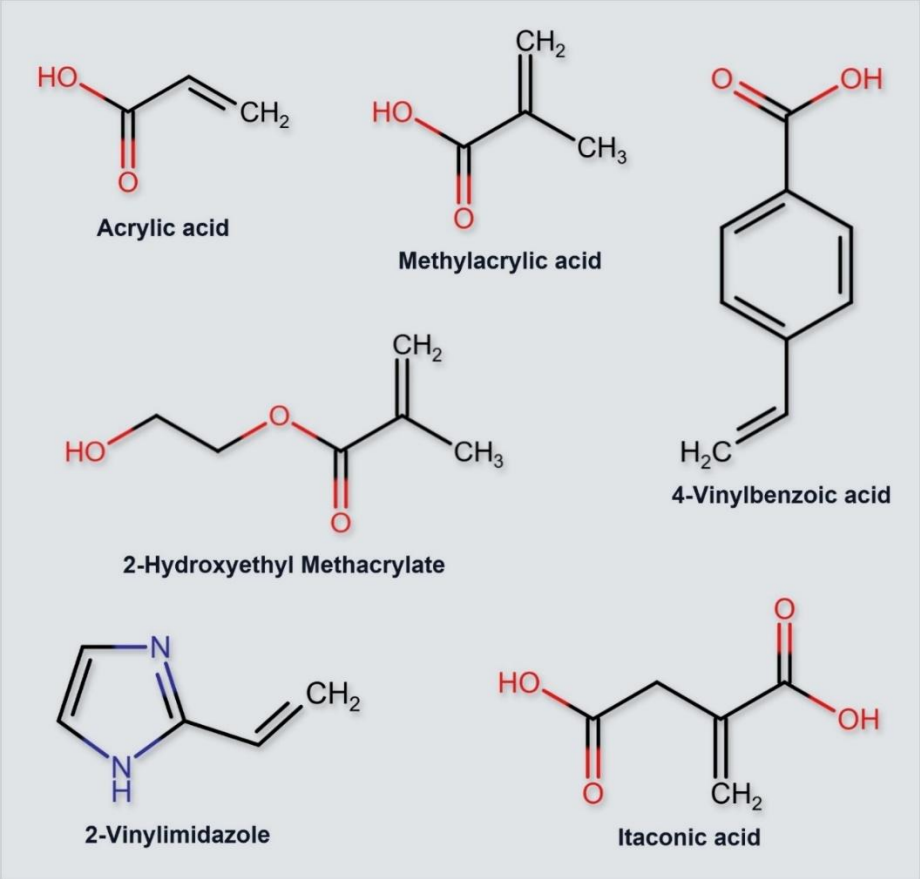

Figure 2.4. Commonly used functional monomers in molecular imprinting technique.

2.4.4.3. Crosslinkers

A crosslinker is used to stabilize the functional monomers around the template molecules, thus creating a highly crosslinked solid polymer even after the target molecules have been removed. These agents control the morphological structures of MIPs, playing an important role in creating stable binding sites. The type and amount of crosslinker have great effects on the selectivity and binding capacity of MIPs. Generally, too low a crosslinker amount will result in a product

with unstable mechanical properties due to the low degree of crosslinking. Too high a crosslinker amount will reduce the number of recognition sites per unit mass of MIPs. Therefore, the ratio of cross-linking agent to functional monomers must be optimized. In this way, polymers with the desired structure can be synthesized (Alexander et al., 2006; Yan & Row, 2006; Golker et al., 2013). Most commonly used crosslinkers in the synthesis of MIPs are given in Figure 2.5.

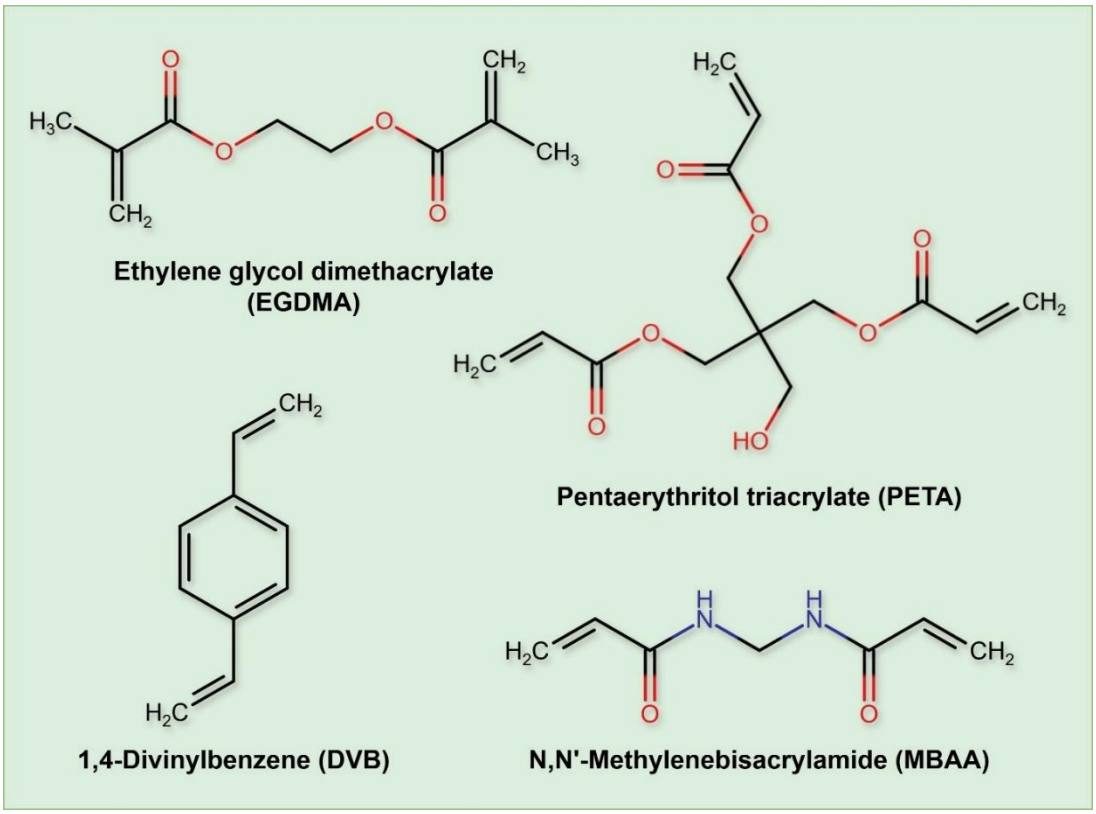

Figure 2.5. Commonly used crosslinkers in molecular imprinting technique.

2.4.4.4. Initiators

Polymerization reactions require a starting force, called initiator or in some cases initiator/catalyst system which induces free radical formation, to initiate free radical polymerization. Some of the well-known and widely used initiators are azobisisobutyronitrile, ammonium persulfate, benzoyl peroxide, dicyclohexyl peroxydicarbonate, lauryl peroxidase, etc., which can be used either alone or mostly together with a catalyst. Polymerization process starts in seconds, after the initiator is added into a polymeric solution (Alexander et al., 2006; Moad, 2019; Pasquardini and Bossi, 2021).

Initiators can be activated by different external stimuli based on their chemical structure. The most common methods include thermal energy, UV light, or redox reactions, which lead to the formation of highly reactive radicals that can interact with monomers (Fuchs et al., 2012; Bonardi et al., 2018; Moad, 2019; Fu et al., 2022). Azobisisobutyronitrile (commonly known as AIBN), undergoes homolytic cleavage when subjected to heat or UV radiation, resulting in the generation of nitrogen gas and two isobutyronitrile radicals which initiate the polymerization reaction. Ammonium persulfate (i.e., APS), a water-soluble initiator that can be activated either thermally or chemically in redox systems. Additionally, benzoyl peroxide (i.e., BPO) is brokendown thermally to create phenyl and benzoate radicals for the initiation of polymerization. Dicyclohexyl peroxydicarbonate is also remarkable since it can be employed in low-temperature polymerizations. In a polymerization process, basically, created radicals target the π-bonds of vinyl monomers, thus initiating the growth of polymer chain. The choice of initiator and its activation method plays a crucial role in determining the efficiency and kinetics of polymer formation (Moad, 2019; Pasquardini and Bossi, 2021).

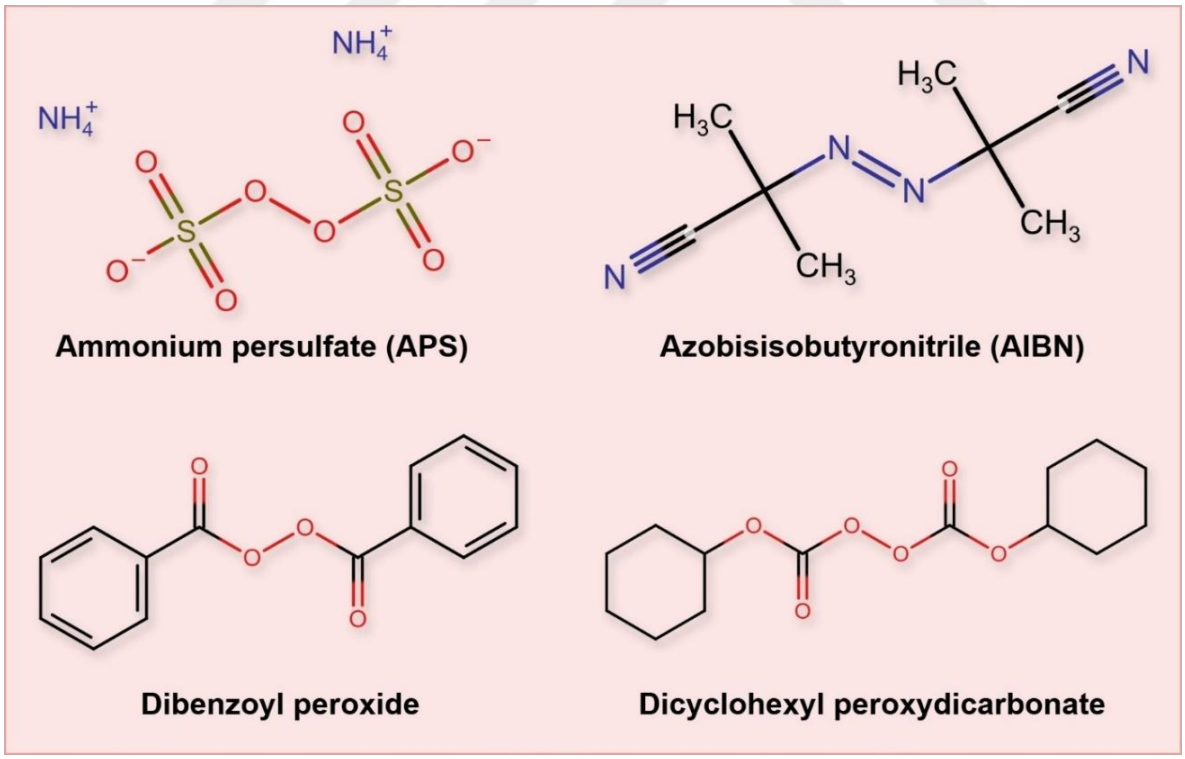

Figure 2.6. Commonly used initiators in molecular imprinting technique.

2.4.4.5. Solvent

Solvent of the polymeric solution is employed as a porogen during the synthesis of MIPs. It is used as the interaction medium to dissolve all these components and to create a interconnected porous network in the polymer. Use of solvent is crucial in the polymerization process (Alexander et al., 2006; Yan and Row, 2006; Vasopollo et al., 2011). Ultrapure water, ethanol, methanol, acetonitrile, chloroform, and toluene are commonly-used solvents in the synthesis of MIPs. Some of them helps the selective identification of specific molecules, while some of them are important in terms of biocompatibility, or other purposes (Gladis & Rao, 2004; Saloni et al., 2013; Ma et al., 2017; Elhachem et al., 2023).

Polarity of the solvent is an important parameter, since the polarity of porogenic solvents can affect the interaction between the target molecule and the functional monomer and therefore the adsorption properties of MIPs, especially in non-covalent interaction systems (Gladis & Rao, 2004; Saloni et al., 2013). Low polarity solvents promote the creation of pre-complexes, while high polarity solvents hinder the interactions required for the pre-complex structure (Włoch and Datta, 2019; Hasanah et al., 2021).

2.5. Advantages of MIPs

MIPs serve as a synthetic substitute for enzymes and antibodies, particularly in cases where natural recognition elements are susceptible to degradation. Their resistance to heat, pH variations, and organic solvents renders them appropriate for application in extreme conditions without the need for refrigeration, which is beneficial for portable and field-ready diagnostics (Saylan et al., 2019).

Selective recognition is the main advantage of MIPs. By choosing appropriate functional monomers and polymerisation conditions, the imprinting process fixes binding sites that can identify one analyte even in complex samples that contain similar compounds (Turiel & Martín-Esteban, 2010). Because the material is fully synthetic, it resists heat, organic solvents, and repeated cleaning cycles with only minimal loss of performance, which supports economical and sustainable long-term use (Chen et al., 2022). During synthesis, chemical anchor groups can be introduced so that the MIP layer attaches directly to a gold-coated quartz crystal or other

sensor surface, allowing the construction of compact, label-free devices (Piletsky & Turner, 2002).

2.6. Nanoparticles

Nanomaterials attract wide interest because they offer high chemical and physical stability, large surface-to-volume ratios, and surfaces that can be modified with ease (Webster et al., 2005). Nanoparticles—the best-known group—measure roughly 1 to 100 nm. At this scale, a large fraction of the atoms sit at the surface, which improves reactivity and shortens binding times. Key traits such as size, shape, crystal structure, and surface charge can all be tuned, giving each particle set its own performance profile (Nergiz et al., 2024).

These adjustable properties make nanoparticles useful across engineering, medicine, and industrial processing. They already appear in products that range from drug carriers and biosensors to textiles, food coatings, and electronic parts (Mondal et al., 2020; Nergiz et al., 2024). Structurally, a typical particle has three zones: a core that provides the main function, a shell that protects the core, and an outer layer whose chemistry can be changed to match a target surface—such as the gold film on a QCM chip (Khan et al., 2019).

2.6.1. Strategies for Nanoparticle Fabrication

Wide variety of processes, under physical, chemical, and biological methods, are used in the synthesis of nanoparticles. These processes can be broadly classified as top-down and bottom-up techniques (Dhand et al., 2015; Khan et al., 2019).

Top-down methods begin with bulk material and use physical forces—milling, lithography, or laser ablation—to break it into nanoscale fragments. These techniques are straightforward and suitable for large-scale production, but they give limited control over particle size and shape. Bottom-up methods take the opposite path: atoms or molecules are assembled into particles through chemical reactions or self-organisation. Chemical reduction, electrochemical growth, sol–gel processing, and biosynthesis are common examples. Because bottom-up routes allow reactant concentrations, temperature, and growth time to be tuned with precision, they deliver particles with narrow size distributions and built-in surface functional groups—attributes that

are especially valuable when the particles will serve as recognition elements in complex biological media.

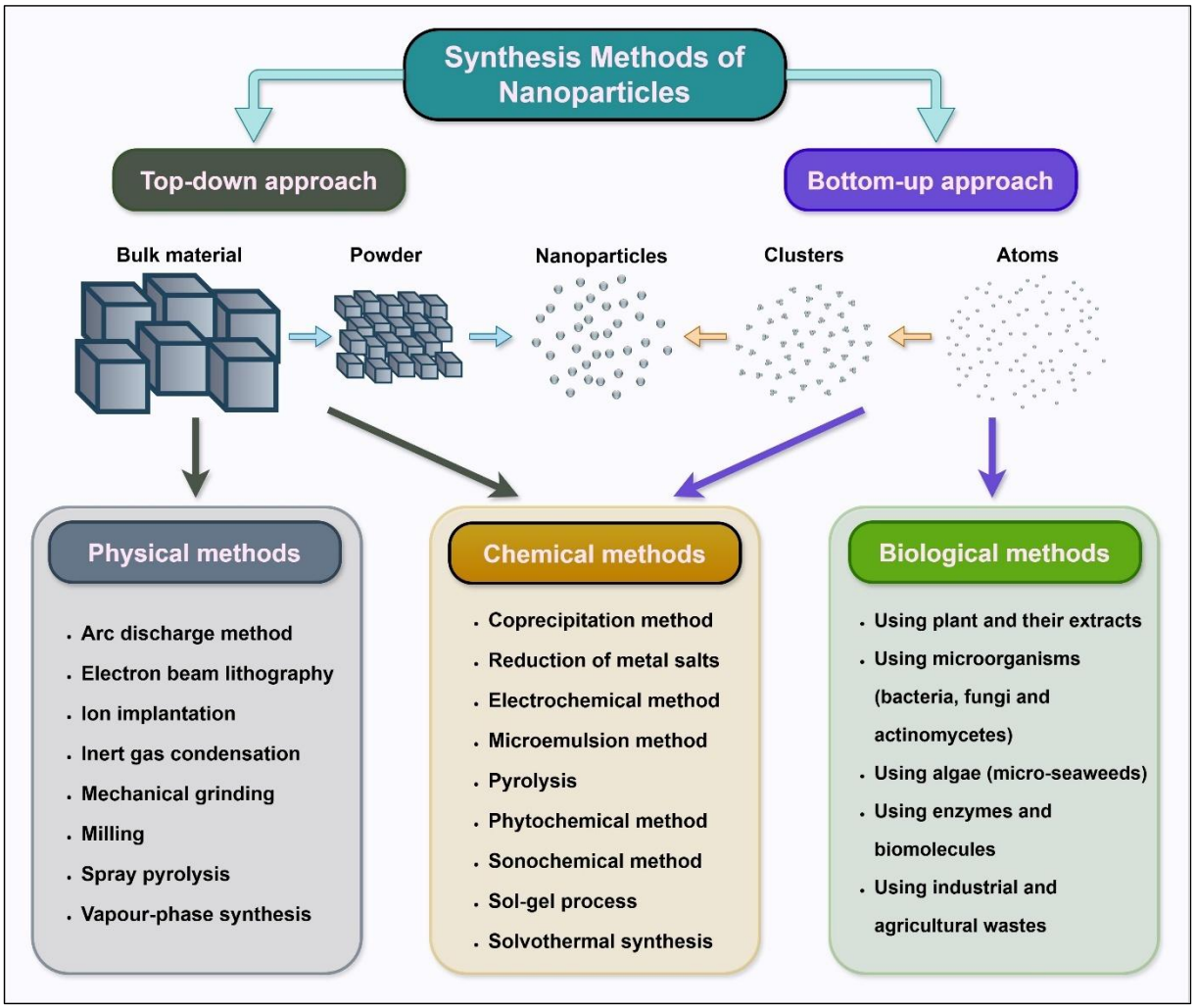

Figure 2.7. Classification of nanoparticle synthesis methods. The synthesis methods are broadly divided into top-down and bottom-up approaches. These approaches are further categorized into physical, chemical, and biological methods based on the process and source materials used.

2.6.2. Advantages of Nanoparticle-Based MIPs

Integrating molecular imprinting tecnique into nanoscale materials has opened new possibilities for designing recognition elements with enhanced selectivity and sensitivity. These so-called nanoMIPs represent a refined generation of synthetic receptors, developed to overcome many

of the limitations seen in conventional MIPs. What makes them especially valuable is their compatibility with biosensing technologies. When coupled with sensitive transducers like QCM, they exhibit rapid response times, favorable surface interactions, and tunable physicochemical features—qualities that are essential for high-performance sensing.

2.6.2.1. High Surface-Area-to-Volume Ratio

A central advantage of nano-MIPs is the large surface-area-to-volume ratio that arises when polymer particles are reduced to tens of nanometres. In bulk MIPs many recognition sites remain buried within the matrix and are reached only slowly, if at all. By contrast, nano-MIPs present a much larger fraction of their cavities on or close to the particle surface, so the number of sites that are effectively available during an assay is greatly increased (Poma et al., 2013). Spherical particles in the 20–100 nm range have diffusion paths on the order of a few nanometres; analyte molecules therefore reach the binding sites quickly, which shortens the time required to achieve equilibrium. The high density of surface sites also improves sensitivity when the target is present at low concentration and competes with structurally similar species in matrices such as serum or urine (Chen et al., 2022).

Their small size further allows nano-MIPs to be combined with other functional nanomaterials—magnetic cores, quantum dots, gold nanorods, and the like—without steric hindrance. Such hybrids can add magnetic separation, fluorescence read-out, or plasmonic amplification in a single construct, enabling multimodal sensing schemes that push detection limits even lower (Kour et al., 2020).

2.6.2.2. Fast Binding Kinetics and Higher Binding Site Accessibility

The same structural features that increase surface area also speed up binding and release. In bulk polymers the diffusion of an analyte into interior cavities is slow, so long incubation or regeneration steps are usually required. Nano-MIPs, however, bring virtually every cavity into immediate contact with the surrounding medium, allowing association and dissociation to occur within minutes (Canfarotta et al., 2016). When surface- or solid-phase imprinting methods are used during synthesis, the orientation and uniformity of these cavities can be controlled even further, producing binding sites whose affinity and selectivity approach those of monoclonal

antibodies. Dissociation constants in the low-nanomolar to picomolar range have been reported for a variety of targets (Poma et al., 2015).

Fast kinetics are especially valuable in real-time transduction formats such as QCM, where the sensor's frequency shift is tracked continuously. Rapid association produces a clear signal in seconds, while rapid dissociation allows multiple measurement cycles on the same chip without lengthy regeneration. The result is a sensor that is not only sensitive and selective but also reusable and operationally efficient.

2.7. Biosensors

2.7.1. Definition and General Working Principle of Biosensors

Biosensors are advanced analytical devices which employ biorecognition elements, such as enzymes, antibodies, nucleic acids, cells, or any artificial mimic structure, to detect any specific analyte and convert changes that occurs upon interaction into readable results (Naresh & Lee, 2021; Morales & Halpern, 2018). Biosensors integrate a biological recognition element with a physicochemical transducer, enabling the identification of target analytes and the conversion of biorecognition events into measurable signals (Liu et al., 2014; Karunakaran et al., 2015; Mehrotra, 2016; Polat et al., 2022).

The fundamental operation of a biosensor is based on three essential components:

- A biorecognition element, which selectively binds to the analyte, e.g., enzymes, antibodies, nucleic acids, aptamers, cells, or synthetic receptors like MIPs (Morales & Halpern, 2018).
- A transducer, which converts the biorecognition process (binding or reaction) into a measurable signal, e.g., electrical, optical, etc. (Polat et al., 2022).
- A signal processing system, which amplifies, interprets, and displays the output signal in a user-readable format (Figure 2.8).

When the target analyte interacts with the biorecognition element, changes such as mass accumulation, charge redistribution, or energy absorption occur at the sensor interface. These changes are detected by the transducer and interpreted in real-time or near-real-time, offering

rapid, sensitive, and often label-free detection (Turner, 2013; Kulkarni et al., 2023). This process enables sensitive and selective analysis of the target analyte, providing information regarding its quantity or presence. Biosensors are widely used in various fields, including drug discovery, disease diagnosis, detection of pathogens and toxins, and monitoring of environmental pollutants (Karunakaran et al., 2015; Yuan and Liu, 2021).

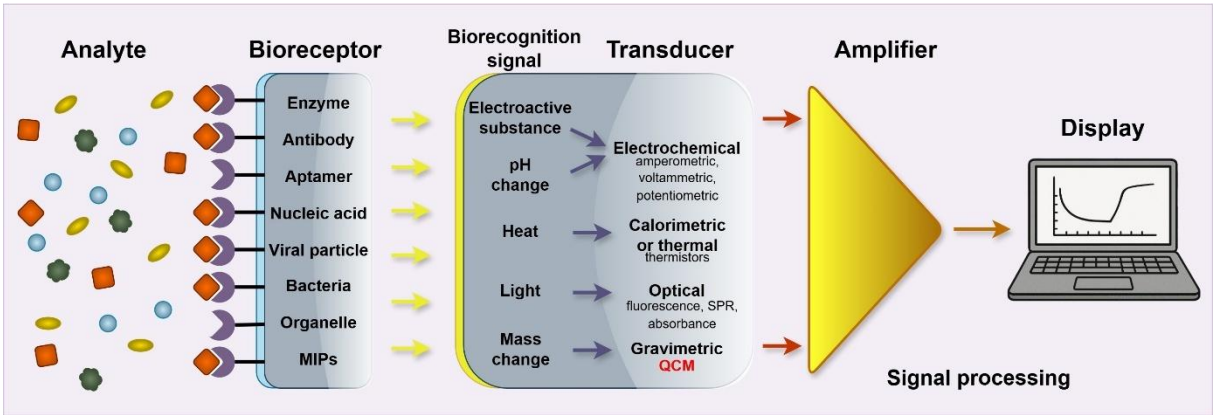

Figure 2.8. Working principle of a biosensor.

Analytes (e.g., ions, proteins, pathogens) interact with specific bioreceptors such as enzymes, antibodies, aptamers, or MIPs, triggering a biorecognition event. This interaction generates a physical or chemical signal (e.g., electroactive substance, pH change, heat, light, or mass change) which is converted into a measurable output by a corresponding transducer (electrochemical, calorimetric, optical, or gravimetric). The signal is then amplified, processed, and displayed as a quantitative output (Kulkarni et al., 2023).

There are a number of remarkable advantages of biosensors over conventional analytical methods and devices, including culture-based assays, ELISA, PCR, and chromatography, which usually come with high costs, take a lot of time to set up, need experts to use, demand a large quantity of samples and reagents, and generally have large instruments (Singh et al., 2021; Ding & Heiden, 2014). Biosensors, on the other hand, is a more accessible alternative with properties like cost-effectiveness, portability, easy-to-use and user-friendly interfaces, and the capability for real-time detection of target analytes. In addition, analysis can be carried out in biosensor with only small amount of sample (Mehrvar & Abdi, 2004; Van Dorst et al., 2010; Saylan et al., 2021; Malik et al., 2023).

2.7.2. Types of Biosensors

Biosensors are often grouped by the physical principle their transducer uses to turn a biochemical event into a readable signal. Two families dominate current practice: electrochemical and optical platforms:

Electrochemical Biosensors

Electrochemical biosensors track changes in electrical variables—current for amperometric devices, potential for potentiometric ones, or impedance for impedimetric formats. When an analyte binds to the recognition layer, it alters charge transfer or ion distribution at the electrode surface, and the shift is recorded in real time. Because the electronics are simple and can be miniaturised, electrochemical sensors remain the method of choice for glucose strips, neurotransmitter assays, and many field-portable environmental tests (Dincer et al., 2019).

Optical Biosensors

Optical biosensors convert binding events into variations in light. Depending on the design, the interaction may change absorbance, trigger or quench fluorescence, emit chemiluminescence, or shift the local refractive index. Detection can be label-based—fluorophores or enzymes are attached to the analyte—or label-free, where the optical response is monitored directly. Surface plasmon resonance (SPR) is the best-known label-free approach: oscillations of surface electrons on a thin gold film respond to nanometre-scale mass changes, giving a continuous read-out of binding kinetics. Newer formats such as localised SPR and SPR imaging improve spatial resolution and support multiplex analysis so that several targets can be evaluated at once (Shrikrishna et al., 2024; Singh et al., 2023).

Beyond SPR, numerous advanced optical configurations have been established. Techniques such as evanescent wave fluorescence, interferometry-based platforms, reflectometric interference spectroscopy, and surface-enhanced Raman scattering demonstrate remarkable sensitivity and selectivity. These sophisticated methods find increasing utilization in detecting a broad spectrum of targets—ranging from viruses and toxins to biomarkers and even whole cells. Optical biosensors find broad application in clinical diagnostics, food safety, and

biodefense, with advances in nanophotonics continuing to drive improvements in speed, sensitivity, and portability (Singh et al., 2023; Uniyal et al., 2023).

Piezoelectric (Mass-Based) Biosensors

Piezoelectric biosensors, such as QCM sensors, rely on the detection of mass changes at the sensor surface. When target molecules bind to the recognition layer, they induce a measurable shift in the oscillation frequency of a quartz crystal. This method is highly sensitive, label-free, and real-time, and is ideal for monitoring biomolecular binding events like antigen-antibody interactions or receptor-ligand binding (Marx, 2003).

Thermal and Calorimetric Biosensors

These measure heat changes resulting from exothermic or endothermic reactions between the analyte and recognition molecule. They are useful in enzyme-based biosensors but are less common due to their relatively lower sensitivity and specificity (Arya et al., 2008).

Mechanical and Micromechanical Biosensors

These detect mechanical properties such as deflection, stress, or strain changes induced by analyte interaction, typically using microcantilevers or nanomechanical resonators. These are still largely in the research phase but offer promising resolution at the single-molecule level (Lavrik & Datskos, 2003).

2.7.3. Importance of Biosensors in Biomarker Detection

Biosensors are uniquely positioned to address the growing demand for rapid, accurate, and accessible biomarker detection technologies, particularly in the context of personalized and point-of-care medicine. Their suitability stems from several key advantages:

High Sensitivity and Selectivity: Biosensors can detect biomarkers at low concentrations (pico- to nanomolar range), which is crucial for early disease diagnosis when biomarker levels are still low (Walla et al., 2014). Selectivity is achieved by tailoring the recognition element—such as using synthetic receptors like MIPs to mimic antibody specificity.

Real-Time and Label-Free Detection: Techniques like QCM and SPR enable real-time monitoring of biomolecular interactions without the need for secondary labeling agents, minimizing assay complexity and preserving the native structure of the biomarker (Walla et al., 2014).

Miniaturization and Portability: Biosensors are amenable to integration into portable and microfluidic platforms, making them ideal for point-of-care applications in clinical diagnostics, including remote or resource-limited settings (Yetisen et al., 2013).

Versatility Across Analyte Types: Biosensors can be engineered to detect a wide range of biomarkers—proteins, peptides, nucleic acids, metabolites—by selecting the appropriate recognition element. In your study, AngII, a small octapeptide, is targeted using MIPs that offer both chemical robustness and reusability (Walla et al., 2014).

Low Sample Volume and Simple Handling: Many biosensors require minimal sample volumes (μL scale) and can operate directly with raw or minimally treated biological fluids like serum, saliva, or urine. This reduces pre-analytical variability and improves throughput in diagnostic workflows (Bahadır & Sezgintürk, 2016).

Integration with Digital Health Technologies: Modern biosensors can be connected to digital interfaces, facilitating data transmission, cloud-based analysis, and remote health monitoring—trends increasingly important in the era of telemedicine (Bahadır & Sezgintürk, 2016).

2.8. Quartz Crystal Microbalance (QCM) Technology

QCM is an exceptionally sensitive and effective method for analyzing significant molecules, including biomarkers. It is extensively utilized for biological and chemical sensing due to its capability to detect very few mass changes on the QCM sensor chip surface in real-time. A QCM device consists of a thin quartz disk sandwiched between a pair of electrodes. It is a piezoelectric sensor, which oscillates mechanically upon the application of alternating voltage. It can be considered as a tiny little scale that measure very small mass changes by tracking how

its oscillation frequency changes (Liu et al., 2021; Aylaz & Andaç, 2022; Karabulut et al., 2022).

QCM is a super sensitive way to check if molecules are binding or not. It offers label-free and real-time detection and can be used in both gaseous and liquid environments (Diltemiz et al., 2017). As illustrated in Figure 1.6, adsorption of mass onto the gold-coated quartz surface lowers the crystal's resonance frequency, and the magnitude of this shift is directly proportional to the added mass (Liu et al., 2021; Aylaz & Andaç, 2022; Aydoğan et al., 2022). Functionalising the surface with selective recognition layers—such as nano-MIPs—ensures that the observed frequency change reflects only target binding, enabling accurate affinity and kinetic analyses even in complex media (Lin et al., 2004; Reimhult et al., 2008; Yang & Zhang, 2009; Diltemiz et al., 2017).

2.8.1. Working Principle of QCM: Mass Change → Frequency Change

Quartz-crystal microbalance (QCM) sensing quantifies extremely small mass changes by tracking the resonance frequency of a piezoelectric quartz crystal. The relationship between added mass and frequency shift is described by the Sauerbrey equation (Sauerbrey, 1959):

$$\Delta f = -\frac{2f_0^2 \Delta m}{A\sqrt{p_q \mu_q}} \quad (1)$$

Where, Δf is the frequency change (Hz), f_0 is the fundamental frequency of the quartz crystal (typically 5-10 MHz), Δm is the mass change per unit area (g/cm²), A is the electrode area, ρ_q and μ_q are the density and shear modulus of quartz, respectively.

When molecules adsorb to or desorb from the functionalized surface of the QCM crystal, this leads to a corresponding increase or decrease in the sensor's oscillation frequency. This direct correlation between mass and frequency enables the detection of extremely small mass changes—on the order of nanograms per square centimeter—making QCM a highly sensitive method for studying molecular interactions (Figure 2.9).

QCM technique can also evaluate the viscoelastic properties of surface-bound layers through the measurement of dissipation, which reflects the energy lost during the oscillatory motion of these layers. An increase in dissipation typically indicates the formation of layers with softer or viscoelastic characteristics at the sensor interface (Lin et al., 2004; Reimhult et al., 2008). By integrating variations in frequency with alterations in dissipation, we can gain deeper insights into molecular interactions on surfaces. This integrated data set demonstrates binding events in real time, detecting subtle variations that alternative approaches may overlook (Diltemiz et al., 2017; Yang and Zhang, 2009).

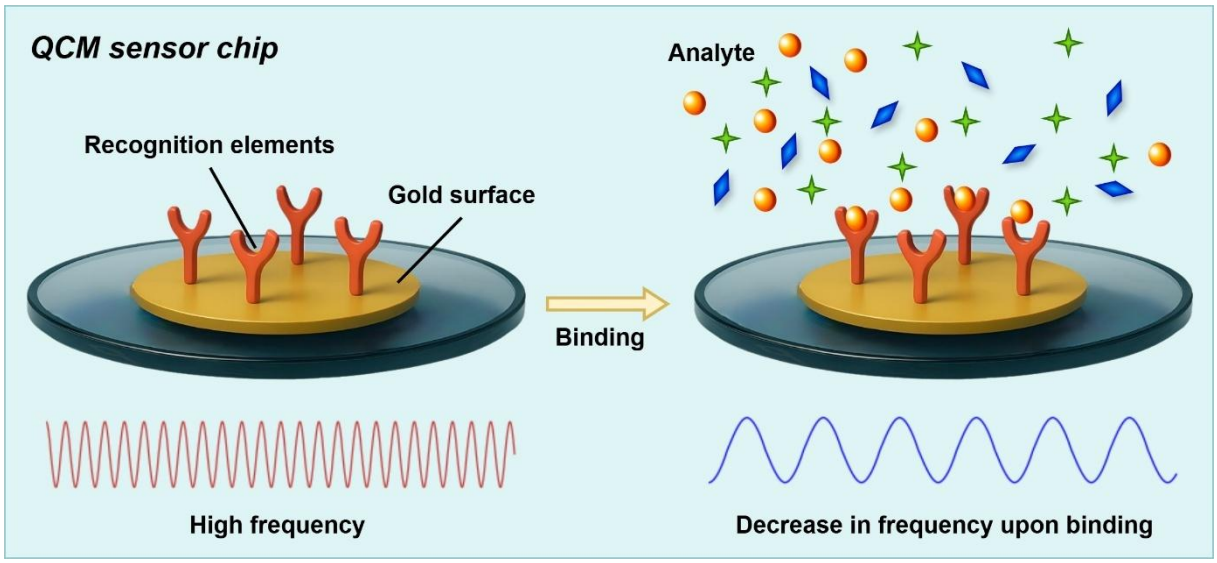

Figure 2.9. Working principle of QCM.

2.8.2. Sensitivity and Real-Time Detection Capability

QCM sensors can register mass additions below one nanogram, allowing them to track small molecules, short peptides, and other low-abundance biomarkers as they bind to a surface (Marx, 2003). Because the crystal can oscillate in either air or liquid, the same instrument serves environmental, pharmaceutical, and biomedical assays without hardware changes. Modern instruments equipped with dissipation monitoring (QCM-D) add a second channel of information: in parallel with the frequency shift that reports mass, they record energy loss in the crystal, which reflects the viscoelastic nature of the adsorbed layer (Reimhult et al., 2008). A stiff protein shell, a loosely bound polymer film, or a water-rich hydrogel will produce different dissipation signatures, giving insight into conformational changes and hydration

without the need for fluorescent or radioactive labels. These label-free measurements preserve the native state of biomolecules and permit full kinetic and thermodynamic analyses on the same chip.

2.8.3. Applications in Biosensing, Especially in Protein/Peptide Recognition

Transducing molecular recognition into a frequency shift has made QCM a versatile platform for biosensing. Once the gold surface is coated with a selective layer—antibodies, aptamers, or MIPs—the crystal can detect targets that range in size from a drug molecule to an intact virus (Katz & Willner, 2004). Protein and peptide assays benefit in particular, because the instrument records association and dissociation in real time, allowing direct determination of affinity constants, on/off rates, and competitive binding in complex media. Representative applications include troponin and cytokine monitoring, hormone assays, and studies of antimicrobial-peptide action (Fogel et al., 2016).

Recent work has pushed QCM toward routine clinical and environmental use. Sensors functionalised with peptide-selective MIPs, for example, distinguish angiotensin II in serum with high selectivity while avoiding the reagents and wash steps required by traditional immunoassays (Diltemiz et al., 2017). Adding nano-MIPs to the crystal amplifies both sensitivity and selectivity: densely packed nanoparticles expand the effective surface area, and their uniform size yields thin, homogeneous recognition layers that minimise energy dissipation and improve the signal-to-noise ratio (Gagliardi & Cecchini, 2025). With this architecture, detection limits for peptide and small-protein biomarkers can reach the low-picomolar or even femtomolar range; examples already reported include neuropeptide Y, atrial natriuretic peptide, and angiotensin II (Saylan et al., 2019). These advances illustrate how nano-MIP/QCM hybrids combine gravimetric precision with synthetic-receptor robustness to meet the demands of real-time, low-level bioanalysis.

Additionally, nanoMIP-coated QCM sensors have numerous technical advantages, such as:

- Label-free detection: no need for fluorescent or radioactive tags.
- Real-time monitoring: continuous data observation during binding and desorption events.

- Multiplexing capability: multiple targets can be simultaneously detected with spatially separated nanoMIP layers.

Such systems are ideal candidates for point-of-care diagnostic tools, where portability, speed, and robustness are essential.

2.9. Existing Methods for AngII Detection and Limitations

2.9.1. Overview of Conventional Methods: ELISA, HPLC, LC-MS/MS

Accurate quantification of Ang II in serum, plasma, or urine underpins many clinical and research studies on cardiovascular, renal, and metabolic disease. Three laboratory methods dominate current practice:

Enzyme-linked immunosorbent assay (ELISA). Commercial ELISA kits exploit antibody–antigen binding and provide straightforward workflows that fit routine hospital and academic laboratories. Throughput is moderate, and reagent costs are relatively low, but assay sensitivity is usually confined to the high-picomolar range and depends on antibody quality.

High-performance liquid chromatography (HPLC). In this approach Ang II is separated from co-eluting compounds before detection by ultraviolet absorbance or—less often—mass spectrometry. HPLC improves specificity over ELISA yet still requires sample pretreatment and delivers limited sensitivity when the peptide is present at only a few picomoles per litre (Basu et al., 2021).

Liquid chromatography–tandem mass spectrometry (LC-MS/MS). Coupling chromatographic separation with selective ion monitoring makes LC-MS/MS the reference method for peptide hormones. The technique resolves Ang II at low-picomolar and, with careful optimisation, femtomolar concentrations in complex matrices, offering unmatched specificity. Its drawbacks are higher capital cost, longer run times, and the need for skilled operation.

2.9.2. Drawbacks: Expensive, Time-Consuming, Labor-Intensive, Not Portable

Techniques such as LC-MS/MS and HPLC need extra cleanup steps—solid-phase extraction or protein precipitation—to remove matrix interferences and concentrate the peptide. These steps lengthen the workflow and add operator-to-operator variability (Rauh et al., 2012). The instruments themselves are costly, require specialised staff, and demand frequent maintenance, so they remain confined to central laboratories. ELISA avoids complex hardware but depends on antibody quality; antibodies can degrade and may cross-react with related angiotensin fragments, leading to inaccurate readings. Turnaround times for all three methods typically range from several hours to more than a day, which is impractical during hypertensive crises or other urgent clinical situations. These constraints have driven interest in portable biosensors that combine MIPs with electrochemical, piezoelectric, or optical transducers, aiming to measure Ang II quickly and inexpensively without sacrificing sensitivity or selectivity.

Table 2.2. Conventional AngII detection techniques.

Method	Detection Limit	Sample Preparation	Time per Sample	Cost & Equipment	Portability	Major Limitations
ELISA	~10-50 pg/mL	Moderate (dilution, blocking)	2-4 hours	Medium; plate reader required	Low	Cross-reactivity, limited sensitivity, antibody dependency.
HPLC-UV	~100 pg/mL	Extensive (filtration, extraction)	2-3 hours	High; requires skilled operator	Very Low	Low sensitivity, lengthy method development.
LC-MS/MS	~1-10 pg/mL	Extensive (SPE, concentration)	4-8 hours	Very High; advanced lab setup	None	Costly, complex instrumentation, non-portable.
MIP-QCM (this study)	~0.15 pg/mL	Minimal (direct serum dilution)	<30 minutes	Low-medium; portable QCM units available	High	Requires MIP synthesis; under clinical validation.

Although ELISA, HPLC, and LC-MS/MS have been indispensable tools for AngII detection, they are not ideal for rapid, affordable, or portable diagnostics. Their limitations highlight the urgent need for next-generation biosensing platforms—such as QCM sensors functionalized

with AngII-imprinted nanoparticles—that can provide real-time, label-free, and selective detection directly from biological fluids. Such systems could revolutionize early diagnosis and monitoring of hypertension-related diseases, enabling decentralized and personalized healthcare solutions.

2.9.3. MIP-Based Studies on the Detection of AngII

In recent years, MIP technology has gained considerable attention as a promising approach for the selective and sensitive detection of AngII in complex biological samples. This section provides an overview of the key studies that have explored MIP-based systems designed to recognize AngII.

Rachkov and Minoura (2004) produced epitope-imprinted polymers in water using the [Sar^{1},Ala^{8}] fragment of Ang II. The polymer gave a linear response from 0.4 μM to 20 μM with a detection limit of ~8 pmol, proving that low-molecular-weight peptides can be imprinted and recovered at physiologically relevant levels (Rachkov and Minoura, 2004).

Yu et al. (2014) reported ligand-specificity-determinant imprinting to obtain nanogel receptors that bound both Ang I and Ang II and neutralised their activity in vitro. The nanogels were evaluated in solution only; no transducer was coupled, so real-time measurement remained unexplored (Yu et al., 2014).

Yıldırım and Baydemir Peşint (2021) fabricated macroporous cryogel columns that extracted Ang II directly from serum. Relative binding factors were 8.27 (vs Ang I) and 14.25 (vs vasopressin), with a capacity of 0.667 mg/g and ~96 % recovery. FTIR, SEM and BET analyses confirmed the material's morphology and surface area (Yıldırım and Baydemir Peşint, 2021).

Using a miniemulsion route, Arısoy and Baydemir Peşint (2025) synthesised HEMA-based nano-MIPs (~50 nm). At an Ang II level of 700 pg/mL the particles adsorbed 4.5 ng/g and showed selectivity factors of 2.8 (Ang I) and 3.2 (Vasp). Binding capacity remained stable over multiple regeneration cycles, indicating suitability for point-of-care assays (Arısoy and Baydemir Peşint, 2025).

The present thesis bridges this gap by introducing the first reported QCM sensor functionalized with AngII-imprinted nanoparticles. This system not only enables selective detection of AngII but also supports real-time, label-free analysis—an important advancement over existing offline or batch-based approaches. By integrating MIP materials with acoustic transduction, this platform allows dynamic monitoring of molecular interactions in complex biological media, offering a valuable tool for next-generation diagnostic technologies.

2.10. Novelty and Contribution of This Research

2.10.1. Development of MIP-Based Nanoparticles Tailored for AngII

This research introduces a novel strategy for the selective detection of AngII by developing MIP nanoparticles specifically designed to recognize and bind this clinically significant peptide. Unlike traditional bulk MIPs, which often suffer from low accessibility to binding sites and slow diffusion kinetics, the MIPs synthesized in this study are fabricated at the nanoscale using a miniemulsion polymerization method. This approach results in monodisperse, spherical nanoparticles with high surface-area-to-volume ratios and abundant surface-accessible imprinted sites (Saylan et al., 2019).

What distinguishes this work is the template-specific design using AngII and VIM as the functional monomer. The careful optimization of template-to-monomer ratios and the use of non-covalent imprinting ensure high affinity, specificity, and selectivity toward AngII, even in the presence of structurally similar analogs like Ang-I and vasopressin. This customized imprinting system enables the molecular recognition of AngII in biologically relevant environments, supporting its potential as a viable biosensing platform (Yıldırım and Baydemir Peşint, 2021; Arısoy and Baydemir Peşint, 2025).

Such peptide-specific MIPs—particularly for small, labile molecules like AngII—remain underexplored in the literature, thus positioning this study as a pioneering contribution to the fields of biorecognition chemistry and MIP-based nanotechnology (Nahhas and Webster, 2021).

2.10.2. Integration with QCM for Real-Time, Label-Free Detection

The integration of AngII-imprinted nanoparticles with a QCM platform represents a key innovation in this study. QCM is an ultrasensitive, label-free mass sensor capable of detecting nanogram-level changes in real time. By immobilizing the synthesized MIP nanoparticles onto the gold surface of the QCM crystal, this work transforms a traditionally chemical sensor into a biomolecular recognition system for AngII.

This integration offers several novel contributions:

- Real-time monitoring of AngII adsorption and desorption kinetics without the need for labels or amplification.
- Quantitative signal output based on frequency shift, correlating directly to the amount of bound analyte.
- Evaluation of selectivity and competitive binding through comparative studies with Ang-I and vasopressin, confirming high target specificity.

While previous QCM studies have explored protein or virus detection using surface-immobilized MIPs, the application of peptide-imprinted nanoparticle coatings for AngII detection is unprecedented. This novel hybrid system demonstrates that nanoMIPs can be effectively used as synthetic bioreceptors in QCM biosensors, enabling ultrasensitive and highly selective detection of small peptide biomarkers (Afzal et al., 2017; Ostrovidov et al., 2023).

2.10.3. Targeting Direct Detection from Human Serum

One of the most significant contributions of this thesis is the successful demonstration of direct detection of AngII from spiked human serum samples. This achievement addresses a critical challenge in biosensing: the interference-rich nature of biological fluids. Unlike conventional methods requiring multistep sample purification, this approach involves only minimal pre-treatment—such as dilution—followed by direct application of serum onto the QCM sensor.

This study confirms that the MIP-coated QCM chip:

- Retains its binding capacity and selectivity even in complex matrices.

- Achieves detection limits in the low picomolar range (1-100 pg/mL), compatible with physiological levels of AngII.
- Maintains high reusability and regeneration capability across multiple detection cycles.

The ability to selectively detect AngII in serum without extensive cleanup or signal interference is an essential step toward clinical translation and confirms the practical viability of this biosensor platform.

This research paves the way for the development of portable, rapid, and affordable biosensors for cardiovascular risk assessment and disease monitoring. Unlike existing immunoassays or LC-MS/MS methods, the proposed system offers:

- Label-free detection, eliminating reliance on costly and unstable antibodies.
- On-site applicability, supported by compact and commercially available QCM devices.
- Cost-effectiveness and scalability, with MIP nanoparticles offering long shelf life and simple synthesis.

These features position the system as a promising tool for point-of-care diagnostics, especially in decentralized or resource-limited settings. In particular, early detection of AngII in conditions such as hypertension, heart failure, renal dysfunction, and sepsis-related hypotension could support faster therapeutic decisions and improved clinical outcomes (Pagliaro & Penna, 2005; Chappell, 2012; Khanna et al., 2017).

Furthermore, this platform can be extended to other disease biomarkers by adjusting the imprinting template, suggesting broad applicability in next-generation biosensing technologies.

3. MATERIALS AND METHODS

3.1. Materials

AngII, AngI Human Acetate and Arg8-Vasopressin Acetate was purchased from Sigmaaldrich, St.Louis, MO , USA. Sodium dodecyl sulfate (SDS), sodium bicarbonate, 2-vinyl imidazole (VIM), 2-hydroxyethyl methacrylate (HEMA), ethylene glycol dimethacrylate (EGDMA), sodium bisulfite and ammonium persulfate (APS) were obtained from Sigma (St. Louis, MO, USA). Other chemicals and equipment used: sodium phosphate dibasic, sodium phosphate monobasic, potassium chloride, acetate buffer, carbonate buffer, PBS, vial with cap, perforator, capped glass bottle 3 mL and 5 mL, peristaltic pump (Watson-Marlow, Wilmington, MA, USA), Refrigerator, pipette set, ethanol, methanol, surface cleaner ethanol, nitric acid, HCl, NaOH, glass baguette, flask, pipette, puar, magnetic stirrer, clamp, tube and laboratory stand rotator, vortex, parafilm, eppendorf, plunger, spatula, pipette tip, syringe, 2.5-3-5 mL, gloves, QCM chips, QCM device, Dremel Lithium Ion (Dremel, Germany) hand tool for cutting metal sheaths from quartz crystals. Piranha solution (3:1 concentrated sulfuric acid and 30% hydrogen peroxide mixture) was used for the cleaning of the QCM chip surface. Allyl mercaptan was employed for the activation of the surface, before nanoparticle immobilization. Ethanol used in washing processes and phosphate buffered saline (PBS) and sodium chloride (NaCl) used in desorption studies were also purchased from Sigma. All chemicals taken are of analytical purity and were stored under appropriate storage conditions until used in experimental studies.

3.2. Synthesis of AngII-imprinted (AngII-MIP) and non-imprinted (NIP) nanoparticles

AngII was used as the template molecule and VIM was used as the functional monomer. The ideal molar ratio of template molecule and functional monomer was determined spectrophotometrically before the synthesis. AngII-VIM pre-complex was prepared (4°C, 4h incubation) in different molar ratios (1:1, 1:2, 1:5, 1:10 and 1:20, n:n) and measured spectrophotometrically.

AngII-MIP and NIP nanoparticles were synthesized according to following procedure:

- Liquid phase 1: SDS (15 mg), PVA (100 mg), and sodium bicarbonate (12,5 mg) in 5 mL ultrapure water,

- Liquid phase 2: SDS (50 mg) and PVA (50 mg) in 100 mL ultrapure water,
- Monomer (or organic) phase: HEMA (0.25 mL) and EGDMA (1 mL)

Monomer phase were added to the liquid phase 1 and the mixture were homogenized using a homogenizer for 30 min at 30000 rpm to obtain miniemulsion (Figure 3.1, left), and further mixing were performed using a magnetic stirrer at 300 rpm for 10 min. 1 mL of AngII:VIM precomplex were added (for AngII-MIP only). Obtaining miniemulsion were added to the liquid phase 2, under constant stirring. Sodium bisulfite and ammonium persulfate were used as initiators. After the addition of initiators, total polymeric solution were taken into round-shaped bottles in order to obtain round-shaped nanoparticles and put into the polymerization reactor (Radleys Carousel 6 Plus Reaction Station) set to 40 °C under constant stirring at 400 rpm for 24 hours (Figure 3.1, middle). After the polymerization process, nanoparticles were separated from the polymer solution performing high speed centrifugation (Figure 3.1, right). Obtaining nanoparticles were washed using ultrapure water for the removal of unreacted monomers and other impurities. Template removal studies will be performed after coating QCM sensor chips with AngII-MIP nanoparticles. Non-imprinted nanoparticles (NIP) were synthesized following the same procedure for control without adding AngII-VIM pre-complex.

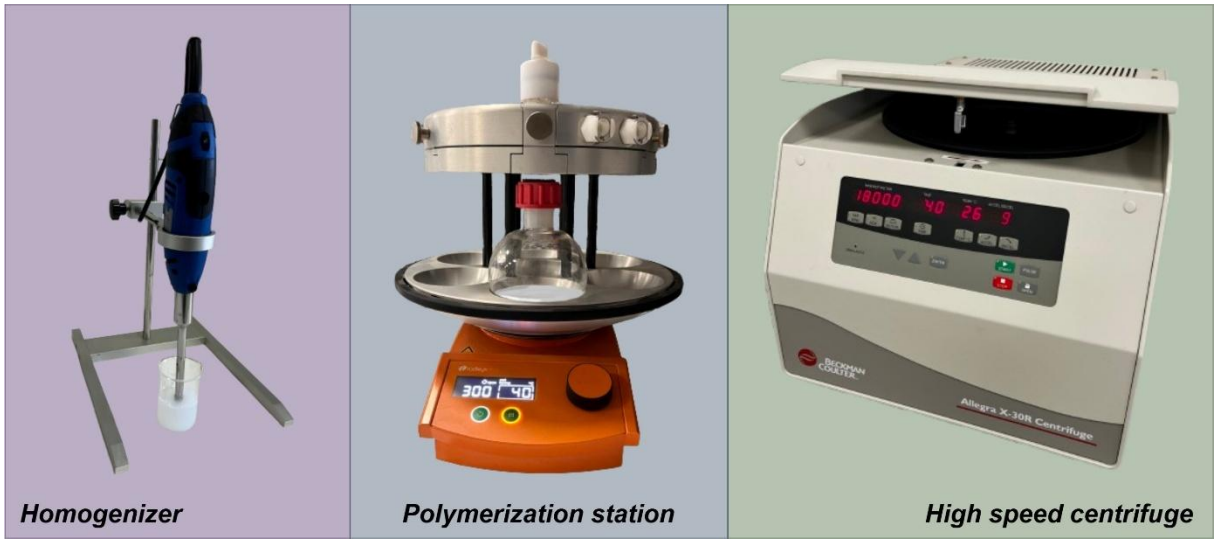

Figure 3.1. Homogenization of polymeric solution using homogenizer (left), polymerization in polymerization station (middle) and high speed centrifuge up to 24,000 rpm (right).

3.3. Characterization of AngII-MIP and NIP Nanoparticles

To provide a comprehensive characterization of the nanoparticles, a variety of analytical techniques, including zeta-sizer analysis, Transmission Electron Microscopy (TEM), Scanning Electron Microscopy (SEM), and Fourier-Transform Infrared Spectroscopy (FTIR) were employed. Particle size distribution and colloidal stability were evaluated using a Zeta-sizer (NanoS90, Malvern Instruments, London, UK). For morphological characterization and precise determination of nanoparticle dimensions, scanning electron microscopy (SEM; FEI, Quanta 650 Field Emission, USA) and transmission electron microscopy (TEM; Hitachi HT-7700, Tokyo, Japan) analyses were performed. These high-resolution imaging techniques complement particle size measurements by offering detailed insights into surface features and structure.

Additionally, FTIR spectroscopy provided insights into chemical composition and functional groups. FTIR identifies characteristic molecular vibrations through infrared absorption, confirming successful molecular imprinting by comparing the spectra of the template, monomer-template complex, and synthesized MIP against corresponding NIPs.

3.3.1. Zeta-sizer Analysis

Hydrodynamic size distributions of the synthesized AngII-MIP and NIP nanoparticles were measured using a Zetasizer Nano S-90, a widely preferred instrument for colloidal analysis based on Dynamic Light Scattering (DLS). In DLS, particle dimensions are determined by analyzing fluctuations in laser light scattered at a 90° angle, caused by the Brownian motion of nanoparticles. Measurements were carried out at 25°C, with refractive index and viscosity parameters of deionized water set to 1.33 and 0.8822 cP, respectively, and polymer absorption defined as 0.001. The Zetasizer automatically verified nanoparticle concentration suitability to ensure accurate results.

To avoid aggregation-related errors during size measurements, nanoparticle suspensions underwent initial ultrasonication and vortex mixing. Samples were carefully diluted through four sequential 1:1 (v:v) steps using ultrapure water, ensuring monodisperse size distributions.

Each dilution step included repeated sonication and vortexing to maintain particle homogeneity. All measurements were performed at room temperature and conducted in triplicate to confirm reliability.

3.3.2. TEM Analysis

To examine the internal structure, morphology, and size distribution of the synthesized nanoparticles with high resolution, TEM analysis was performed. During sample preparation, ethanol was added to the nanoparticle pellet to promote uniform dispersion and minimize aggregation. The suspension was then carefully sonicated in an ultrasonic bath to ensure homogeneity. A small aliquot of the resulting solution was gently dropped onto a copper grid coated with a formvar film. To preserve particle integrity and prevent morphological distortion, the sample was left to air-dry at room temperature without applying any external heat or vacuum. Following the drying step, the grids were mounted onto the TEM sample holder and imaged. This process allowed for a detailed visualization of the particle size distribution, shape uniformity, and dispersion state. The technique was particularly useful in distinguishing between individual particles and aggregated structures, thereby offering valuable insights into the structural quality of the molecular imprinting process.

3.3.3. SEM Analysis

SEM was employed to characterize morphological properties and size distributions of AngII-MIP and NIP nanoparticles. Initially, nanoparticles were precipitated with ethanol, briefly sonicated, and subsequently resuspended in ultrapure water. To preserve particle morphology, suspensions were frozen at -80°C and lyophilized. After freeze-drying, the powder was evenly dispersed onto glass coverslips, mounted onto SEM stubs using conductive adhesive, and sputter-coated with gold-palladium alloy (40/60). This procedure minimized electron beam charging effects, producing high-quality images suitable for detailed morphological evaluation.

3.3.4. FTIR Analysis

FTIR spectroscopy, a rapid and non-destructive analytical method, was used to investigate the chemical composition and confirm the successful synthesis of AngII-MIP and NIP nanoparticles. FTIR spectra were collected for AngII, VIM, their pre-polymerization complex

(1:10 molar ratio), as well as AngII-MIP and NIP, using a Jasco FT/IR 6700 spectrometer (Japan). Nanoparticles were centrifuged, freeze-dried, and analyzed, while other samples were measured directly without further preparation. Spectral data ranging from 400 to 4000 cm^{-1} provided crucial insights into the incorporation of functional groups and molecular interactions, clearly distinguishing between imprinted and non-imprinted polymers.

3.4. Fabrication of Nanoparticle-coated QCM Chips

QCM is a technique that measures the mass change of a quartz crystal resonator due to the adsorption or desorption of molecules on its surface. QCM chips coated with AngII-MIPs and NIPs were fabricated. For this purpose, QCM chips were washed in 15 mL of piranha solution in an ultrasonic bath for 20 minutes. Piranha solution is a powerful oxidizing agent that can remove organic contaminants from surfaces. Then, QCM chips were rinsed with distilled water for 15 minutes, with pure ethanol for 15 minutes and left to dry for 1 hour. After the surface was completely dry, 15 µL of allyl mercaptan was dropped onto the middle of the gold surface of the chips to activate the chip surfaces with mercaptan groups and the chips were left overnight for the activation. Allyl mercaptan is an organosulfur compound that can form self-assembled monolayers on gold surfaces. After the surfaces were activated with allyl mercaptan, one of the chips was dropped with AngII-MIPs, and the other with non-imprinted nanoparticles (NIP) as a control group, and they were kept under UV lamp for 20 minutes to ensure the attachment of the nanoparticles to the surface (Figure 3.2). QCM chips coated with nanoparticles and other residues that could not adhere were washed with distilled water for 15 minutes, with pure ethanol for 15 minutes and left to dry for 1 hour.

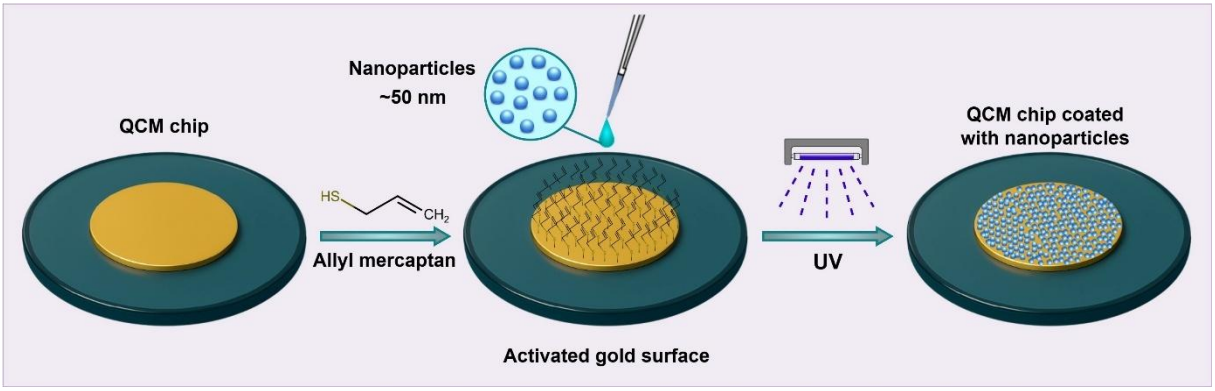

Figure 3.2. Representative illustration of fabrication of nanoparticle-coated QCM chips.

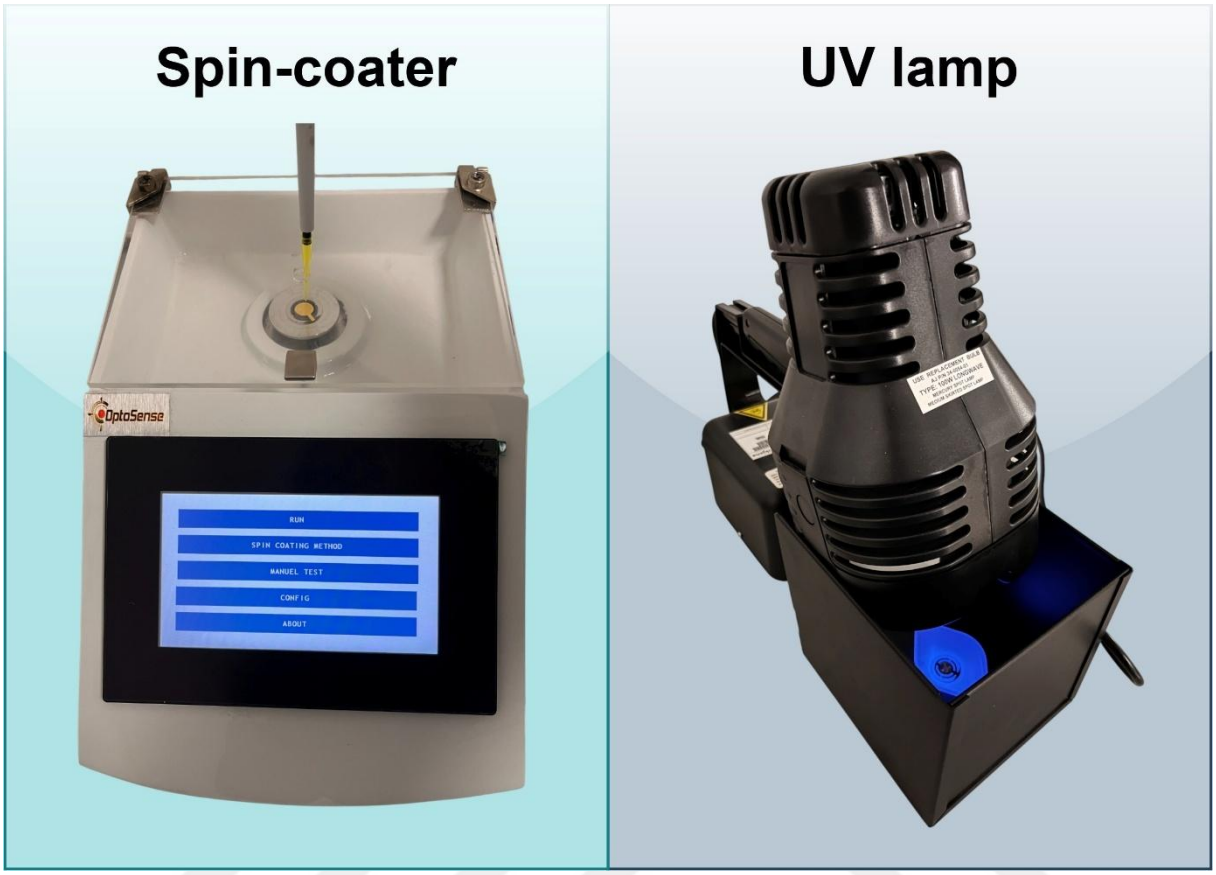

Figure 3.3. Spin-coating of activated QCM chip with nanoparticles (left) and UV immobilization of nanoparticles onto QCM chip (right).

Further washing step before getting into template removal and binding studies was applied with ultrapure water using QCM tools in a continious system to make sure there is no residual elements. This step was continued until the frequency stabilizes.

3.5. Characterization of Nanoparticle-coated QCM Chips

The surface morphology and physicochemical properties of AngII-MICqcm and NICqcm chips were analyzed using atomic force microscopy (AFM) and contact angle measurements. These complementary techniques provided topographical and interfacial data critical for understanding nanoparticle deposition. Contact angle analysis (Attension Theta Lite, Biolin Scientific, Sweden) assessed surface wettability, with differences between MIP and NIP coatings indicating variations in hydrophilic/hydrophobic behavior due to surface-bound

functional groups. AFM analysis (Park NX10, Park Systems, South Korea) confirmed nanoparticle immobilization and revealed differences in roughness, depth, and distribution. These high-resolution scans also qualitatively evaluated coverage homogeneity, key to sensor reproducibility.

3.5.1. Atomic Force Microscopy Analysis

Optimizing sensor performance requires a detailed understanding of surface architecture at the nanoscale. Atomic force microscopy (AFM) enables such analysis by using a sharp cantilever tip to interact with the sample surface, generating high-resolution, three-dimensional images that reveal subtle differences in texture, depth, and morphology. AFM was utilized to reveal differences in nanoparticle distribution, surface roughness, and morphology between AngII-MIP and NIP nanoparticle-coated QCM chips (AngII-MICqcm and NICqcm, respectively). Measurements were conducted using a Park NX10 AFM system (Park Systems, South Korea) operated in semi-contact mode, minimizing mechanical stress on the polymer-coated surfaces while preserving resolution. Samples were carefully fixed onto the AFM stage using double-sided adhesive tape, ensuring stable and consistent imaging. This analysis provided nanoscale evidence of structural variations resulting from molecular imprinting..

3.5.2. Contact Angle

Surface wettability of QCM chips coated with AngII-MIP and NIP nanoparticles was assessed by contact angle measurements, highlighting changes in hydrophilicity or hydrophobicity due to molecular imprinting. Ultrapure water droplets were placed onto chip surfaces using an Attension Theta Lite contact angle goniometer (Biolin Scientific Ltd., Sweden). Droplet shapes were recorded in real-time, and to minimize the effect of local surface variations, measurements were repeated on at least two distinct chip regions. Final contact angle values were reported as the average of these multiple readings, enabling precise comparison of surface chemistry modifications caused by imprinting.

3.6. AngII Binding and Kinetic Analysis Studies with AngII-MICqcm/NICqcm

Following the preparation of QCM sensors, either AngII-imprinted (AngII-MICqcm) or non-imprinted (NICqcm), binding and kinetic analysis studies were carried out. These experiments were conducted using the SRS200 model QCM system (Stanford Research Systems) available

in our laboratory. The setup consisted of a peristaltic pump for sample delivery, a flow cell to facilitate molecular interaction, an oscillator for real-time frequency shift measurements, and a computer for signal processing and analysis.

Kinetic analyses were performed using AngII protein solutions at various concentrations. In each experiment, the QCM chip was placed into the sensor unit and rinsed with deionized water for 15 minutes. It was then equilibrated at room temperature with phosphate buffer (pH 7.4), and the initial resonance frequency (f_0) was recorded. After 3 minutes of stabilization with the phosphate buffer, AngII solutions at different concentrations (0.25-100 pg/mL) were sequentially introduced into the system. The shifts in resonance frequency (Δf) were continuously monitored in real-time.

Once equilibrium was reached, desorption was performed using a 1 M NaCl solution prepared in PBS (10 mM, pH 7.4). After each measurement, the QCM chip was rinsed with deionized water and re-equilibrated with phosphate buffer (pH 7.4). The resonance frequency changes obtained from interactions of each solution with the QCM sensor surface were recorded, and the kinetic data were analyzed using SRSQCM 200 software.

QCM, which consists of a thin vibrating quartz crystal placed between two metal excitation electrodes, was used to detect interfacial mass changes based on resonance frequency shifts. The correlation between the frequency shift (Δf) and the mass change (Δm) of the bound and desorbed AngII molecules was determined according to the simplified Sauerbrey equation (Equation 2), which defines the mass-frequency relationship on the QCM surface.

$$\Delta m = -Cqcm \times \Delta f \qquad (2)$$

In this equation, Δm represents the change in mass, while Δf denotes the frequency shift. For AT-cut QCM crystals operating at a fundamental frequency of 5 MHz, the mass sensitivity constant (Cqcm) is defined as 17.7 $ng \cdot cm^{-2} \cdot Hz^{-1}$. In this study, a calibration curve was constructed using standard AngII solutions of known concentrations based on the linear

correlation between the resonance frequency shift (Δf) and the corresponding mass change (Δm).

This calibration curve was then used to determine the confidence interval, the Limit of Detection (LOD), and the Limit of Quantification (LOQ). The sensitivity of the AngII-MICqcm sensor was periodically evaluated using a standard AngII solution. All measurements were performed in triplicate, and the confidence interval was established accordingly. For each data set, standard statistical methods were applied to calculate the mean values and standard deviations.

The concentration corresponding to the signal that could be reliably distinguished from the blank (control) was considered the minimum detectable concentration of the method. In analytical science, the ability of a method to detect lower concentrations is regarded as a critical indicator of its sensitivity and overall performance.

The Limit of Detection (LOD) and the Limit of Quantification (LOQ) for the AngII-MICqcm sensor were calculated using the following equations:

$$LOD = 3.3\ s/m \quad (3)$$

$$LOQ = 10\ s/m \quad (4)$$

In these equations, s denotes the standard deviation of the response, and m represents the slope of the calibration curve. These calculations were performed in accordance with previously reported methodologies (Şener et al., 2010; Diltemiz et al., 2017; Aydoğan, 2018; Kartal et al., 2019).

3.7. Competitive Binding Studies with AngII-MICqcm and NICqcm Chips

At this stage, the study focused on the selective binding of AngII molecules to QCM sensor surfaces modified with AngII-MIP and NIP nanoparticles (Şener et al., 2010; Aydoğan, 2018; Diltemiz et al., 2017; Kartal et al., 2019). To evaluate the selectivity of the QCM sensor

functionalized with MIP and NIP nanoparticles, 15 pg/mL solutions of AngII (target analyte), and its structural analogues AngI and Vasp (competitor molecules), were prepared.

AngI and Vasp were selected as competitor molecules due to their structural and molecular weight similarities with AngII (Figure 3.4). Solutions of AngII, AngI, and Vasp were prepared in 10 mM phosphate buffer (pH 7.4) at a concentration of 15 pg/mL and were sequentially introduced over the surface of the QCM chip.

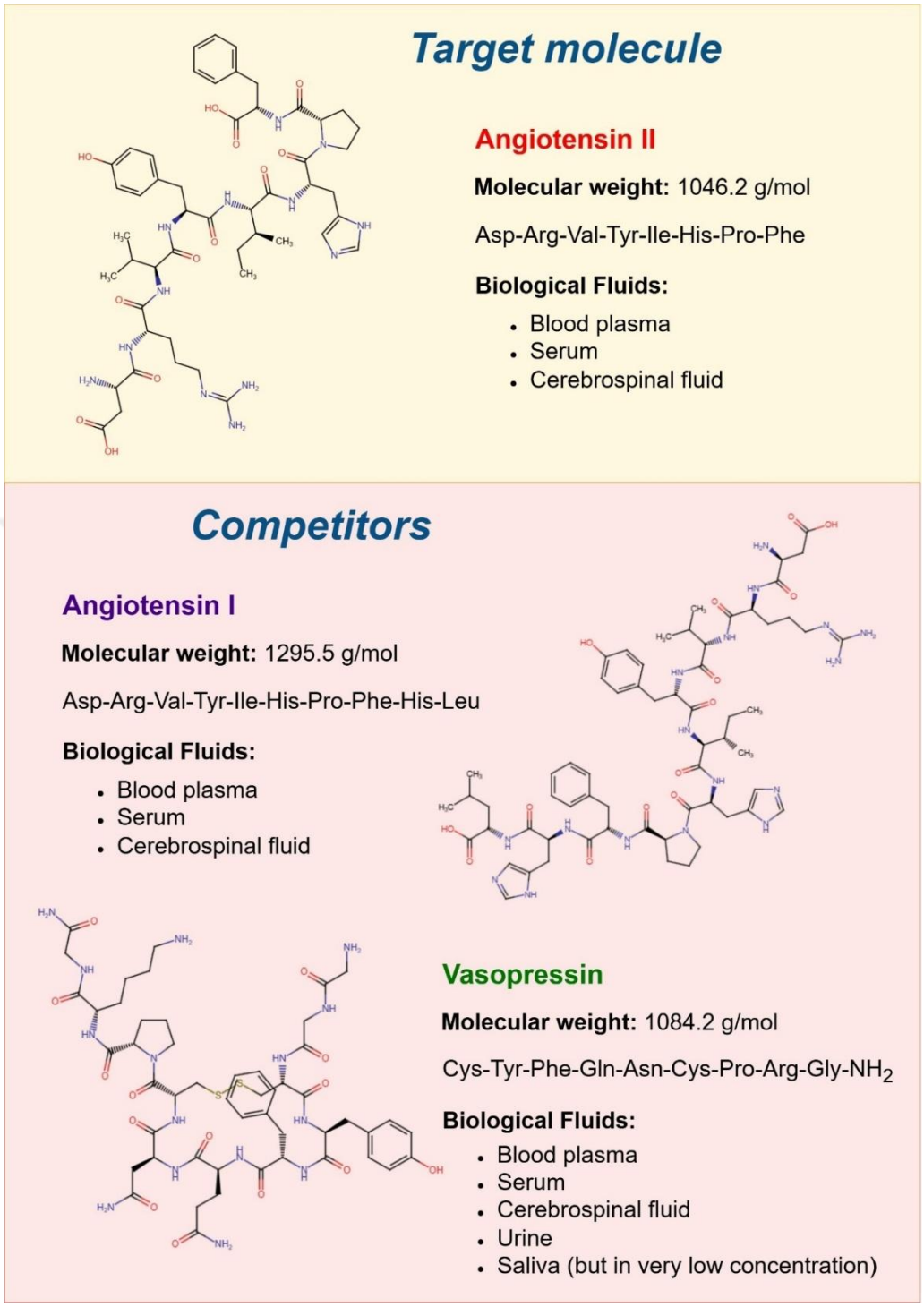

Figure 3.4. Selectivity Studies. Molecular structures and characteristics of template molecule (AngII) and competitors (AngI and Vasp).

The relationship between the resonance frequency shift (Δf) and the corresponding mass change (Δm) due to the binding and desorption of the analyte and competitor molecules was determined

based on the Sauerbrey equation (Equation 2). The obtained kinetic data were analyzed using the SRSQCM 200 software.

The selectivity coefficients (K) for AngII relative to the competitor molecules were calculated using the following equation:

$$K = \Delta m_{AngII/} \Delta m_{competitor} \quad (5)$$

Furthermore, the relative selectivity of AngII-MICqcm compared to NICqcm was determined using the following equation:

$$K' = K_{AngII\text{-}MICqcm}/K_{NICqcm} \quad (6)$$

The imprinting factor (IF) tells us how much more strongly the MIP binds the target than the non-imprinted polymer (NIP). It is simply the ratio:

$$IF = K_{MIP}/K_{NIP} \quad (7)$$

where K is any binding coefficient you use (for example, adsorbed amount divided by equilibrium concentration). An IF greater than 1 means imprinting improved selectivity; the larger the number, the bigger the gain.

3.8. Reusability Studies

The reusability of the QCM chip was evaluated by analyzing the Δf variations obtained from ten repeated binding experiments performed under identical conditions using the same sensor chip. To assess the reusability of the QCM sensor chip, ten consecutive adsorption-desorption cycles were conducted with aqueous AngII solution.

In each cycle, the QCM chip surface was first stabilized with phosphate buffer solution (pH 7.4) for 3 minutes, followed by interaction with AngII solution for 5 minutes. Subsequently, desorption was carried out for 2 minutes using 1 M NaCl in PBS (10 mM, pH 7.4). After each

cycle, the system was evaluated to determine whether the same baseline frequency was reestablished, indicating sensor surface stability and reproducibility.

These procedures were repeated at least three times independently, and average values were used in the data analysis. Standard deviations were calculated to assess the variability and reproducibility of the results. This methodology is consistent with previously reported studies (Şener et al., 2010; Aydoğan, 2018; Diltemiz et al., 2017; Kartal et al., 2019).

3.9. AngII Detection from Human Serum Samples

Commercially obtained human serum samples were used in the study. The serum samples were diluted at a ratio of 1:4 with 10 mM phosphate buffer (pH 7.4). Serum samples without added AngII served as the blank controls. These blank samples were spiked with AngII at concentrations ranging from 10 pg/mL to 100 pg/mL. The samples were then introduced into the system, and the relationship between the resonance frequency shift (Δf) and the corresponding mass change (Δm) of the bound and desorbed AngII molecules was determined according to the Sauerbrey equation (Equation 2) (Kartal et al., 2019).

4. ANALYSIS AND DISCUSSION

4.1. Preparation of AngII-VIM Pre-complex and Synthesis of AngII-MIP and NIP Nanoparticles

AngII-VIM pre-complex was prepared in different molar ratios and measured spectrophotometrically. According to results, there was no remarkable change in the peak after 1:10 molar ratio (Figure 4.1). So, the best molar ratio was determined as 1:10 (AngII:VIM, V:V). This molar ratio was used for the preparation of AngII-VIM precomplex. AngII-MIP and NIP nanoparticles were synthesized according to given protocol (Figure 4.2). Optical photographs of AngII-MIP (A) and NIP (B) nanoparticles, before and after centrifugation, are given in Figure 4.3.

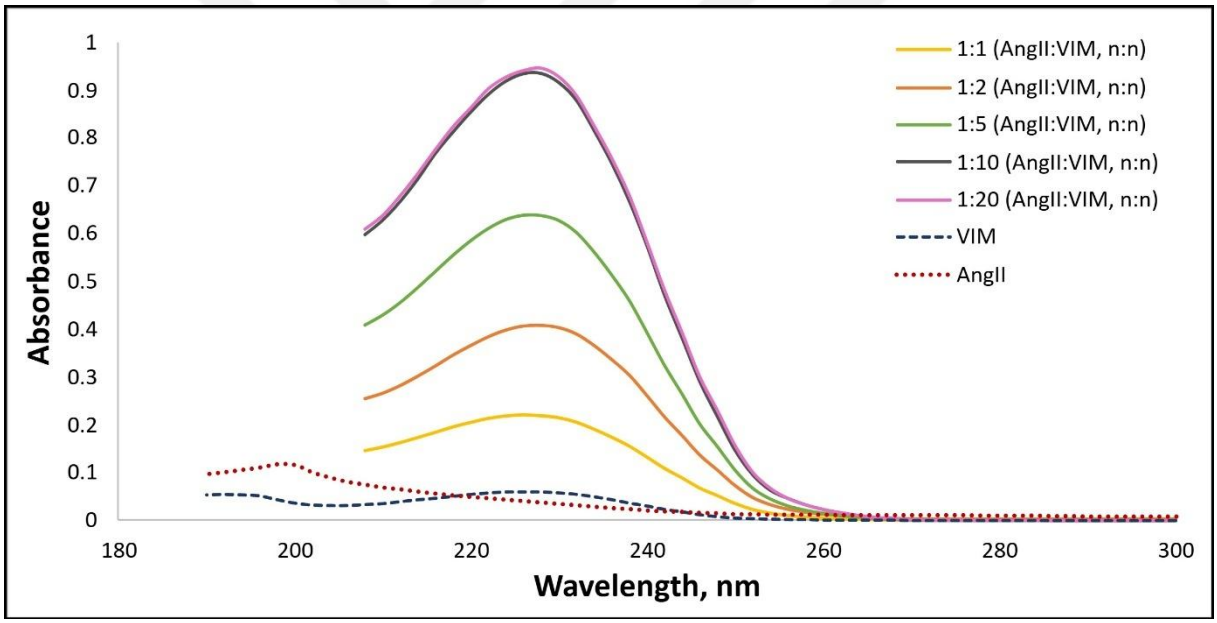

Figure 4.1. UV-VIS absorption spectra of AngII:VIM (n:n) mixtures prepared in 1:1, 1:2, 1:5, 1:10 and 1:20 ratios and AngII and VIM samples (VIM: 2-Vinylimidazole).

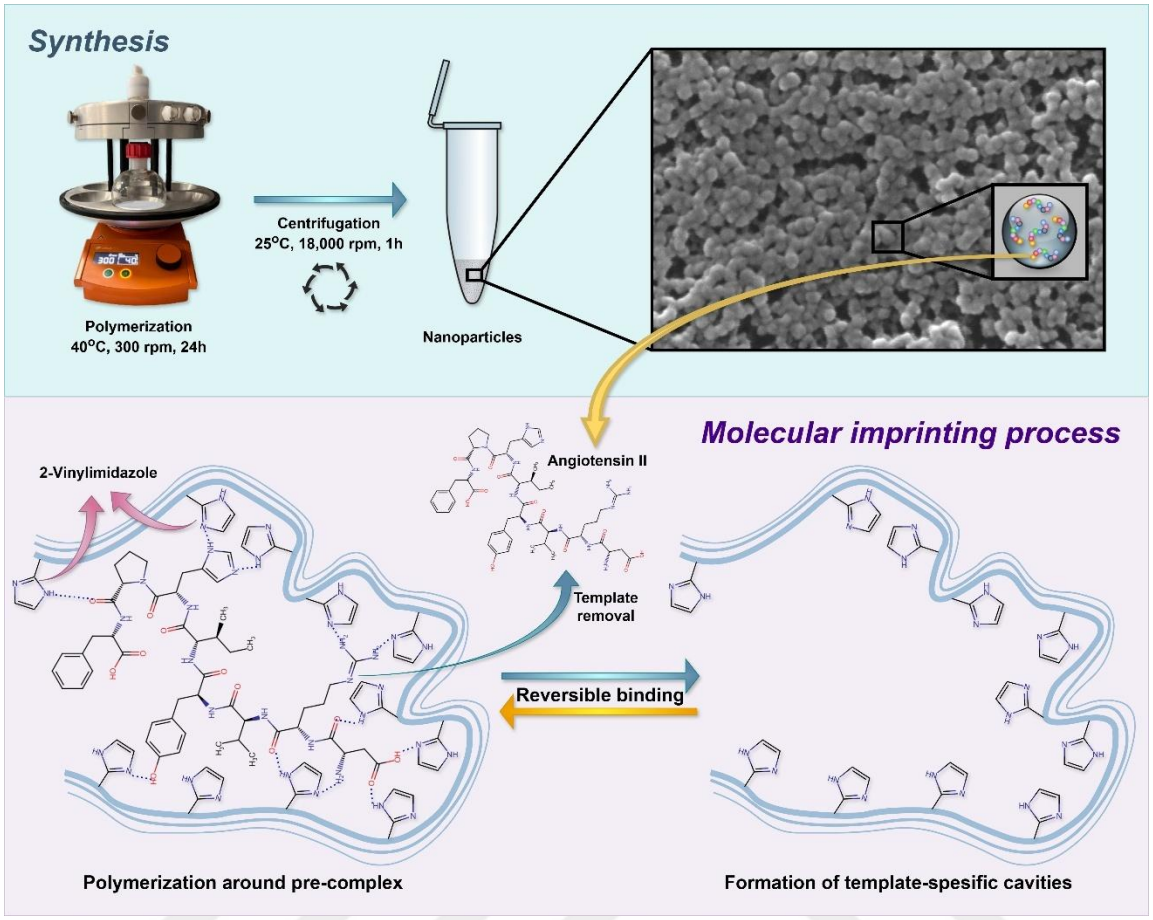

Figure 4.2. Schematic representation of the synthesis and molecular imprinting process for AngII-imprinted nanoparticles.

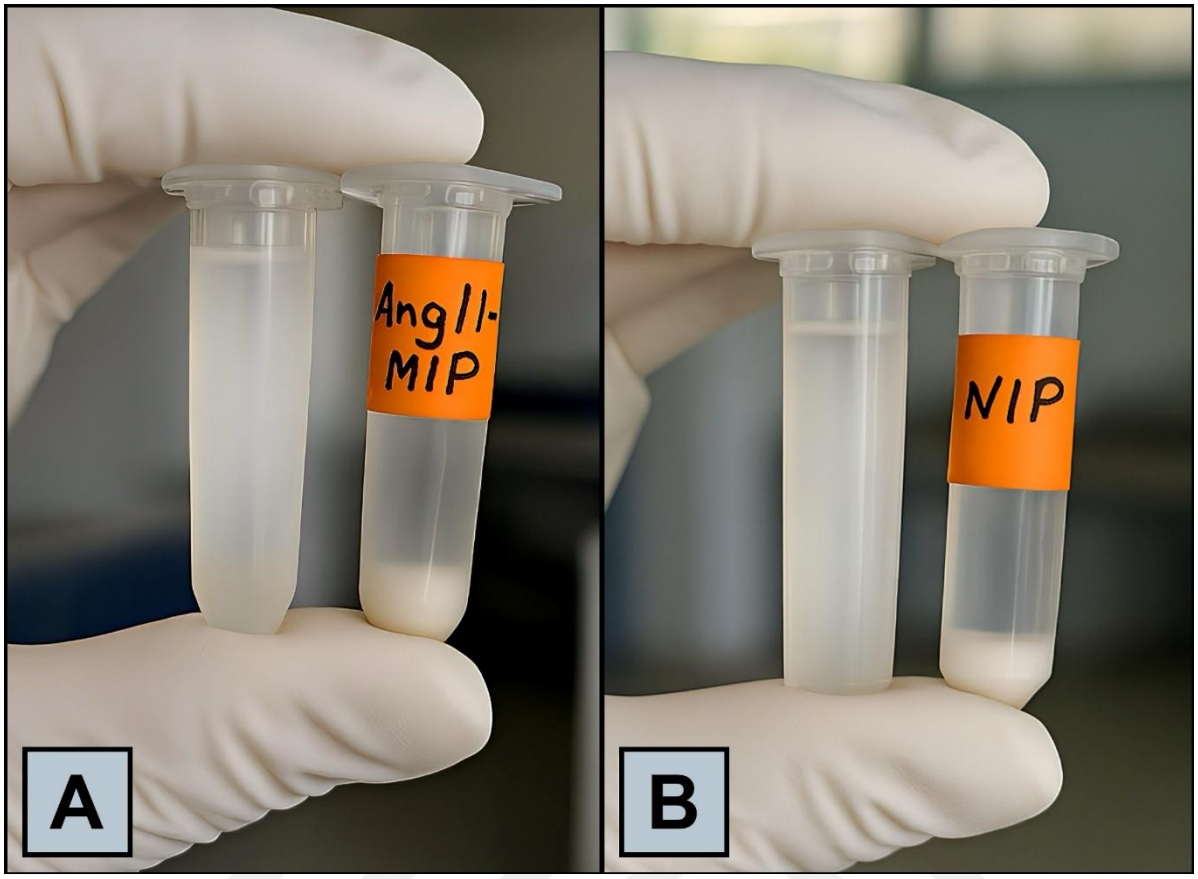

Figure 4.3. Optical photographs of **A)** AngII-MIP and **B)** NIP nanoparticles, before and after centrifuge.

4.2. Characterization of Synthesized AngII-MIP and NIP Nanoparticles

4.2.1. Zeta-sizer Analysis

According to zeta-sizer analysis results, average diameter size of AngII-MIP and NIP were found to be 47.73 and 46.03, respectively (Figure 4.4). Detection of particles below 50 nm with good result quality indicates that stable cross-linked polymers are obtained. In Figure 4.4, one and smooth peaks for both AngII-MIP and NIP demonstrate that there is no aggregation of particles and there is no micro-size particles.

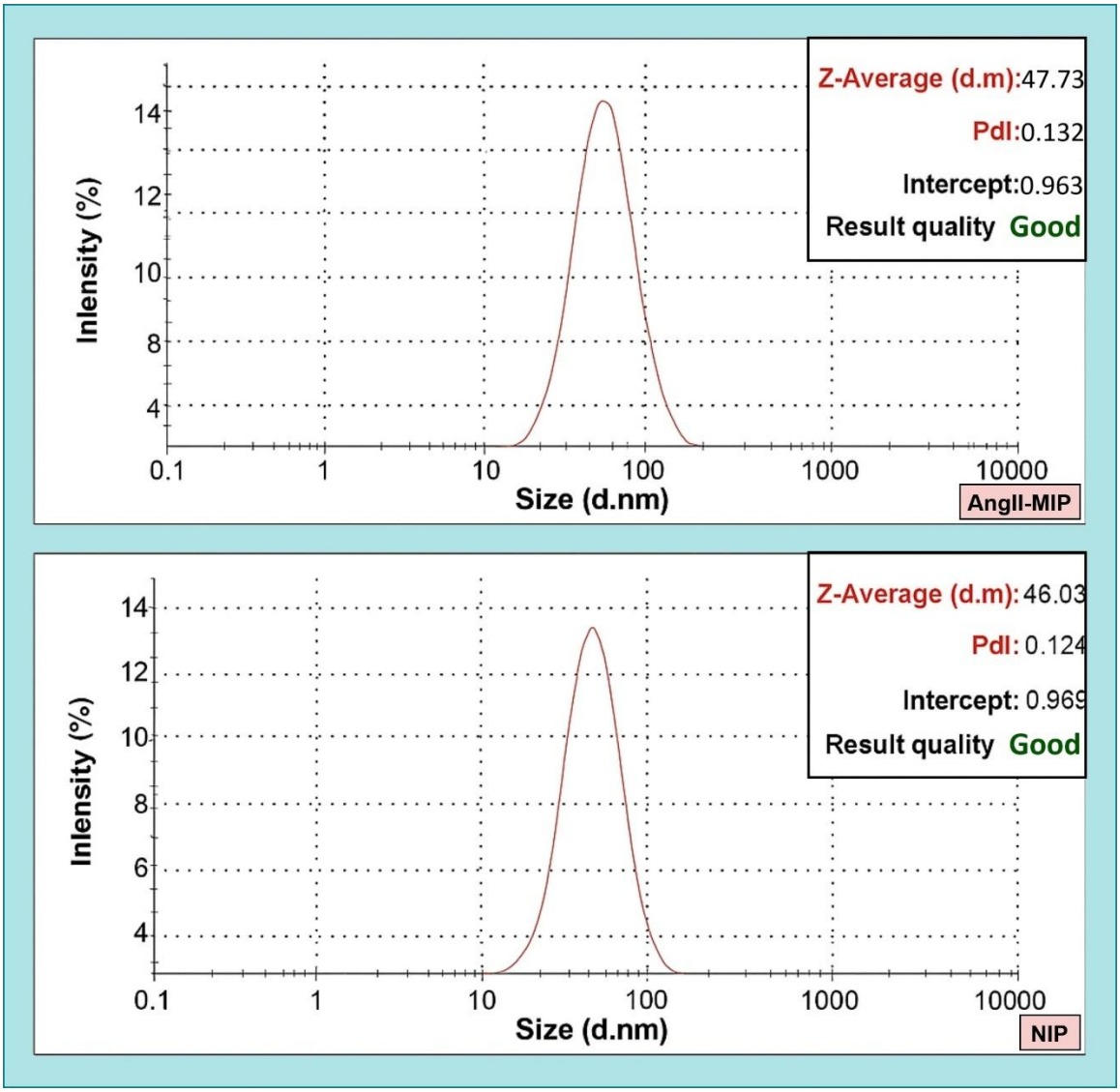

Figure 4.4. Results of size analysis of AngII-MIP and NIP nanoparticles via zeta-sizer.

The morphological characteristics of the synthesized nanoparticles were first examined using SEM. As shown in Figure 4.5, the nanoparticles were uniformly distributed across the surface without significant aggregation, indicating effective colloidal stability during synthesis. The majority of particles were below 50 nm in diameter, which is in agreement with the hydrodynamic diameter results obtained from zeta-sizer. The use of a miniemulsion polymerization technique—combined with suitable surfactants and stabilizers—enabled the controlled nucleation and growth of nanoparticles. The confined aqueous domains within the emulsion droplets served as effective nanoreactors, promoting uniform particle formation and limiting overgrowth or agglomeration.

Further insights into particle morphology and size were obtained through TEM. As illustrated in Figure 4.6, the nanoparticles displayed a predominantly spherical shape with well-defined boundaries and discrete dispersion. The average particle size was measured to be approximately 50 nm, consistent with both SEM and zeta-sizer results. The uniform contrast observed in TEM images suggests homogeneity in the internal structure and confirms that the imprinting and template removal steps did not compromise particle integrity. Overall, the combined SEM and TEM analyses demonstrate that the applied polymerization strategy successfully yields spherical, monodisperse nanoparticles below 50 nm, making them suitable for subsequent surface functionalization and biosensing applications.

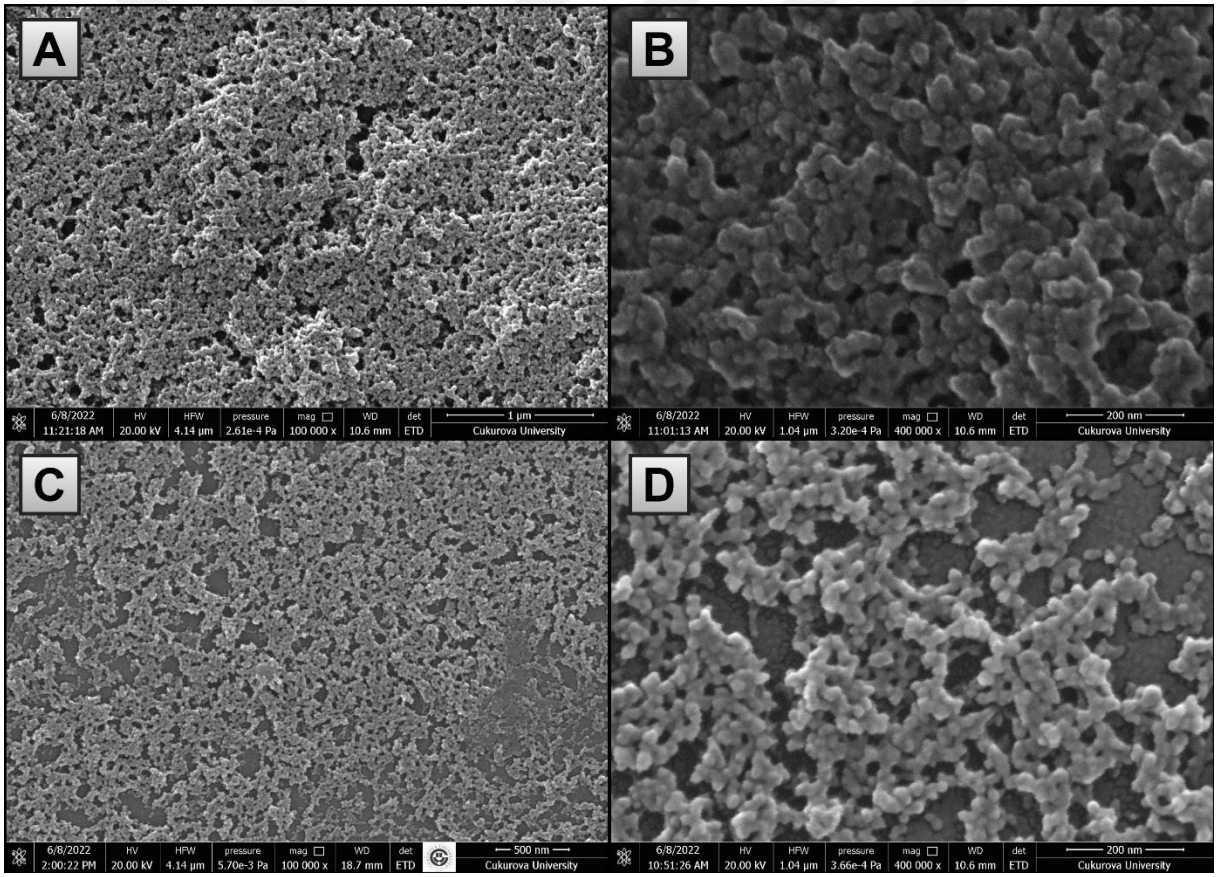

Figure 4.5. SEM images of AngII-MIP and NIP nanoparticles. **A, B)** AngII-MIP (100KX and 400KX magnification); **C, D)** NIP (100KX and 400KX magnification).

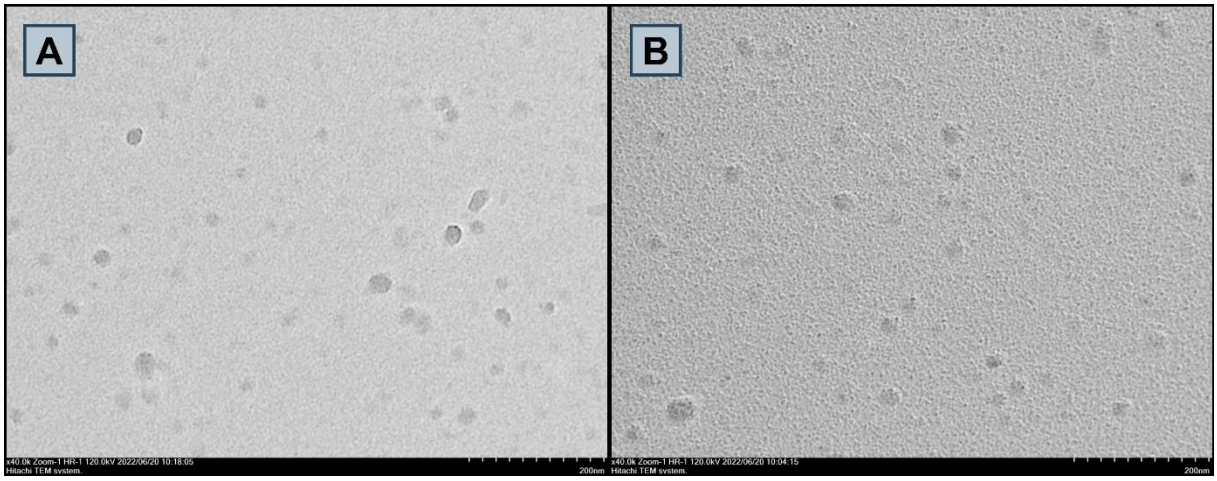

Figure 4.6. TEM images of **A)** AngII-MIP nanoparticles (40X magnification); **B)** NIP nanoparticles (40X magnification).

FTIR spectroscopy was used to analyze the chemical structures of VIM, AngII, their precomplex, as well as the AngII-MIP and NIP nanoparticles. The formation of the precomplex was confirmed by significant changes in characteristic FTIR peaks, indicating secondary interactions such as hydrogen bonding between VIM and AngII (Figure 4.7).

In the FTIR spectrum of AngII, characteristic peaks include the C=C stretching vibration near 1625 cm^{-1}, aromatic C-H bending around 1500-1512 cm^{-1}, and broad O-H stretching in the range of 3600-3500 cm^{-1}. Additionally, C-H stretching at ~2960 cm^{-1} and C-O stretching around 1249 cm^{-1} are evident. For VIM, the N-H stretching band appears between 2820-3000 cm^{-1}, with a notable carboxylic acid O-H stretch near 3112 cm^{-1}, along with imidazole ring vibrations such as C=N-C aromatic ring stretching around 1504 cm^{-1} and C-N ring bending at 1024 cm^{-1} (Arısoy and Baydemir Peşint, 2025). Upon complexation, the FTIR spectrum of the AngII-VIM precomplex revealed a broad and intensified O-H stretching band around 3400 cm^{-1}, suggesting the formation of strong hydrogen bonds. Additionally, a shift in the C=N stretching band to lower wavenumbers and an increase in the intensity of the C=N-C aromatic ring vibration confirmed the presence of π-π stacking and electrostatic interactions. Perturbations in other functional group regions such as amide I/II (~1650-1550 cm^{-1}), C-H bending (~1112 cm^{-1}), and C-N stretching (~1024 cm^{-1}) further supported successful precomplexation. These spectral shifts collectively confirm the formation of a stable molecular precomplex, essential for effective molecular imprinting (Figure 4.7).

In the FTIR spectra of both AngII-MIP and NIP nanoparticles, the main absorption bands largely reflect the presence of HEMA and EGDMA, which are the dominant components. Both nanoparticles show a broad O-H stretching band at 3331 cm^{-1}, attributed to HEMA. Aliphatic C-H stretching bands appear around 2950 cm^{-1} due to methyl groups in HEMA and EGDMA, while the C=O stretching bands from EGDMA are observed between 1700-1730 cm^{-1}. Additionally, both samples exhibit C-O stretching bands near 1140 cm^{-1}. Distinctive differences between AngII-MIP and NIP are also evident, confirming successful imprinting. In AngII-MIP, an absorption band around 1200 cm^{-1} is observed, corresponding to the stretching vibrations of amine groups. This band is absent in the NIP spectrum, indicating the presence of amine functionalities within the imprinted cavities of AngII-MIP. Furthermore, AngII-MIP displays a peak near 1630 cm^{-1}, which can be attributed to C=C and C=N stretching vibrations, likely originating from the AngII-VIM precomplex. Compared to NIP, AngII-MIP also exhibits a more intense peak at 1245 cm^{-1}, associated with the C-O group from VIM, and a carboxyl group band at 1140 cm^{-1}, further supporting the incorporation of VIM into the AngII-MIP structure. Overall, the observed shifts and additional peaks in the AngII-MIP spectrum, relative to NIP, demonstrate the successful incorporation of VIM and AngII into the polymer matrix, confirming the formation of specific recognition sites in the MIP (Figure 4.8).

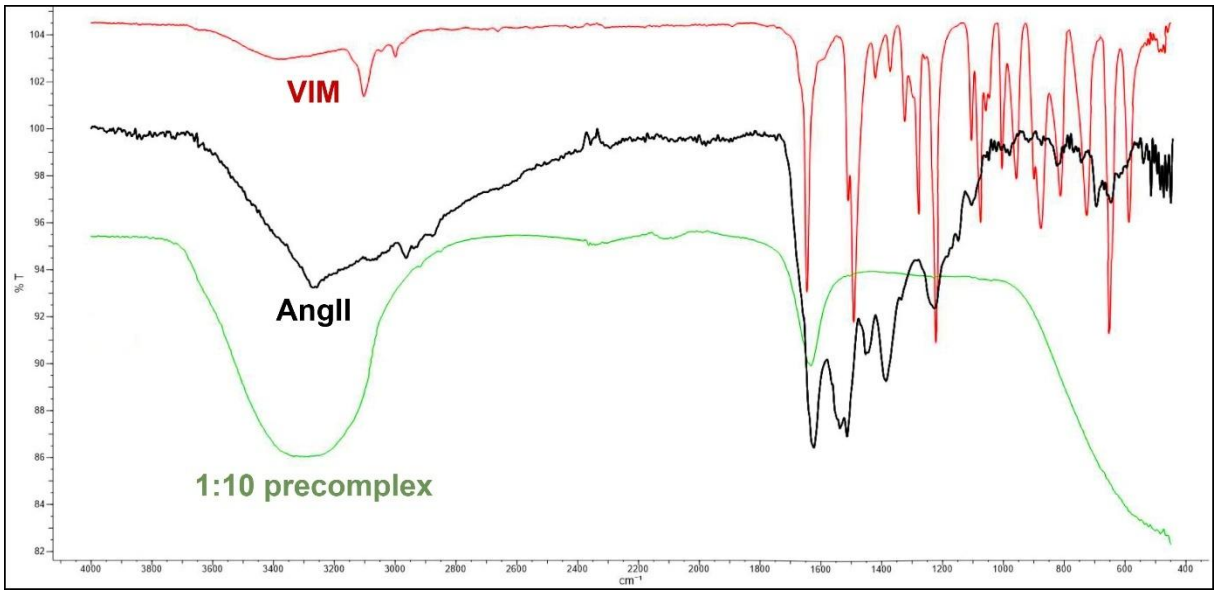

Figure 4.7. FTIR Spectra of Ang II, VIM and AngII:VIM (1:10, n:n) precomplex.

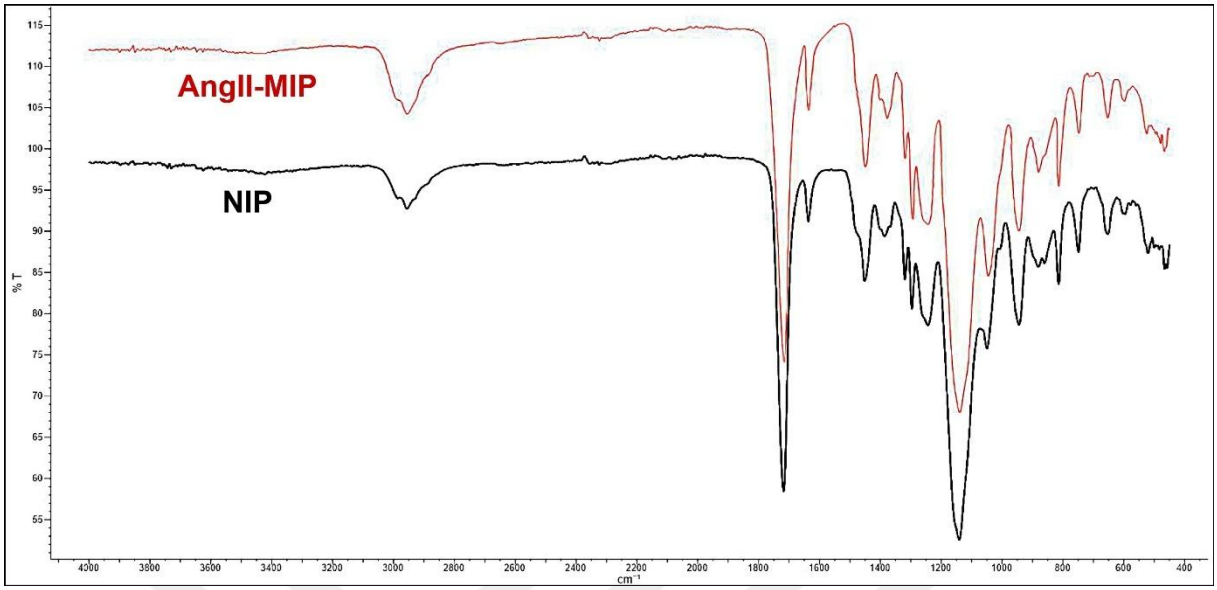

Figure 4.8. FTIR Spectra of AngII-MIP and NIP nanoparticles.

4.3. Fabrication of Nanoparticle-coated QCM Chips

QCM chips coated with AngII-MIPs and NIPs were fabricated. For this purpose, QCM chips were washed for 3 minutes in piranha solution, a strong oxidizing agent that can remove organic contaminants from acidic surfaces. Next, the QCM chips were washed for 15 minutes with distilled water, followed by 15 minutes with pure ethanol, and then left to dry for 1 hour. Once the surface was completely dry, 15 µL of allyl mercaptan was dropped onto the center of the gold surface of the chips to activate the surface with mercaptan groups. The chips were then left overnight in a fume hood for activation. After activation with allyl mercaptan, AngII-MIPs were applied to one chip, while NIPs were applied to another as a control group. To ensure the nanoparticles adhered to the surface, the chips were exposed to UV light for 20 minutes. Finally, the QCM chips coated with nanoparticles (Figure 4.9) were washed for 15 minutes with distilled water, followed by 15 minutes with pure ethanol, and left to dry for 1 hour.

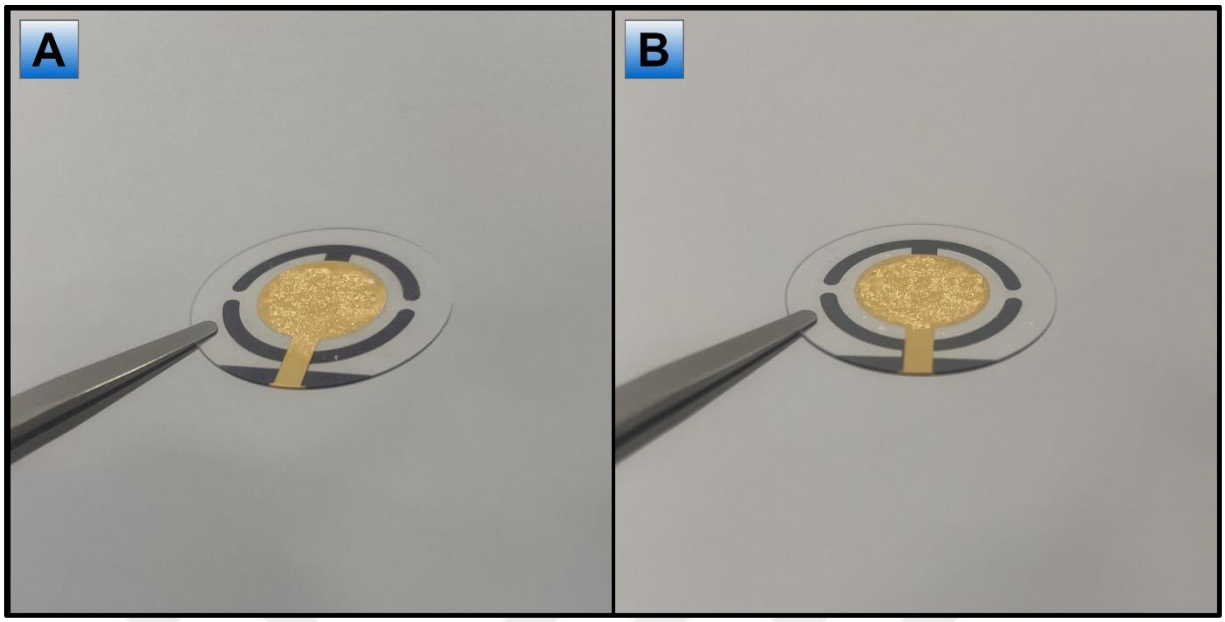

Figure 4.9. Optical photographs of **A)** AngII-MICqcm and **B)** NICqcm.

Washing step before getting into template removal and binding studies was applied with ultrapure water using QCM tools in a continious system to make sure there is no residual elements. This step was continued until the frequency stabilizes. AngII-imprinted nanoparticles were immobilized on the QCM chip without removing the template molecule. After the washing process was completed, the removal of the template molecule was initiated. During this process, a 0.03 M NaCl solution prepared in phosphate buffer at pH 7.4 was used to simulate physiological conditions. Continuous interaction with the QCM device was maintained, circulating the solution in the system until the frequency stabilized. The stabilization of the frequency theoretically indicates that the template molecule has been completely removed from the QCM chip (Figure 4.10).

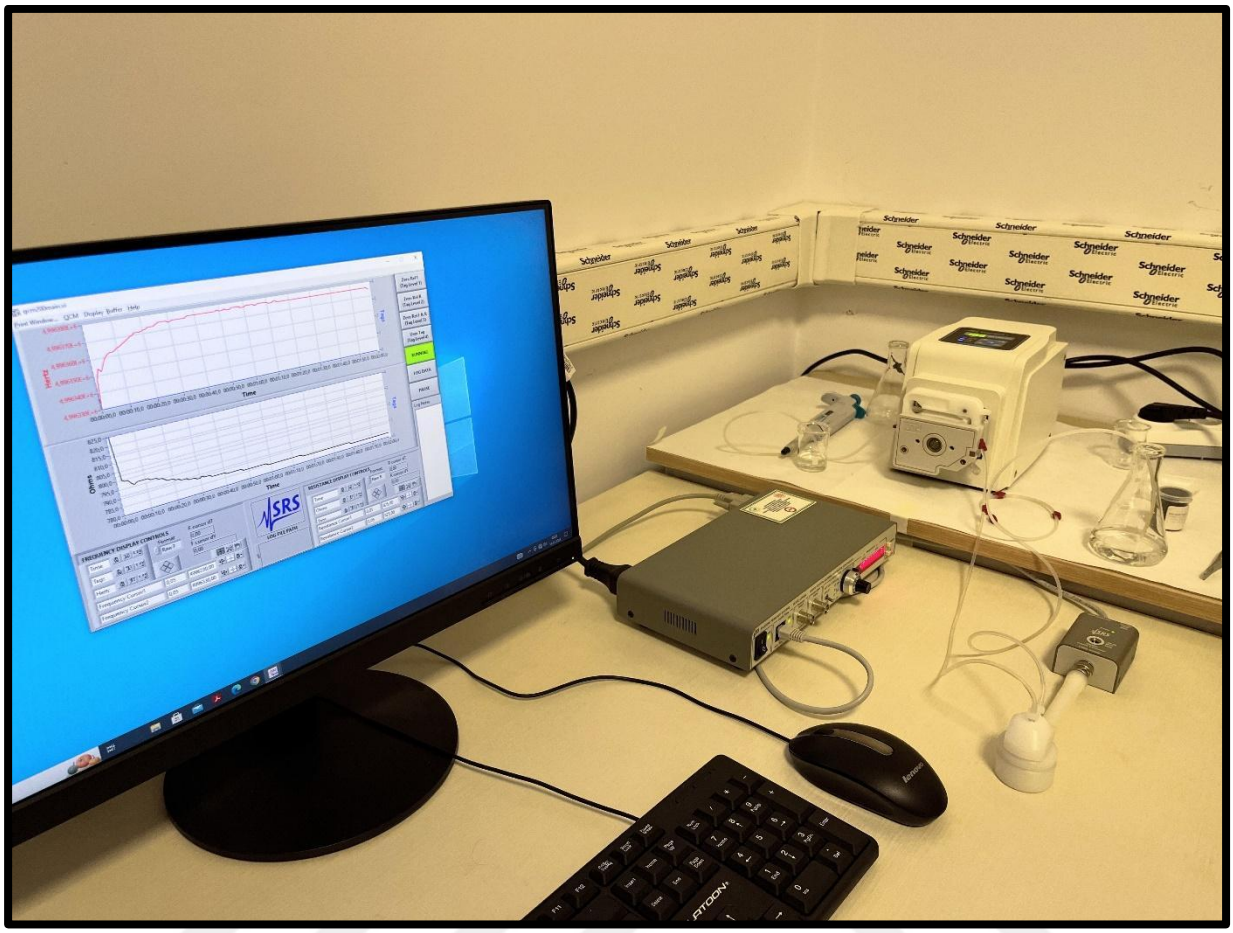

Figure 4.10. Washing QCM chip in a continuous system using QCM tools until frequency stabilizes.

4.4. Characterization of QCM Chips

4.4.1. Contact Angle

According to contact angle measurements, it can be seen that the contact angle value of the AngII-MICqcm chip is lower compared to the contact angle value of the NIPqcm chip. The decrease in the contact angle of the AngII-MICqcm chip indicates that the hydrophilicity of the surface increases. This can be explained by the VIM and AngII content in the AngII-MICqcm chip. The contact angle was used to determine the hydrophobic/hydrophilic properties of QCM chip surfaces modified with allyl mercaptan, including AngII-imprinted (AngII-MIP) and non-imprinted (NIP) surfaces. The contact angle values of unmodified chips, as well as those coated with AngII-MIP and NIP, were measured by placing a drop of water on the chip surface using an Attension Theta Lite device (Biolin Scientific Ltd., Sweden). Measurements were taken from

at least three different positions on the chip, and the average of these measurements was calculated to determine the contact angle values. Upon evaluating the results, the contact angle values for the unmodified, AngII-MICqcm and NICqcm chips were found to be, 57.07°, and 63.87°, respectively (Figure 4.11).

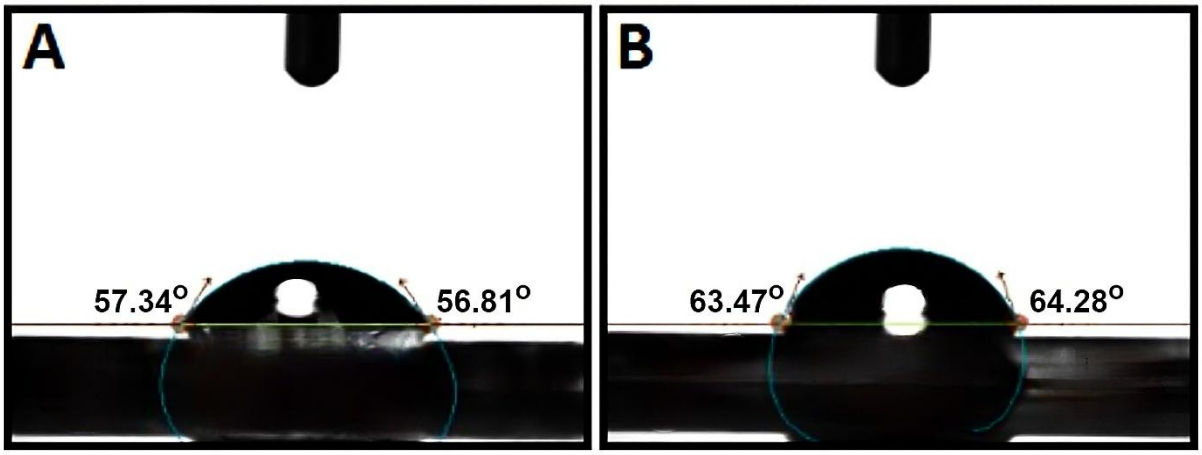

Figure 4.11. Contact angle measurements of **A)** AngII-MICqcm and **B)** NICqcm chip.

It is observed that the contact angle value of the AngII-MICqcm chip is lower compared to that of the NICqcm chip. The decrease in the contact angle of the AngII-MICqcm indicates an increase in the hydrophilic property of the surface. For the imprinted and non-imprinted QCM chips prepared for the detection of AngII in human serum, 2-hydroxyethyl methacrylate (HEMA), which possesses hydrophilic properties, was used as the main monomer. Therefore, coating the chip surface with a hydrophilic polymer has increased the surface's hydrophilicity.

4.4.2. Atomic Force Microscopy Analysis

Atomic force microscopy (AFM) was employed to characterize the surface morphology and topography of the unmodified QCM chip, the NICqcm chip, and the AngII-MICqcm chip. AFM imaging was performed in semi-contact mode using a Park Systems NX10 AFM (South Korea). The samples were fixed onto the sample holder using double-sided adhesive tape.

Figure 4.12 presents the AFM images and surface profile analyses. The unmodified QCM chip (Figure 4.12A) exhibited a relatively smooth surface, with a maximum surface height of approximately 4.5 nm. In contrast, the NIP-coated chip (Figure 4.12B) displayed increased

surface roughness, with particulate structures and a maximum height of around 33 nm. The AngII-MICqcm chip (Figure 4.12C) exhibited the most prominent surface features, with a highly textured morphology and a maximum height reaching approximately 55 nm.

The increased surface roughness observed in the AngII-MICqcm chip indicates the successful deposition of the imprinted polymer layer. The more structured topography suggests a higher polymer density and more complex surface architecture, likely due to the incorporation of AngII during the imprinting process. These results confirm the effective surface modification of the QCM chip through molecular imprinting and support the presence of a distinct imprinted layer suitable for selective AngII detection.

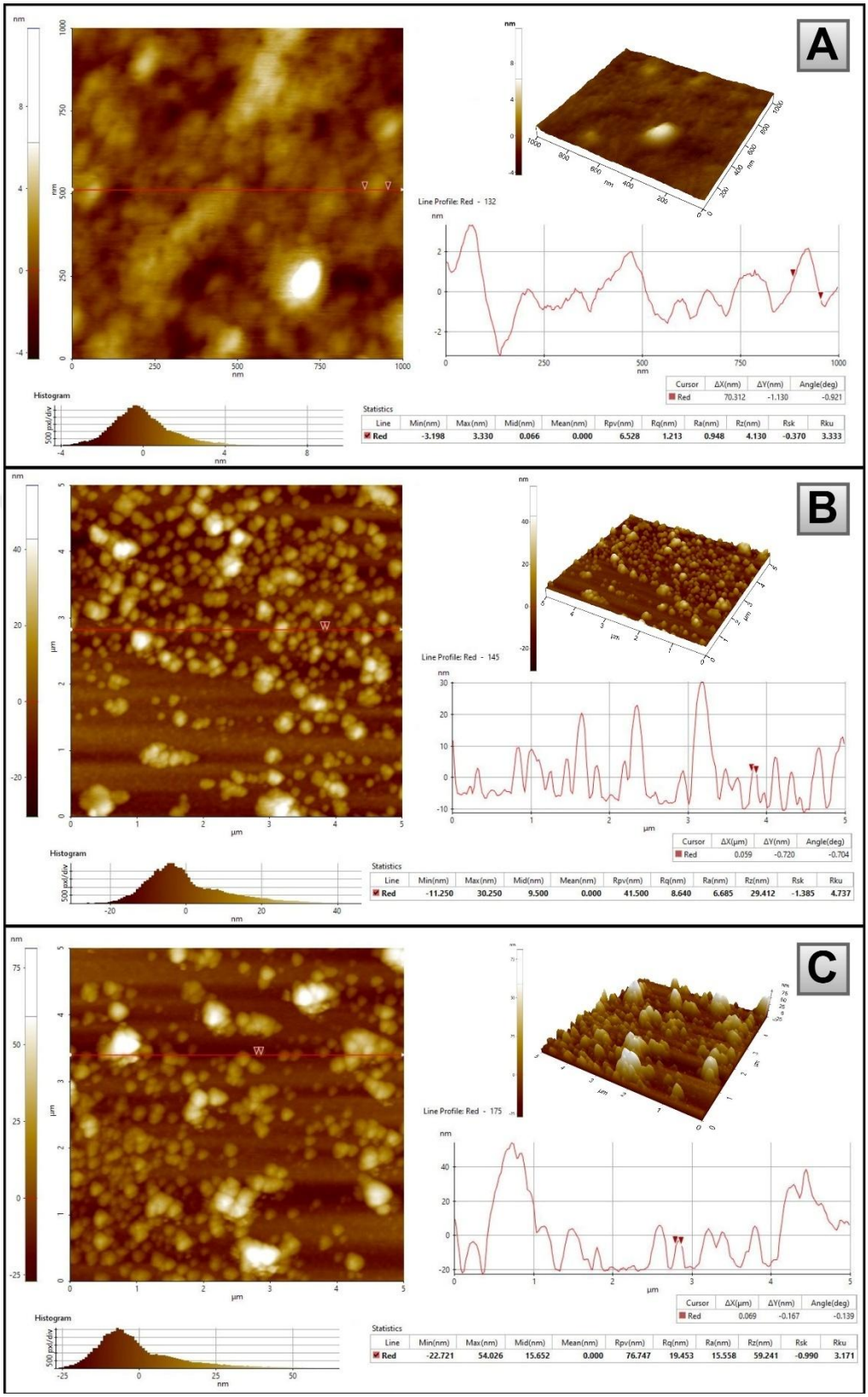

Figure 4.12. AFM results of **A)** plain QCM chip, **B)** NICqcm and **C)** AngII-MICqcm.

4.4.3. SEM Analysis of Nanoparticle coated QCM Chips

After attaching the nanoparticles to the surface of the QCM chips, SEM analysis (FEI, Quanta 650 Field Emission SEM, USA) was performed to demonstrate that the nanoparticles were not released from the surface during the washing processes. Prior to the analysis, the AngII-MIPqcm/NIPqcm chips were dried in an oven at 40°C. Following the drying process, nanoparticle samples were fixed onto an SEM sample plate using a conductive adhesive for imaging. To make the surface conductive, the sample surface was coated with gold under vacuum, and SEM images were obtained (Figure 4.13). According to the SEM images, it was observed that the AngII-MIP and NIP nanoparticles were not released from the QCM chip surface and were evenly distributed across the surface.

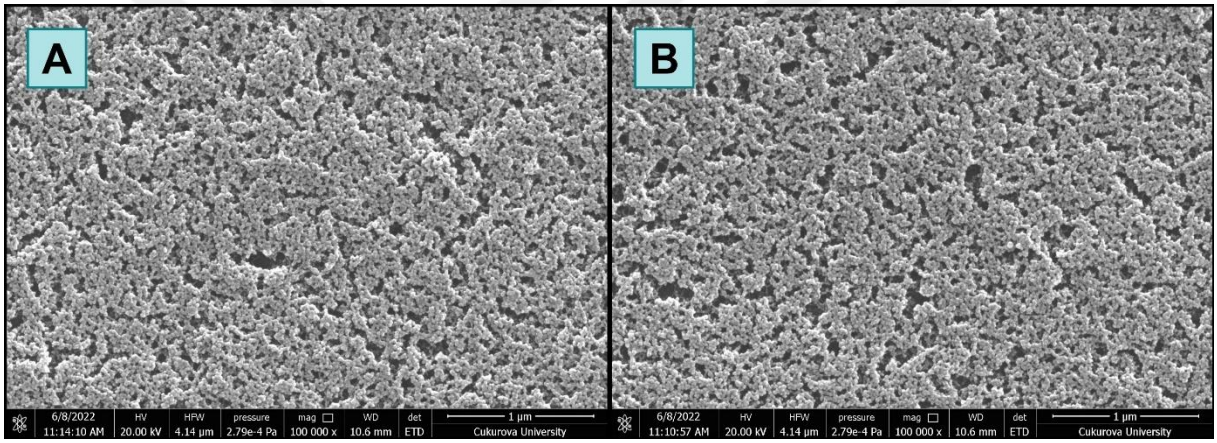

Figure 4.13. SEM images of **A)** AngII-MICqcm chip, **B)** NICqcm chip (100,000X magnification).

4.5. AngII Binding and Kinetic Analysis Studies with AngII-MICqcm/NICqcm

The frequency changes observed during the adsorption of AngII solutions at different concentrations (0.25, 0.5, 1, 2.5, 5, 10, 15, 25, 50, and 100 pg/mL) onto the QCM chip coated with AngII-imprinted nanoparticles are presented in Figure 4.14. For each concentration, the chip was first washed with pure water to return it to its initial conditions. After the washing process, the AngII solution was introduced onto the chip, causing the frequency to rapidly decrease. From approximately the 10th minute onward, no significant change in frequency was observed, indicating that the adsorption process was complete. After adsorption was complete, the chip was washed again with pure water. During this step, nonspecific bindings were

removed, and the frequency change reflecting the true adsorption amount was obtained. Following the washing process, the desorption phase began. Desorption was continued until the frequency value reached equilibrium again. These frequency changes demonstrate the extent to which AngII binds to the MIP-coated sensor surface and how effectively nonspecific bindings were removed during the washing steps.

Figure 4.14 presents the QCM sensor responses of the AngII-MICqcm chip upon exposure to AngII solutions at increasing concentrations. Part A shows the real-time frequency shifts (ΔF) during baseline, adsorption, washing, and desorption phases. Part B displays the calibration curve based on maximum frequency changes, while Part C presents the corresponding mass change (Δm) values calculated using the Sauerbrey equation. Both ΔF and Δm increased proportionally with AngII concentration, demonstrating a clear concentration-dependent response and indicating the high sensitivity of the AngII-MICqcm sensor in the picogram per milliliter range.

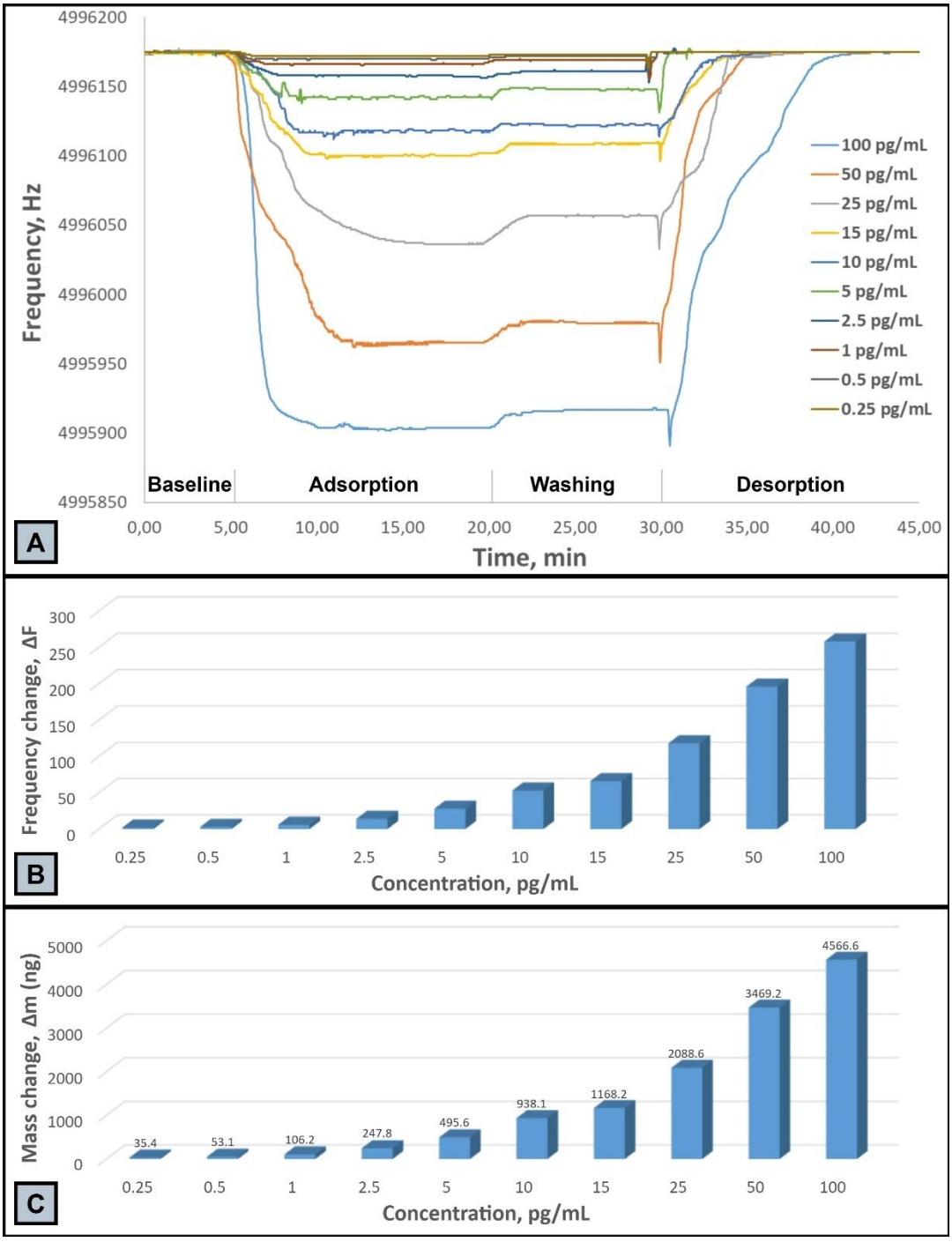

Figure 4.14. QCM sensor responses of the AngII-MICqcm chip at varying AngII concentrations. **A)** Real-time frequency shifts (ΔF) recorded during baseline, adsorption, washing, and desorption phases. **B)** Maximum frequency changes (ΔF) observed during adsorption of AngII solutions (0.25-100 pg/mL). **C)** Corresponding mass changes (Δm) calculated from ΔF values using the Sauerbrey equation.

The analytical sensitivity of the developed QCM sensor was assessed by calculating the limit of detection (LOD) and limit of quantification (LOQ), using Equations 3 and 4, respectively. For these calculations, the slope (S = 70.21 ng/pg·mL) from the calibration curve and the standard deviation (σ = 3.0 Hz) from blank frequency measurements (without AngII) were utilized. Calculated values indicated an LOD of approximately 0.141 pg/mL and an LOQ of about 0.427 pg/mL, confirming the system's capability for ultra-sensitive detection at sub-picogram concentrations. The obtained LOQ slightly exceeding the lowest tested concentration (0.25 pg/mL) indicates reliable quantitative accuracy within the tested range. However, the determined LOD lies below the minimum experimentally validated concentration, and thus should be regarded as theoretical. To empirically confirm detection performance at lower concentrations, additional experimental validation below 0.25 pg/mL is necessary.

4.5.1. Adsorption Isotherm Models

Adsorption isotherms are mathematical models describing analyte binding onto solid surfaces. Among the commonly employed isotherms are Langmuir, Freundlich, and Langmuir-Freundlich models. The Langmuir model assumes monolayer binding with uniform adsorption energy across the surface and negligible interaction between adsorbed molecules. Conversely, the Freundlich model considers surface heterogeneity, allowing multilayer adsorption with varying energy levels and interactions among neighboring molecules. The Langmuir-Freundlich isotherm merges both perspectives, describing heterogeneity in adsorption energies. At low analyte concentrations, it behaves similarly to the Freundlich model, while at higher concentrations it transitions towards Langmuir characteristics.

Experimental findings from this study revealed that adsorption at lower AngII concentrations fitted better to the Freundlich model, implying surface heterogeneity and potential multilayer interactions. At higher concentrations, however, the data were better aligned with the Langmuir isotherm, suggesting saturation of binding sites and dominance of monolayer adsorption.

In this context, it can be stated that the adsorption process on a gold surface coated with nanoMIPs follows the Freundlich isotherm, which considers heterogeneity and multilayer adsorption, at low concentrations (0.25-50 pg/mL) and the Langmuir isotherm, which describes homogeneous and monolayer adsorption, at high concentrations (0.5-100 pg/mL). This suggests

that the binding sites on the surface vary in terms of both energy and occupancy, causing adsorption behavior to change across different concentration ranges (Figure 4.15).

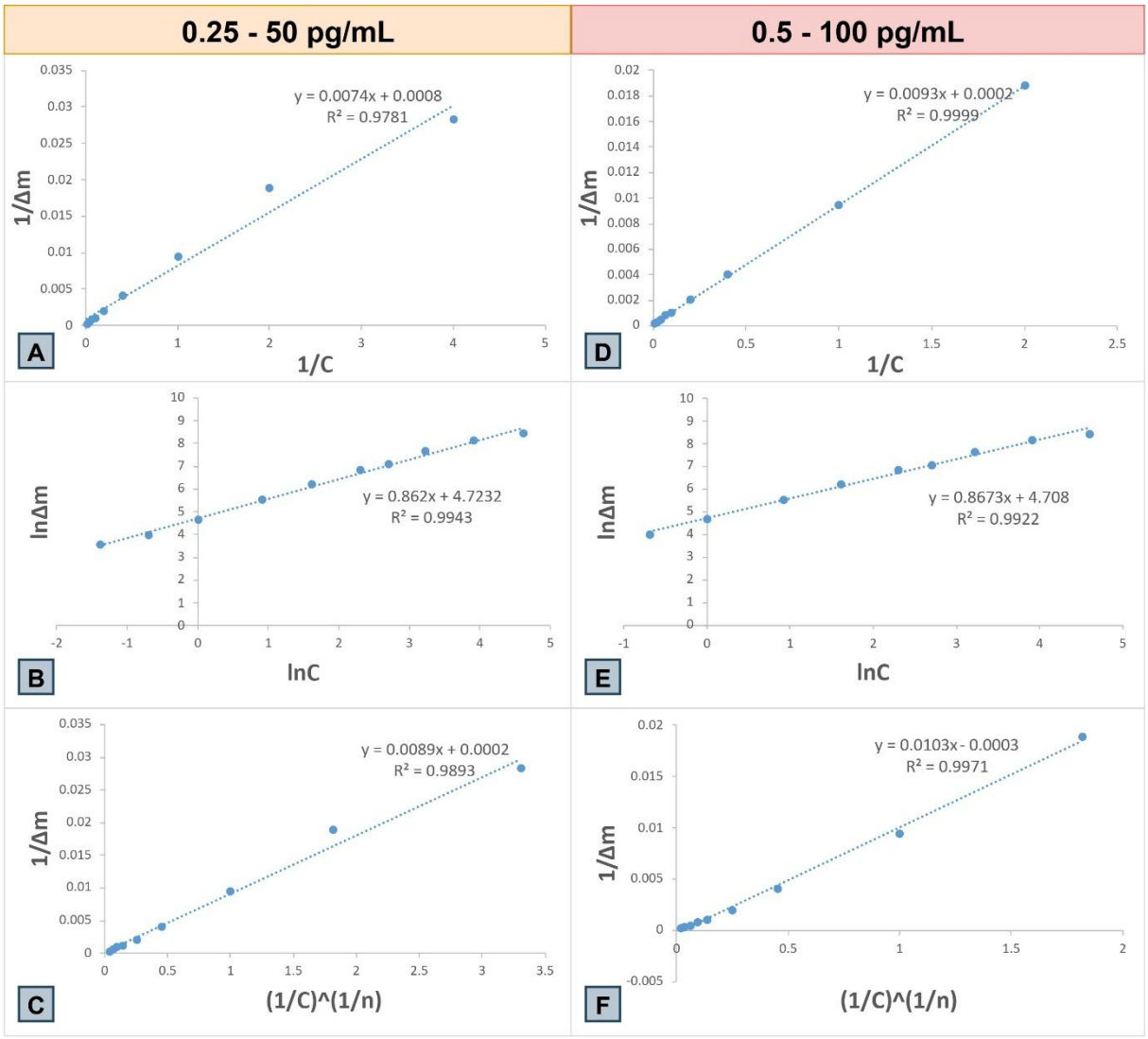

Figure 4.15. Adsorption isotherm linearization plots for AngII-MICqcm sensor: **A-C)** 0.25-50 pg/mL concentration range and **D-F)** 0.5-100 pg/mL. A and D correspond to Langmuir, B and E to Freundlich, and C and F to Langmuir-Freundlich models.

4.6. Competitive Binding Analysis of AngII Using AngII-MICqcm/NICqcm

The AngII molecule exhibits the highest frequency and mass changes on the AngII-MICqcm chip, demonstrating the high affinity and selectivity of the AngII-MICqcm chip for AngII. Specifically, the Δm value for AngII adsorption on the AngII-MICqcm chip was calculated as 1185.9 ng, representing a remarkably high binding capacity. In contrast, the Δm values on the

same AngII-MICqcm chip were considerably lower for AngI (194.7 ng) and Vasp (159.3 ng), clearly demonstrating the selective nature of the imprinted surface toward AngII.

To quantify this selectivity, selectivity coefficients ($K_{AngII\text{-}MICqcm}$) were calculated, yielding values of 6.09 for AngI and 7.44 for Vasp. These high $K_{AngII\text{-}MICqcm}$ values indicate that the AngII-MICqcm chips have significantly greater affinity for AngII compared to structurally related molecules. Additionally, imprinting factors (IF), representing the enhancement of selectivity due to imprinting, were determined as 5.58 for AngII, 3.67 for AngI, and 4.5 for Vasp. These IF values further underline the high specificity of the AngII-MICqcm chips, as they effectively distinguish AngII while minimizing nonspecific interactions observed in NICqcm chips.

Interestingly, while the AngII-MICqcm chips show significantly different adsorption capacities for AngII compared to other molecules, the adsorption differences among molecules on the NICqcm chips were much smaller, reflecting non-specific binding behavior. Thus, AngII-MICqcm chips effectively discriminate AngII from other structurally similar molecules, such as AngI and Vasp, even at low concentrations (Figure 4.16). This feature underscores the potential utility of these selective AngII-MICqcm chips in clinical diagnostic settings as reliable and sensitive biosensing platforms..

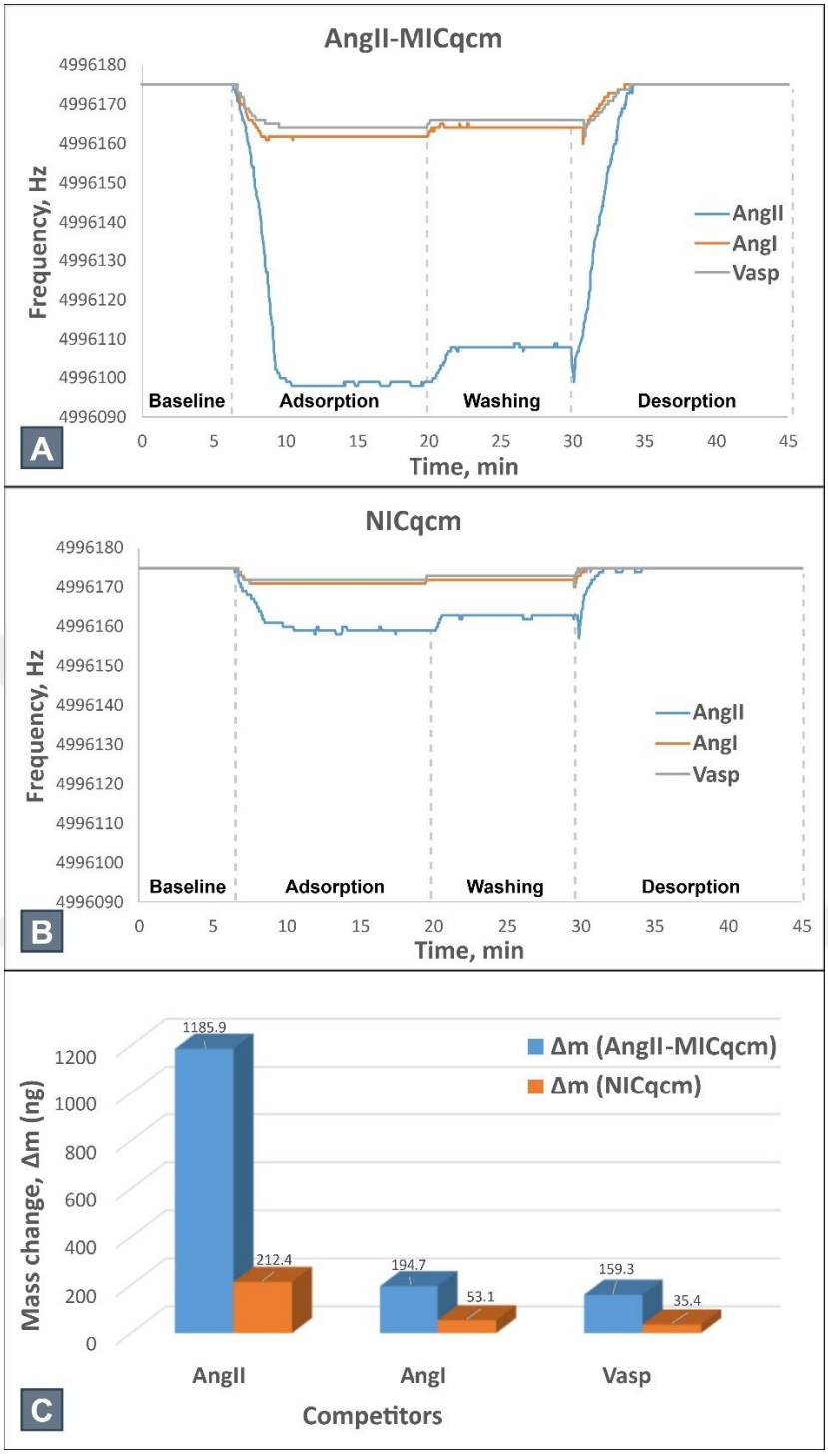

Figure 4.16. Selectivity Studies. **A)** Frequency changes caused by AngII, AngI, and Vasp molecules bound to the AngII-MICqcm chip, **B)** Frequency changes caused by AngII, AngI, and Vasp molecules bound to the NICqcm chip, **C)** Mass change values (Δm) induced by the molecules bound to the chip surfaces.

Table 4.1. Selectivity studies with AngII-MICqcm ve NICqcm.

Competitors	Δm (MIP) ng	kMIP	Δm (NIP) ng	kNIP	IF
AngII	1185.9	-	212.4	-	5.58
AngI	194.7	6.09	53.1	4	3.66
Vasp	159.3	7.45	35.4	6	4.5

4.7. Reusability Studies

The reusability and stability of AngII-MICqcm chips modified with nanoparticles were evaluated. For this purpose, 10 consecutive adsorption-desorption cycles were performed to determine whether the AngII adsorption capacity was maintained during each cycle. The experiments were conducted using a 15 pg/mL AngII solution, and the adsorption capacity of the chip surface was measured after each cycle. The results indicated that the adsorption-desorption process could be successfully repeated without a noticeable loss in adsorption capacity after each cycle. It was found that after the 10th cycle, the QCM chip retained approximately 96% of its AngII adsorption capacity. These high-performing chips demonstrated significant advantages in terms of longevity and reusability. The 96% retention in adsorption capacity suggests minimal loss of functional groups on the chip surface (Figure 4.17).

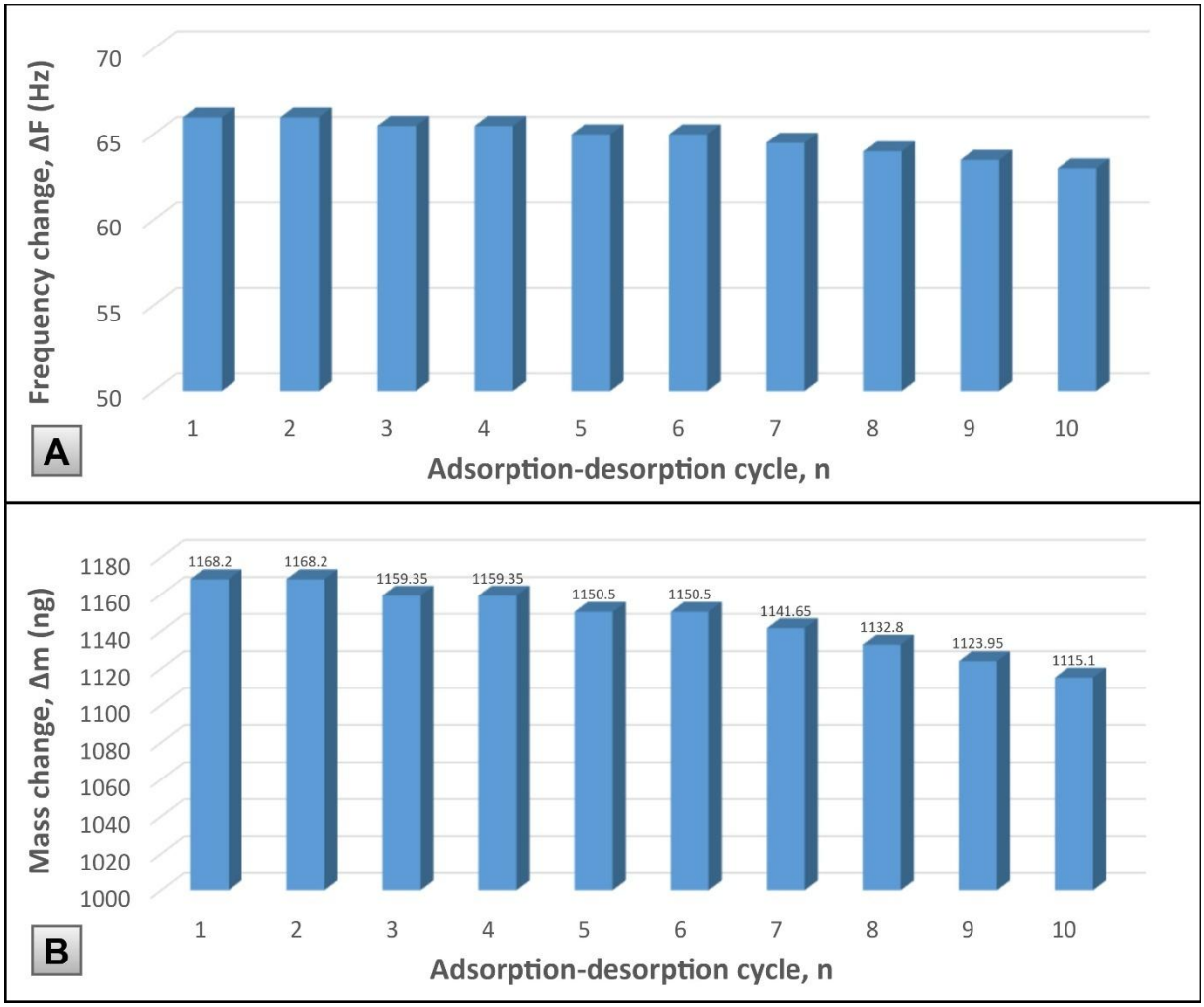

Figure 4.17. Reusability performance of the AngII-MICqcm chip over 10 adsorption-desorption cycles. **A)** Frequency change (ΔF), **B)** Mass change (Δm).

4.8. Detection of AngII in Human Serum Samples Enriched with AngII

In this part of the study, AngII-MICqcm chips were tested for detecting AngII in serum samples enriched at concentrations ranging from 1 to 100 pg/mL. Frequency changes (ΔF) caused by AngII adsorption were measured to evaluate sensor performance. Since QCM detection relies on mass changes, AngII binding resulted in measurable decreases in frequency. As presented in Figure 4.18, frequency shifts became more prominent with higher AngII concentrations, clearly reflecting increased molecular binding to the chip surface. Even at the lowest concentration tested (1 pg/mL), the sensor produced distinct frequency responses compared to control samples, emphasizing the sensor's high sensitivity.

These findings confirm that the developed QCM sensor is both sensitive and selective, effectively detecting AngII from serum samples at extremely low concentrations. Moreover, the negligible frequency shift observed in blank serum samples indicates minimal nonspecific interactions, further underscoring the selectivity and reliability of this QCM-based sensing approach (Figure 4.18).

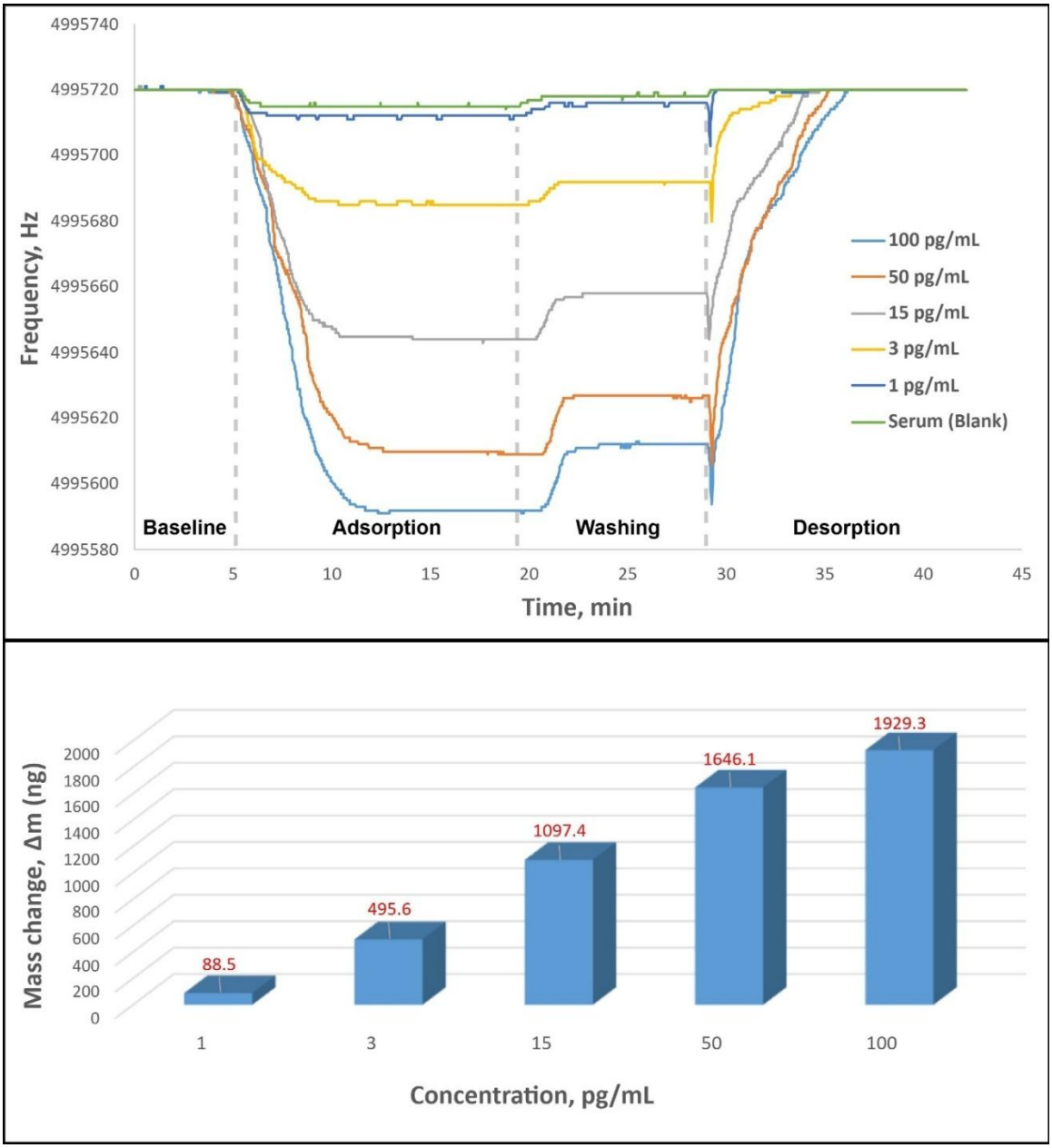

Figure 4.18. Determination of AngII molecule in serum samples enriched with varying concentrations of the AngII molecule.

5. CONCLUSION

AngII is a significant effector peptide of the RAAS and serves as a critical biomarker in the diagnosis and monitoring of various pathological conditions, including infectious diseases, neoplasms, and, most notably, cardiovascular disorders. However, the spontaneous detection of AngII remains challenging due to its low physiological concentration, instability, and the complex nature of biological fluids.

Despite their analytical power, the conventional methods for the analysis of AngII suffer from several limitations that restrict their application in routine diagnostics, especially at the point of care, such as complex sample preparation, high instrumentation cost and maintenance, limited portability and point-of-care feasibility, time-consuming workflows, or antibody limitations in case of ELISA. False positives or inaccurate readings are common in conventional methods.

In this study, molecularly imprinted nanoparticles (~50 nm) were synthesized and well-characterized, and employed as recognition elements in QCM sensor chips for the selective, ultra-sensitive, real-time and label-free detection of AngII in human serum. Integration of molecularly imprinted nanoparticles into ultra-sensitive sensor platforms presented remarkable advantages including high surface area to volume ratio, fast binding kinetics and higher binding site accessibility. On the other hand, QCM provided label-free detection (no need for fluorescent or radioactive tags), real-time monitoring even at very low concentrations (as low as 0.25 pg/mL), fast analysis, and ultra-sensitive detection. So, molecularly imprinted nanoparticle-coated QCM chips are ideal candidates for point-of-care diagnostic tools, where portability, speed, and robustness are essential.

Following the fabrication and characterization of AngII-MICqcm and NICqcm sensor chips, they were used in kinetic binding studies. LOD and LOQ values were calculated as approximately 0.141 pg/mL and 0.427 pg/mL, respectively. These results demonstrate that the developed QCM sensor system possesses ultra-sensitive detection capabilities for AngII, allowing for reliable signal discrimination at sub-picogram concentrations. The fact that the LOQ is slightly above the lowest tested concentration (0.25 pg/mL) confirms the system's ability to provide accurate and repeatable quantification within the studied range. Selectivity

studies revealed the ability of the sensor to discriminate AngII from structurally similar molecules. In competition with AngI and Vasp, AngII-MICqcm sensor yielded selectivity ratios of 6.09 and 7.44, respectively, in favor of AngII. Furthermore, IF values were calculated as 5.58 for AngII, 3.67 for AngI, and 4.50 for Vasp, confirming the successful imprinting process, so the formation of specific recognition sites with minimal nonspecific interactions. These results highlight the AngII-MICqcm sensor chip's exceptional selectivity for AngII, demonstrating its ability to strongly distinguish AngII from other molecules while effectively suppressing nonspecific binding compared to the NICqcm chip. Upon reusability studies, it was found that after the 10th cycle, the QCM chip retained approximately 96% of its AngII adsorption capacity. These high-performing chips demonstrated significant advantages in terms of longevity and reusability. The 96% retention in adsorption capacity suggests minimal loss of functional groups on the chip surface. This consistent performance highlights not only its physical and chemical stability but also its reliability for repeated diagnostic applications, making it both a practical and cost-effective solution. As the final stage of the thesis, performance of AngII-MICqcm sensor was validated in a complex biological matrix. Human serum samples enriched with varying concentrations of AngII were used in studies to detect AngII using the AngII-MICqcm chip. Even in this complex environment, the instrument was able to detect incredibly minute amounts of AngII (1 pg/mL). This ability to function effectively in serum emphasizes the platform's practical viability and diagnostic relevance.

In conclusion, this thesis study successfully demonstrated the synhesis and characterization of AngII-imprinted nanoparticle and the fabrication of molecularly imprinted nanoparticle-based QCM biosensors for the direct, real-time, and label-free detection of AngII in human serum. To the best of current literature knowledge, this is the first study employing AngII-imprinted nanoparticles within QCM-based biosensors, representing a significant step forward in biomarker detection technologies.

REFERENCES

Abdella, A. A., & Ulber, R. (2025). Dummy-template molecularly imprinted polymers as an approach for improved efficiency for analytical applications: A mini review. Microchemical Journal, 209, 112768.

Afzal, A., Mujahid, A., Schirhagl, R., Bajwa, S. Z., Latif, U., & Feroz, S. (2017). Gravimetric viral diagnostics: QCM based biosensors for early detection of viruses. Chemosensors, 5(1), 7.

Akgönüllü, S., Kılıç, S., Esen, C., & Denizli, A. (2023). Molecularly imprinted polymer-based sensors for protein detection. Polymers, 15(3), 629.

Alexander, C., Andersson, H. S., Andersson, L. I., Ansell, R. J., Kirsch, N., Nicholls, I. A., ... & Whitcombe, M. J. (2006). Molecular imprinting science and technology: a survey of the literature for the years up to and including 2003. Journal of Molecular Recognition: An Interdisciplinary Journal, 19(2), 106-180.

Andersson, L. I., Muller, R., Vlatakis, G., & Mosbach, K. (1995). Mimics of the binding sites of opioid receptors obtained by molecular imprinting of enkephalin and morphine. Proceedings of the National Academy of Sciences, 92(12), 4788–4792. https://doi.org/10.1073/pnas.92.12.4788

Ardaillou, R. (1998). Angiotensin II-complexities beyond AT. Nephrol Dial Transplant, 13, 2988-2990.

Arısoy, P., & Baydemir Peşint, G. (2025). Development of molecularly imprinted nanoparticles for the detection of cardiovascular diseases biomarker Angiotensin II in human serum. Journal of Applied Polymer Science, 142(1), e56304.

Arya, S. K., Saha, S., Ramirez-Vick, J. E., Gupta, V., Bhansali, S., & Singh, S. P. (2008). Recent advances in ZnO nanostructures and thin films for biosensor applications: review. Analytica Chimica Acta, 616(1), 1–17. https://doi.org/10.1016/j.aca.2008.03.030

Aydoğan, N., Aylaz, G., Bakhshpour, M., Tugsuz, T., & Andaç, M. (2022). Molecularly designed ion-imprinted nanoparticles for real-time sensing of Cu (II) ions using quartz crystal microbalance. Biomimetics, 7(4), 191.

Aylaz, G., & Andaç, M. (2022). Affinity recognition based gravimetric nanosensor for equilin detection. Chemosensors, 10(5), 172.

Bahadır, E. B., & Sezgintürk, M. K. (2016). Applications of electrochemical biosensors for early clinical diagnostics. Talanta, 132, 162–174. https://doi.org/10.1016/j.talanta.2014.08.055

Bajaj, A., Buchholz, M., Choudhary, S., & Altintas, Z. (2023). Molecularly imprinted polymer sensors: a bridge to advanced diagnostics. In Fundamentals of Sensor Technology (pp. 475-504). Woodhead Publishing.

Balke, S. T., & Hamielec, A. E. (1973). Bulk polymerization of methyl methacrylate. Journal of applied Polymer science, 17(3), 905-949.

Basu, R., Poglitsch, M., Yogasundaram, H., Thomas, J., Rowe, B. H., & Oudit, G. Y. (2021). Roles of angiotensin peptides and recombinant human ACE2 in heart failure. Journal of the American College of Cardiology, 77(15), 1969–1983. https://doi.org/10.1016/j.jacc.2021.02.035

Baydemir, G., & Denizli, A. (2015). Heparin removal from human plasma using molecular imprinted cryogels. Artificial Cells, Nanomedicine, and Biotechnology, 43(6), 403-412.

Bedair, A., Hamed, M., El Hassab, M., Kannouma, R. E., Abdelhameed, R. M., & Mansour, F. R. (2025). Dummy template molecularly imprinted polymer-based sensors in analytical and bioanalytical applications. Talanta Open, 100431.

BelBruno, J. J. (2018). Molecularly imprinted polymers. Chemical reviews, 119(1), 94-119.

Benigni, A., Cassis, P., & Remuzzi, G. (2010). Angiotensin II revisited: new roles in inflammation, immunology and aging. EMBO Molecular Medicine, 2(7), 247–257. https://doi.org/10.1002/emmm.201000080

Bonardi, A. H., Bonardi, F., Morlet-Savary, F., Dietlin, C., Noirbent, G., Grant, T. M., ... & Lalevée, J. (2018). Photoinduced thermal polymerization reactions. Macromolecules, 51(21), 8808-8820.

Bossi, A. M., Bonini, F., Turner, A. P., & Piletsky, S. A. (2012). Molecularly imprinted polymers for the recognition of proteins: the state of the art. Biosensors and Bioelectronics, 26(4), 1171–1181. https://doi.org/10.1016/j.bios.2010.07.017

Bowen, R. A., & Remaley, A. T. (2014). Interferences from blood collection tube components on clinical chemistry assays. Biochemia medica, 24(1), 31-44.

Böttger, R., Hoffmann, R., & Knappe, D. (2017). Differential stability of therapeutic peptides with different proteolytic cleavage sites in blood, plasma and serum. PloS one, 12(6), e0178943.

Braunwald, E. (2008). Biomarkers in heart failure. New England Journal of Medicine, 358(20), 2148-2159.

Brenner, B. M., Cooper, M. E., de Zeeuw, D., et al. (2001). Effects of losartan on renal and cardiovascular outcomes in patients with type 2 diabetes and nephropathy. New England Journal of Medicine, 345(12), 861–869. https://doi.org/10.1056/NEJMoa011161

Brooks, B. (2010). Suspension polymerization processes. Chemical Engineering & Technology, 33(11), 1737-1744.

Brosnihan, K. B., & Chappell, M. C. (2017). Measurement of angiotensin peptides: HPLC-RIA. Hypertension: Methods and Protocols, 81-99.

Burnier, M., & Brunner, H. R. (2000). Angiotensin II receptor antagonists. The Lancet, 355(9204), 637-645.

Busse, L. W., Wang, X. S., Chalikonda, D. M., Finkel, K. W., Khanna, A. K., Szerlip, H. M., ... & Chawla, L. S. (2017). Clinical experience with IV angiotensin II administration: a systematic review of safety. Critical Care Medicine, 45(8), 1285.

Canfarotta, F., Poma, A., Guerreiro, A., & Piletsky, S. (2016). Solid-phase synthesis of molecularly imprinted nanoparticles. Nature Protocols, 11(3), 443–455. https://doi.org/10.1038/nprot.2016.024

Carey, R. M., Wang, Z. Q., & Siragy, H. M. (2018). Role of the angiotensin type 2 receptor in the regulation of blood pressure and renal function. Hypertension, 72(3), 710–717. https://doi.org/10.1161/HYPERTENSIONAHA.118.11154

Catt, K. J., Cain, M. C., & Coghlan, J. P. (1967). Measurement of angiotensin II in blood. The Lancet, 290(7524), 1005-1007.

Cavalier, E., CARLISI, I., Bekaert, A. C., Rousselle, O., Chapelle, J. P., & Delanaye, P. (2012). New insights on the stability of the parathyroid hormone as assayed by an automated 3rd generation PTH assay. Clinica Chimica Acta, 413(1-2).

Chappell, M. C. (2012). The non-classical renin-angiotensin system and renal function. Comprehensive Physiology, 2(4), 2733.

Chaudhary, V., & Sharma, S. (2019). Suspension polymerization technique: parameters affecting polymer properties and application in oxidation reactions. Journal of Polymer Research, 26(5), 102.

Chen, L., Wang, X., Lu, W., Wu, X., & Li, J. (2016). Molecular imprinting: perspectives and applications. Chemical Society Reviews, 45(8), 2137–2211. https://doi.org/10.1039/C5CS00404A

Chen, L., Xu, S., & Li, J. (2011). Recent advances in molecular imprinting technology: current status, challenges and highlighted applications. Chemical Society Reviews, 40(5), 2922-2942.

Chen, X., Zhang, W., Zhang, Z., et al. (2022). Recent advances of molecularly imprinted polymers in sensing applications. Sensors and Actuators B: Chemical, 368, 132131. https://doi.org/10.1016/j.snb.2022.132131

Cheng, Z. J., Vapaatalo, H., & Mervaala, E. (2005). Angiotensin II and vascular inflammation. Med Sci Monit, 11(6), 194-205.

Choi, J., Ghaffari, R., Baker, L. B., & Rogers, J. A. (2021). Skin-interfaced systems for sweat collection and analytics. Science Advances, 7(4), eabe5749. https://doi.org/10.1126/sciadv.abe5749

Chong, B., Jayabaskaran, J., Jauhari, S. M., Chan, S. P., Goh, R., Kueh, M. T. W., ... & Chan, M. Y. (2024). Global burden of cardiovascular diseases: projections from 2025 to 2050. European journal of preventive cardiology, zwae281.

Crapnell, R. D., Dempsey-Hibbert, N. C., Peeters, M., Tridente, A., & Banks, C. E. (2020). Molecularly imprinted polymer based electrochemical biosensors: Overcoming the challenges of detecting vital biomarkers and speeding up diagnosis. Talanta Open, 2, 100018.

Crowley, S. D., & Coffman, T. M. (2012). Recent advances involving the renin–angiotensin system. Experimental Cell Research, 318(9), 1049–1056. https://doi.org/10.1016/j.yexcr.2012.02.016

Crowley, S. D., & Coffman, T. M. (2014). The inextricable role of the kidney in hypertension. The Journal of clinical investigation, 124(6), 2341-2347.

Dainiak, M. B., Galaev, I. Y., Kumar, A., Plieva, F. M., & Mattiasson, B. (2007). Chromatography of living cells using supermacroporous hydrogels, cryogels. Cell separation: fundamentals, analytical and preparative methods, 101-127.

Demir, M. M., Castignolles, P., Akbey, Ü., & Wegner, G. (2007). In-situ bulk polymerization of dilute particle/MMA dispersions. Macromolecules, 40(12), 4190-4198.

Deng, F., Wang, R., Wu, L., Yang, G., Su, R., & Liu, Y. (2024). Angiotensin detection: A comprehensive review of current methods and novel technologies. Microchemical Journal, 111592.

Dhand, C., Dwivedi, N., Loh, X. J., Ying, A. N. J., Verma, N. K., Beuerman, R. W., ... & Ramakrishna, S. (2015). Methods and strategies for the synthesis of diverse nanoparticles and their applications: a comprehensive overview. Rsc Advances, 5(127), 105003-105037.

Dietl, S., Sobek, H., & Mizaikoff, B. (2021). Epitope-imprinted polymers for biomacromolecules: Recent strategies, future challenges and selected applications. TrAC Trends in Analytical Chemistry, 143, 116414.

Diltemiz, S. E., Keçili, R., Ersöz, A., & Say, R. (2017). Molecular imprinting technology in quartz crystal microbalance (QCM) sensors. Sensors, 17(3), 454. https://doi.org/10.3390/s17030454

Dincer, C., Bruch, R., Costa-Rama, E., Fernández-Abedul, M. T., Merkoçi, A., Manz, A., … & Urban, G. A. (2019). Disposable sensors in diagnostics, food, and environmental monitoring. Advanced Materials, 31(30), 1806739. https://doi.org/10.1002/adma.201806739

Ding, S., Lyu, Z., Niu, X., Zhou, Y., Liu, D., Falahati, M., ... & Lin, Y. (2020). Integrating ionic liquids with molecular imprinting technology for biorecognition and biosensing: a review. Biosensors and Bioelectronics, 149, 111830.

Ding, X., & Heiden, P. A. (2014). Recent developments in molecularly imprinted nanoparticles by surface imprinting techniques. Macromolecular Materials and Engineering, 299(3), 268-282.

Dong, C., Shi, H., Han, Y., Yang, Y., Wang, R., & Men, J. (2021). Molecularly imprinted polymers by the surface imprinting technique. European Polymer Journal, 145, 110231.

Emdin, M., Fatini, C., Mirizzi, G., Poletti, R., Borrelli, C., Prontera, C., ... & Vergaro, G. (2015). Biomarkers of activation of renin-angiotensin-aldosterone system in heart failure: how useful, how feasible?. Clinica Chimica Acta, 443, 85-93.

Erdös, E. G. (1976). Conversion of angiotensin I to angiotensin II. The American journal of medicine, 60(6), 749-759.

Ertürk, G., & Mattiasson, B. (2017). Molecular imprinting techniques used for the preparation of biosensors. Sensors, 17(2), 288.

Ferrario, C. M., & Varagic, J. (2010). The ANG-(1–7)/ACE2/mas axis in the regulation of nephron function. American Journal of Physiology-Renal Physiology, 298(6), F1297–F1305. https://doi.org/10.1152/ajprenal.00110.2010

Fogel, R., Limson, J., & Seshia, A. A. (2016). Acoustic biosensors. Essays in biochemistry, 60(1), 101-110.

Forrester, S. J., Booz, G. W., Sigmund, C. D., Coffman, T. M., Kawai, T., Rizzo, V., ... & Eguchi, S. (2018). Angiotensin II signal transduction: an update on mechanisms of physiology and pathophysiology. Physiological reviews, 98(3), 1627-1738.

Fu, D., Chen, T., Liu, H., Cheng, Y., Zong, H., Zhang, Y., ... & Liu, J. (2022). An ultraviolet self-initiated polymerized platform for specific recognition and elimination of caffeic acid based on the molecular imprinting technology. Sensors and Actuators B: Chemical, 361, 131659.

Fuchs, Y., Soppera, O., & Haupt, K. (2012). Photopolymerization and photostructuring of molecularly imprinted polymers for sensor applications—A review. Analytica chimica acta, 717, 7-20.

Gagliardi, M., & Cecchini, M. (2025). Core/shell molecularly imprinted nanoparticles: optimized synthesis and application in QCM-D biosensing. RSC advances, 15(23), 18310-18323.

Gaidai, O., Cao, Y., & Loginov, S. (2023). Global cardiovascular diseases death rate prediction. Current problems in cardiology, 48(5), 101622.

Geyer, P. E., Holdt, L. M., Teupser, D., & Mann, M. (2017). Revisiting biomarker discovery by plasma proteomics. Molecular Systems Biology, 13(9), 942. https://doi.org/10.15252/msb.20177781

Gladis, J. M., & Rao, T. P. (2004). Effect of porogen type on the synthesis of uranium ion imprinted polymer materials for the preconcentration/separation of traces of uranium. Microchimica Acta, 146, 251-258.

Golker, K., Karlsson, B. C., Olsson, G. D., Rosengren, A. M., & Nicholls, I. A. (2013). Influence of composition and morphology on template recognition in molecularly imprinted polymers. Macromolecules, 46(4), 1408-1414.

Haupt, K., & Mosbach, K. (2000). Molecularly imprinted polymers and their use in biomimetic sensors. Chemical Reviews, 100(7), 2495–2504. https://doi.org/10.1021/cr990099w

Haupt, K., Medina Rangel, P. X., & Bui, B. T. S. (2020). Molecularly imprinted polymers: antibody mimics for bioimaging and therapy. Chemical reviews, 120(17), 9554-9582.

Henein, M. Y., Vancheri, S., Longo, G., & Vancheri, F. (2022). The role of inflammation in cardiovascular disease. International journal of molecular sciences, 23(21), 12906.

Homola, J. (2008). Surface plasmon resonance sensors for detection of chemical and biological species. Chemical Reviews, 108(2), 462–493. https://doi.org/10.1021/cr068107d

IUPAC. (1999). Pure and Applied Chemistry, 71(12), 2333–2348. https://doi.org/10.1351/pac199971122333

Kalecki, J., Iskierko, Z., Cieplak, M., & Sharma, P. S. (2020). Oriented immobilization of protein templates: a new trend in surface imprinting. ACS sensors, 5(12), 3710-3720.

Kappelgaard, A. M., Nielsen, M. D., & Giese, J. (1976). Measurement of angiotensin II in human plasma: technical modifications and practical experience. Clinica Chimica Acta, 67(3), 299-306.

Karabulut, G., Beköz Üllen, N., & Karakuş, S. (2022). Nanostructures in Biosensors: Development and Applications. IntechOpen. doi: 10.5772/intechopen.108508

Kario, K. (2018). Nocturnal hypertension: new technology and evidence. Hypertension, 71(6), 997-1009.

Karnik, S. S., Unal, H., Kemp, J. R., et al. (2015). International union of basic and clinical pharmacology. XCIX. Angiotensin receptors: interpreters of pathophysiological angiotensinergic stimuli. Pharmacological Reviews, 67(4), 754–819. https://doi.org/10.1124/pr.114.010454

Kartal, F., & Denizli, A. (2014). Surface molecularly imprinted magnetic microspheres for the recognition of albumin. Journal of separation science, 37(15), 2077-2086.

Katz, E., & Willner, I. (2004). Probing biomolecular interactions at conductive and semiconductive surfaces by impedance spectroscopy: routes to electrochemical sensors. Electroanalysis, 16(1–2), 19–44. https://doi.org/10.1002/elan.200302851

Khan, I., Saeed, K., & Khan, I. (2019). Nanoparticles: Properties, applications and toxicities. Arabian journal of chemistry, 12(7), 908-931.

Khanna, A., English, S. W., Wang, X. S., et al. (2017). Angiotensin II for the treatment of vasodilatory shock. New England Journal of Medicine, 377(5), 419–430. https://doi.org/10.1056/NEJMoa1704154

Khumsap, T., Corpuz, A., & Nguyen, L. T. (2021). Epitope-imprinted polymers: applications in protein recognition and separation. RSC advances, 11(19), 11403-11414.

Kour, R., Arya, S., Young, S. J., Gupta, V., Bandhoria, P., & Khosla, A. (2020). Recent advances in carbon nanomaterials as electrochemical biosensors. Journal of The Electrochemical Society, 167(3), 037555.

Kulkarni, M. B., Ayachit, N. H., & Aminabhavi, T. M. (2023). A short review on miniaturized biosensors for the detection of nucleic acid biomarkers. Biosensors, 13(3), 412.

Laghlam, D., Jozwiak, M., & Nguyen, L. S. (2021). Renin–angiotensin–aldosterone system and immunomodulation: a state-of-the-art review. Cells, 10(7), 1767.

Lavrik, N. V., & Datskos, P. G. (2003). Femtogram mass detection using photothermally actuated nanomechanical resonators. Applied Physics Letters, 82(16), 2697–2699. https://doi.org/10.1063/1.1570930

Leal, C. R. V., Costa, L. B., Ferreira, G. C., de Melo Ferreira, A., Reis, F. M., & e Silva, A. C. S. (2022). Renin-angiotensin system in normal pregnancy and in preeclampsia: A comprehensive review. Pregnancy hypertension, 28, 15-20.

Li, G. L., Möhwald, H., & Shchukin, D. G. (2013). Precipitation polymerization for fabrication of complex core–shell hybrid particles and hollow structures. Chemical Society Reviews, 42(8), 3628-3646.

Li, R., Feng, Y., Pan, G., & Liu, L. (2019). Advances in molecularly imprinting technology for bioanalytical applications. Sensors, 19(1), 177.

Li, W. J., Liu, Y., Wang, J. J., Zhang, Y. L., Lai, S., Xia, Y. L., ... & Li, H. H. (2016). “Angiotensin II memory” contributes to the development of hypertension and vascular injury via activation of NADPH oxidase. Life Sciences, 149, 18-24.

Lin, T. Y., Hu, C. H., & Chou, T. C. (2004). Determination of albumin concentration by MIP-QCM sensor. Biosensors and Bioelectronics, 20(1), 75-81.

Liu, S., Liu, X., Pan, Q., Dai, Z., Pan, M., & Wang, S. (2021). A portable, label-free, reproducible quartz crystal microbalance immunochip for the detection of zearalenone in food samples. Biosensors, 11(2), 53.

Liu, Y., Shi, Q., Wang, J., & Yu, H. (2019). Recent advances in protein detection by nanomaterial-based biosensors. Analyst, 144(10), 2859–2873. https://doi.org/10.1039/C9AN00101F

Lovell, P. A., & Schork, F. J. (2020). Fundamentals of emulsion polymerization. Biomacromolecules, 21(11), 4396-4441.

Luque-Garcia, J. L., & Neubert, T. A. (2007). Sample preparation for serum/plasma profiling and biomarker identification by mass spectrometry. Journal of Chromatography A, 1153(1-2), 259-276.

Maisel, A., et al. (2019). The role of biomarkers in the diagnosis and management of heart failure. Clinical Chemistry, 65(1), 116–127. https://doi.org/10.1373/clinchem.2018.288902

Malik, S., Singh, J., Goyat, R., Saharan, Y., Chaudhry, V., Umar, A., ... & Baskoutas, S. (2023). Nanomaterials-based biosensor and their applications: A review. Heliyon, 9(9).

Maranduca, M. A., Clim, A., Pinzariu, A. C., Statescu, C., Sascau, R. A., Tanase, D. M., ... & Serban, I. L. (2023). Role of arterial hypertension and angiotensin II in chronic kidney disease. Experimental and Therapeutic Medicine, 25(4), 153.

Marx, K. A. (2003). Quartz crystal microbalance: a useful tool for studying thin polymer films and complex biomolecular systems at the solution–surface interface. Biomacromolecules, 4(5), 1099–1120. https://doi.org/10.1021/bm020116i

Mensah, G. A., Fuster, V., Murray, C. J., Roth, G. A., & Global Burden of Cardiovascular Diseases and Risks Collaborators. (2023). Global burden of cardiovascular diseases and risks, 1990-2022. Journal of the American College of Cardiology, 82(25), 2350-2473.

Mills, K. T., Stefanescu, A., & He, J. (2020). The global epidemiology of hypertension. Nature Reviews Nephrology, 16(4), 223-237.

Miura, S. I., Karnik, S. S., & Saku, K. (2011). Angiotensin II type 1 receptor blockers: class effects versus molecular effects. Journal of the Renin-Angiotensin-Aldosterone System, 12(1), 1-7.

Moad, G. (2019). A critical assessment of the kinetics and mechanism of initiation of radical polymerization with commercially available dialkyldiazene initiators. Progress in Polymer Science, 88, 130-188.

Mogensen, C. E., Neldam, S., Tikkanen, I., et al. (2000). Randomised controlled trial of dual blockade of renin–angiotensin system in patients with hypertension, microalbuminuria, and non-insulin dependent diabetes: the CALM study. BMJ, 321(7270), 1440–1444. https://doi.org/10.1136/bmj.321.7270.1440

Mondal, P., Anweshan, A., & Purkait, M. K. (2020). Green synthesis and environmental application of iron-based nanomaterials and nanocomposite: A review. Chemosphere, 259, 127509.

Morales, M. A., & Halpern, J. M. (2018). Guide to selecting a biorecognition element for biosensors. Bioconjugate chemistry, 29(10), 3231-3239.

Morsi, S. M., Abd El-Aziz, M. E., & Mohamed, H. A. (2023). Smart polymers as molecular imprinted polymers for recognition of target molecules. International Journal of Polymeric Materials and Polymeric Biomaterials, 72(8), 612-635.

Mueller, C., McDonald, K., deBoer, R. A., Maisel, A., GF, J., Cleland, N. K., ... & Jr16, J. L. J. Heart Failure Association of the European Society of Cardiology Practical.

Murdaya, N., Triadenda, A. L., Rahayu, D., & Hasanah, A. N. (2022). A review: using multiple templates for molecular imprinted polymer: is it good?. Polymers, 14(20), 4441.

Nahhas, A. F., & Webster, T. J. (2021). The promising use of nano-molecular imprinted templates for improved SARS-CoV-2 detection, drug delivery and research. Journal of Nanobiotechnology, 19(1), 305.

Naresh, V., & Lee, N. (2021). A review on biosensors and recent development of nanostructured materials-enabled biosensors. Sensors, 21(4), 1109.

National Center for Biotechnology Information (2022). PubChem Compound Summary for CID 172198, Angiotensin II. Retrieved October 10, 2022 from https://pubchem.ncbi.nlm.nih.gov/compound/Angiotensin-II.

Nazir, S., & Iqbal, R. A. (2023). Biosensor for rapid and accurate detection of cardiovascular biomarkers: Progress and prospects in biosensors. Biosensors and Bioelectronics: X, 14, 100388.

Nergiz, M., Zenger, O., & Peşint, G. B. (2024). L-proline determination by molecularly imprinted nanoparticles: A potential nanoscale tool for the diagnosis of metabolic disorders. Journal of Chromatography A, 1730, 465106.

Ng, K. K. F., & Vane, J. R. (1967). Conversion of angiotensin I to angiotensin II. Nature, 216(5117), 762-766.

Nguyen Dinh Cat, A., & Touyz, R. M. (2011). A new look at the renin-angiotensin system—focusing on the vascular system. Peptides, 32(10), 2141–2150. https://doi.org/10.1016/j.peptides.2011.07.021

Nikolaidis, A. K., Achilias, D. S., & Karayannidis, G. P. (2011). Synthesis and characterization of PMMA/organomodified montmorillonite nanocomposites prepared by in situ bulk polymerization. Industrial & engineering chemistry research, 50(2), 571-579.

Niu, J., Du, M., Wu, W., Yang, J., & Chen, Q. (2024). Advances in the selection of functional monomers for molecularly imprinted polymers: A review. Journal of Separation Science, 47(16), 2400353.

Okay, O., & Lozinsky, V. I. (2014). Synthesis and structure–property relationships of cryogels. In Polymeric cryogels: Macroporous gels with remarkable properties (pp. 103-157). Cham: Springer International Publishing.

Oparil, S., & Schmieder, R. E. (2015). New approaches in the treatment of hypertension. Circulation research, 116(6), 1074-1095.

Ostrovidov, S., Ramalingam, M., Bae, H., Orive, G., Fujie, T., Hori, T., ... & Kaji, H. (2023). Molecularly imprinted polymer-based sensors for the detection of skeletal-and cardiac-muscle-related analytes. Sensors, 23(12), 5625.

Pagliaro, P., & Penna, C. (2005). Rethinking the renin-angiotensin system and its role in cardiovascular regulation. Cardiovascular drugs and therapy, 19, 77-87.

Pasquardini, L., & Bossi, A. M. (2021). Molecularly imprinted polymers by epitope imprinting: a journey from molecular interactions to the available bioinformatics resources to scout for epitope templates. Analytical and Bioanalytical Chemistry, 413(24), 6101-6115.

Perazella, M. A., & Setaro, J. F. (2003). Renin-angiotensin-aldosterone system: fundamental aspects and clinical implications in renal and cardiovascular disorders. Journal of Nuclear Cardiology, 10(2), 184-196.

Piletsky, S. A., & Turner, A. P. (2002). Electrochemical sensors based on molecularly imprinted polymers. Electroanalysis, 14(5), 317–323. https://doi.org/10.1002/1521-4109(200203)14:5<317::AID-ELAN317>3.0.CO;2-9

Pisitkun, T., Shen, R. F., & Knepper, M. A. (2006). Identification and proteomic profiling of exosomes in human urine. Proceedings of the National Academy of Sciences, 101(36), 13368–13373. https://doi.org/10.1073/pnas.0403453101

Plebani, M. (2016). Harmonization in laboratory medicine: requests, samples, measurements and reports. Critical Reviews in Clinical Laboratory Sciences, 53(3), 184-196.

Polat, E. O., Cetin, M. M., Tabak, A. F., Bilget Güven, E., Uysal, B. Ö., Arsan, T., ... & Gül, S. B. (2022). Transducer technologies for biosensors and their wearable applications. Biosensors, 12(6), 385.

Poma, A., Guerreiro, A., & Piletsky, S. (2013). Solid-phase synthesis of molecularly imprinted polymer nanoparticles with a reusable template – a step closer to antibody replacement. Advanced Functional Materials, 23(21), 2821–2827. https://doi.org/10.1002/adfm.201203822

Poma, A., Turner, A. P. F., & Piletsky, S. A. (2015). Advances in the manufacture of MIP nanoparticles. Trends in Biotechnology, 33(12), 653–661. https://doi.org/10.1016/j.tibtech.2015.09.005

Puoci, F., Iemma, F., & Picci, N. (2008). Stimuli-responsive molecularly imprinted polymers for drug delivery: A review. Current drug delivery, 5(2), 85-96.

Rao, T. P., Kala, R., & Daniel, S. (2006). Metal ion-imprinted polymers—novel materials for selective recognition of inorganics. Analytica Chimica Acta, 578(2), 105-116.

Rauh, M. (2012). LC–MS/MS for protein and peptide quantification in clinical chemistry. Journal of Chromatography B, 883, 59-67.

Reimhult, K., Yoshimatsu, K., Risveden, K., Chen, S., Ye, L., & Krozer, A. (2008). Characterization of QCM sensor surfaces coated with molecularly imprinted nanoparticles. Biosensors and Bioelectronics, 23(12), 1908-1914.

Rossi, G. P., Lenzini, L., Caroccia, B., Rossitto, G., & Seccia, T. M. (2021). Angiotensin peptides in the regulation of adrenal cortical function. Exploration of Medicine, 2(3), 294-304.

Roth, G. A., Mensah, G. A., Johnson, C. O., Addolorato, G., Ammirati, E., Baddour, L. M., ... & GBD-NHLBI-JACC Global Burden of Cardiovascular Diseases Writing Group. (2020). Global burden of cardiovascular diseases and risk factors, 1990–2019: update from the GBD 2019 study. Journal of the American college of cardiology, 76(25), 2982-3021.

Saloni, J., Walker, K., & Hill Jr, G. (2013). Theoretical investigation on monomer and solvent selection for molecular imprinting of nitrocompounds. The Journal of Physical Chemistry A, 117(7), 1531-1534.

Sauerbrey, G. (1959). Verwendung von Schwingquarzen zur Wägung dünner Schichten und zur Mikrowägung. Zeitschrift für Physik, 155(2), 206–222.

Saylan, Y., Akgönüllü, S., Yavuz, H., Ünal, S., & Denizli, A. (2019). Molecularly imprinted polymer based sensors for medical applications. Sensors, 19(6), 1279.

Saylan, Y., Özgür, E., & Denizli, A. (2021). Recent advances of medical biosensors for clinical applications. Medical Devices & Sensors, 4(1), e10129.

Saylan, Y., Yilmaz, F., Özgür, E., Derazshamshir, A., Yavuz, H., & Denizli, A. (2017). Molecular imprinting of macromolecules for sensor applications. Sensors, 17(4), 898.

Schirhagl, R. (2014). Bioapplications for molecularly imprinted polymers. Analytical chemistry, 86(1), 250-261.

Sellergren, B. (2001). Molecularly Imprinted Polymers: Man-Made Mimics of Antibodies and Their Applications in Analytical Chemistry. Elsevier.

Shanks, J., & Ramchandra, R. (2021). Angiotensin II and the cardiac parasympathetic nervous system in hypertension. International journal of molecular sciences, 22(22), 12305.

Shrikrishna, N. S., Sharma, R., Sahoo, J., Kaushik, A., & Gandhi, S. (2024). Navigating the landscape of optical biosensors. Chemical Engineering Journal, 490, 151661.

Singh, A. K., Mittal, S., Das, M., Saharia, A., & Tiwari, M. (2023). Optical biosensors: A decade in review. Alexandria Engineering Journal, 67, 673-691.

Singh, A., Sharma, A., Ahmed, A., Sundramoorthy, A. K., Furukawa, H., Arya, S., & Khosla, A. (2021). Recent advances in electrochemical biosensors: Applications, challenges, and future scope. Biosensors, 11(9), 336.

Spagnolie, S. E. (2015). Complex fluids in biological systems. Biological and Medical Physics, Biomedical Engineering.

Sparks, M. A., Crowley, S. D., Gurley, S. B., Mirotsou, M., & Coffman, T. M. (2014). Classical renin-angiotensin system in kidney physiology. Comprehensive physiology, 4(3), 1201.

Sriramula, S., Haque, M., Majid, D. S., & Francis, J. (2008). Involvement of tumor necrosis factor-α in angiotensin II–mediated effects on salt appetite, hypertension, and cardiac hypertrophy. Hypertension, 51(5), 1345-1351.

Suzuki, Y., Ruiz-Ortega, M., Lorenzo, O., Ruperez, M., Esteban, V., & Egido, J. (2003). Inflammation and angiotensin II. The international journal of biochemistry & cell biology, 35(6), 881-900.

Swiderski, J., Gadanec, L. K., Apostolopoulos, V., Moore, G. J., Kelaidonis, K., Matsoukas, J. M., & Zulli, A. (2023). Role of angiotensin II in cardiovascular diseases: introducing bisartans as a novel therapy for coronavirus 2019. Biomolecules, 13(5), 787.

Şerbetçi, T., & Boğa, B. (2022). Renin-Anjiyotensin-Aldosteron Sistemine Etkili Tıbbi Bitkilerin Potansiyel Kullanımı. KTO Karatay Üniversitesi Sağlık Bilimleri Dergisi, 3(1), 105-118.

Tang, W., Han, J., Zhang, W., Li, H., Chen, J., Song, W., & Wang, L. (2024). Molecularly imprinted polymer sensors for biomarker detection in cardiovascular diseases. Analyst, 149(23), 5617-5637.

Thickett, S. C., & Gilbert, R. G. (2007). Emulsion polymerization: State of the art in kinetics and mechanisms. Polymer, 48(24), 6965-6991.

Titirici, M. M., & Sellergren, B. (2004). Peptide recognition via hierarchical imprinting. Analytical and bioanalytical chemistry, 378(8), 1913-1921.

Turiel, E., & Martín-Esteban, A. (2010). Molecularly imprinted polymers for sample preparation: a review. Analytica Chimica Acta, 668(2), 87–99. https://doi.org/10.1016/j.aca.2010.05.020

Turner, A. P. (2013). Biosensors: sense and sensibility. Chemical Society Reviews, 42(8), 3184–3196. https://doi.org/10.1039/c3cs35528d

Uniyal, A., Srivastava, G., Pal, A., Taya, S., & Muduli, A. (2023). Recent advances in optical biosensors for sensing applications: a review. Plasmonics, 18(2), 735-750.

Vahabi, S., Salman, B. N., & Javanmard, A. (2013). Atomic force microscopy application in biological research: a review study. Iranian journal of medical sciences, 38(2), 76.

Vasapollo, G., Sole, R. D., Mergola, L., Lazzoi, M. R., Scardino, A., Scorrano, S., & Mele, G. (2011). Molecularly imprinted polymers: present and future prospective. International journal of molecular sciences, 12(9), 5908-5945.

Verma, K., Pant, M., Paliwal, S., Dwivedi, J., & Sharma, S. (2021). An insight on multicentric signaling of angiotensin II in cardiovascular system: a recent update. Frontiers in Pharmacology, 12, 734917.

Wackerlig, J., & Lieberzeit, P. A. (2015). Molecularly imprinted polymer nanoparticles in chemical sensing–Synthesis, characterisation and application. Sensors and Actuators B: Chemical, 207, 144-157.

Walla, P. J. (2014). Modern biophysical chemistry: detection and analysis of biomolecules. John Wiley & Sons.

Wang, S., Zhang, L., Zeng, J., Hu, X., Wang, X., Yu, L., ... & Zhang, Z. (2023). Multi-templates molecularly imprinted polymers for simultaneous recognition of multiple targets: From academy to application. TrAC Trends in Analytical Chemistry, 166, 117173.Canfarotta, F., Poma, A., Guerreiro, A., & Piletsky, S. (2016). Solid-phase synthesis of molecularly imprinted nanoparticles. Nature protocols, 11(3), 443-455.

World Health Organization (2021). Hypertension. https://www.who.int/news-room/fact-sheets/detail/hypertension

World Health Organization (2023). Cardiovascular diseases (CVDs). https://www.who.int/news-room/fact-sheets/detail/cardiovascular-diseases-(cvds)

Wu, Z., & McGoogan, J. M. (2020). Characteristics of and important lessons from the coronavirus disease 2019 (COVID-19) outbreak in China: summary of a report of 72 314 cases from the Chinese Center for Disease Control and Prevention. jama, 323(13), 1239-1242.

Wulff, G. (1995). Molecular imprinting in cross-linked materials with the aid of molecular templates—a way towards artificial antibodies. Angewandte Chemie International Edition in English, 34(17), 1812–1832.

Xu, S., Wang, L., & Liu, Z. (2021). Molecularly imprinted polymer nanoparticles: an emerging versatile platform for cancer therapy. Angewandte Chemie International Edition, 60(8), 3858-3869.

Yan, H., & Row, K. H. (2006). Characteristic and synthetic approach of molecularly imprinted polymer. International journal of molecular Sciences, 7(5), 155-178.

Yang, Z. P., & Zhang, C. J. (2009). Designing of MIP-based QCM sensor for the determination of Cu (II) ions in solution. Sensors and Actuators B: Chemical, 142(1), 210-215.

Yetisen, A. K., Akram, M. S., & Lowe, C. R. (2013). Paper-based microfluidic point-of-care diagnostic devices. Lab on a Chip, 13(12), 2210–2251. https://doi.org/10.1039/c3lc50169h

Yıldırım, M., & Baydemir Peşint, G. (2021). Molecularly imprinted spongy columns for Angiotensin (II) recognition from human serum. Biotechnology Progress, 37(2), e3112.

Yusuf, S., Sleight, P., Pogue, J., Bosch, J., Davies, R., & Dagenais, G. (2000). Effects of an angiotensin-converting–enzyme inhibitor, ramipril, on cardiovascular events in high-risk patients. New England Journal of Medicine, 342(3), 145–153. https://doi.org/10.1056/NEJM200001203420301

Zenger, O., & Peşint, G. B. (2022). Preparation of molecularly imprinted bilayer cryogel columns for selective protein depletion. Process Biochemistry, 117, 90-100.

Zhang, R., Gao, R., Gou, Q., Lai, J., & Li, X. (2022). Precipitation polymerization: a powerful tool for preparation of uniform polymer particles. Polymers, 14(9), 1851.